Magnetically Targeted Drug Delivery:

Contributions In Magnetic Nanoparticle Uptake And Manipulation

A Thesis

Submitted to the Faculty

Of

Drexel University

by

Cristin Marie MacDonald

in partial fulfillment of the

requirements for the degree

of

Doctor of Philosophy

July 2011

Dedications

This thesis is dedicated to my grandfather, Seaman Harry MacDonald, for constantly reminding me about the important things in life.

Acknowledgements

I would like to express my deep and sincere gratitude to my supervisors, Dr Boris Polyak and Dr Kenneth Barbee. Without their constant show of support and dedication to teaching, I would not be where I am today. A special thanks to Dr Boris Polyak for stepping in to take the reigns on my project and helping to make sure I made it to the finish, as well as our fantastic lab memories of searching for boxes, hot glass and other words of wisdom. Dr. Barbee was a fantastic mentor that has helped steer me in the right direction whether through his academic inspirations or athletic ones.

I would like to thank committee members Dr. Gary Friedman for his wisdom and guidance in a field I was not all too familiar with at the beginning. Dr. Ari Brooks for providing me space to work with and the start that I needed at Drexel. As well as, Dr. Margaret Wheatley for her help and providing a fantastic softball team name and a lighthearted story in the break room. Special thanks to Dr. Elisabeth Papazoglou for being an inspiring committee member and to Dr. Fred Allen for helping to lead me through the final push and thoroughly reviewing my work.

Without the help of Dr. Banu Onaral's fantastic leadership and inspiring passion, my degree would not be nearly as much as it is today. Similarly, thank you to Dr. Rami Seliktar for his role in getting me to Drexel University. A very special thanks to the Biomed front office for all of their hard work and leading me through all of the red tape, most especially Lisa, Natalia, Aylin and Caryn.

Thank you to my fellow Drexel students, past and present for being there to share in the joys, tears, dreads and uniqueness that is a PhD program. Allison Andrews, Danielle

Figueroa, John Eisenbrey, Kelleny Oum, Manuel Figueroa, Michael Gormley, Mihir Shahnbag, Nicola Francis, Patrick Kirby, Raha Dastgheyb, Rob Hart and Valentina Cecchi. You all made even the truly lowest days a lot brighter.

To my friends near and far, who learned quickly to never ask, “how much longer”, especially Kristen Holahan, Colleen Riddle and Lori Anderson, Stef Cahill, Megan Sebstian, Krissy Blaston and Katie Herbst. To Travis Weber who helped me to survive the final months of stress and tears, despite stresses of his own. And most importantly my family: Caitlin, Marisa, Sabrina, Aunt Rosie and Uncle Bob for being there through thick and thin. Aunt Sharon for talking me off the ledge every time I wanted to throw in the towel. Grandmom and Grandpops for their unconditional love and confidence in me. My Mom and Dad, for their love, support and encouragement. Thank you Mom for always being proud of me and teaching me to be an independent woman and being there for me whether you were near or far. Thank you Dad for the trips to Dominics when school had me down in the dumps and for being a mirror image of grandpop and an equally inspirational human being. Words can never define how proud I am to call you my dad.

Table of Contents

Index of Tables and Figures

Abstract

Magnetically Targeted Drug Delivery:

Contributions In Magnetic Nanoparticle Uptake And Manipulation

Cristin Marie MacDonald

Currently, there are multiple approaches to targeted therapies being researched that involve the use of magnetic micro/nanoparticles. Their high biocompatibility as a result of magnetite's composition and the ability to position the magnetite in biocompatible polymer coatings such as PLA and PLGA makes them a potential resource for cancer treatment and gene delivery. Magnetic targeting utilizes an external magnetic field in combination with MNPs to allow delivery of particles to the desired target area and fixation to a local site while the medication is released and acts locally. This technique allows for decreased dosage of chemical therapies that may otherwise cause deleterious systemic effects. While much work has been completed on functionalizing MNPs and targeting them *in vitro*, there is minimal work that examines how these MNPs can move through soft tissues to treat disease.

Our work uses an alternating magnetic field, applied perpendicularly to a static magnetic gradient to increase magnetic nanoparticle motion through a simulated soft tissue. In order to increase magnetic susceptibility highly superparamagnetic nanoparticles were synthesized with magnetite concentrations of up to 70% (w/w). We found that magnetic nanoparticle uptake is a force dependent process and that an increase in MNP magnetite concentration not only leads to an increase in magnetic force applied to the cell but also increases MNP uptake. Using this process we were able to load bovine aortic endothelial cells with up to 15% of their cell volume without any

deleterious effects to the cytoskeletal or mitochondrial function. As a result of the minimal toxic effects, we tested the ability to manipulate the movement of loaded cells and showed that under the influence of a magnetic gradient from a permanent magnet there was significant increase in MNP loaded cell migration through a collagen coated transwell membrane in comparison to control cells. The loaded cells offer less toxic magnetically targeted vectors with a much higher magnetic susceptibility in comparison to MNPs alone. Further research is needed to determine if the “shaking” effect exhibited in the MNP viscous fluid study would work with MNP loaded endothelial cells.

This thesis analyzes magnetic nanoparticle synthesis with varying magnetite incorporation and how these differences affect magnetic nanoparticle motion with and without an alternating magnetic field. Through this research it has been found that we can load magnetite crystals into polymer nanoparticles up to 70% w/w without affecting the structural integrity of the particle. As a result, the particles synthesized were on average 250 nm in diameter and were significantly more responsive to external magnetic fields in comparison to standard commercially available nanoparticles that are approximately 30-40% w/w. The increase in magnetic responsiveness yields an increase in magnetic nanoparticle velocity through a viscous fluid, under the influence of a magnetic field provided by a neodymium magnet. The velocity in which particles moved increased linearly with respect to the amount of magnetite incorporated into the particle. The addition of the alternating current field that was applied perpendicular to the line of movement allowed the leading edge of the MNP group to move a 10 mm distance more quickly than the static only group. Additionally, the MNPs exposed to the alternating current field, also had an increase in the percentage of particles that made it the entire 10 mm length.

The increase in magnetic responsiveness was also examined when loading MNPs into bovine aortic endothelial cells (BAEC). It was found that an increase in magnetite concentration led to an increase in magnetic nanoparticle uptake into BAEC. This effect was determined to be a function of the magnetic force applied to nanoparticles since MNP uptake was minimal without the influence of a magnetic field.

Lastly, these highly loaded magnetic cells were used in two dimensional and three dimensional migration assays to determine if the MNP loadings had any positive or negative effects on migratory function. In two-dimensional studies, it was determined that highly loaded BAEC were not inhibited from migrating. In fact, 10% and 70% MNP loaded cells experienced migration rates that were significantly higher than that of the control, while 30% MNP loaded cells exhibited a higher migration rate that was not statistically significant. This implied that the functionality of the cytoskeleton for its role of migration was not impaired by the presence of the MNPS. The addition of a magnetic field, resulting from a neodymium magnet was added to 3-D migration in order to determine if MNP loaded BAEC would migrate through a Boyden chamber more quickly than non-loaded BAEC. It was found that the 70% MNP loaded BAEC were able to migrate across the membrane at speeds equal to that of control cells that were encouraged to migrate through the membrane with the assistance of FBS gradients. This study showed successful implementation of MNP loaded cell movement manipulation through a membrane.

The overall study has shown that increased magnetite concentration in polymer MNPs yields higher MNP uptake into endothelial cells. The increased MNP concentration in the cytoskeleton of the endothelial cells allows for an increase in magnetic responsiveness. The increase in MNP concentration shows minimal cellular function impairment. The ability to load these cells and manipulate them through the

body with minimal deleterious effects to their functionality makes them excellent candidates as vehicles for gene, drug or cellular deliveries.

Chapter 1: Background and Introduction

1.1 Thesis Overview

Biocompatible magnetic micro/nanoparticles are currently being developed as targeted drug and gene delivery agents, magnetic resonance imaging contrast agents and as thermoablation mechanisms. The potential of magnetic micro/nanoparticles for these applications results from their small size (comparable to a cell (micro) or protein (nano)), their biocompatibility, and most importantly their ability to be directed to a specific site through the use of an applied magnetic field gradient. However, the potential of magnetic particles for medical applications has not been fully realized due to limitations in the capability to accurately control the movement of the particles *in vivo* and to adequately concentrate the particles at the target site.

For example, the use of magnetic particles for thermoablation of cancerous tumors has been limited by the inability to move the particles within the tumor in order to obtain a homogeneous distribution and uniform heating. For many applications the magnetic particles must migrate through soft tissue under the influence of an applied field to reach the desired location. A better understanding of the factors that influence the movement of magnetic nanoparticles (MNP) through soft tissue is required to fully exploit the potential of these particles. Surprisingly little work has been performed on this important aspect of the overall problem.

Magnetically loaded cells have also been investigated as potential targeted delivery vectors that would allow circumnavigation of the immune system, as well as increase the magnetic susceptibility of the vector. Loading a cell with therapeutics attached to the MNPs or genetic materials to deliver genetically altered cells to specific areas are two potential ways that targeted drug delivery can be improved. In order to determine the

feasibility of this option, it is important to determine how these particles enter into a cell. In the past, work has been performed that shows an increase in transfection in cells with nanoparticles as gene delivery vectors; however, the mechanism of uptake is still unknown due to the difficulties in eliminating one endocytotic pathway without affecting another. Lastly, the uptake of these particles must be examined due to their cytotoxic effects. MNPs have been shown to be toxic both *in vivo* and *in vivo* and size and concentration both influence the toxic effects these particles exhibit.

In support of these concepts, this thesis contains a series of studies that address various important questions relevant to making magnetically targeted drug delivery one step closer to incorporation in a clinical setting. This thesis analyzes magnetic nanoparticle synthesis with varying magnetite incorporation and how these differences affect magnetic nanoparticle motion with and without an alternating magnetic field. The thesis takes the first step in analyzing magnetic transport through soft tissues by looking at the cellular level how MNPs of various iron oxide concentrations enter a cell, affect cell function and health as well as a feasibility study involving three-dimensional migration of particle loaded cells. The specific aims of this work are:

- Chapter 2: Synthesize magnetic nanoparticles of varying magnetite concentrations and examine how their motion through a viscous fluid is affected by a time-varying magnetic field.
- Chapter 3: Determine whether the mechanism of uptake is force driven and clarify the effects of cholesterol depletion and cytochalasin-D on uptake to offer a potential uptake mechanism. Quantify particle loading in cells.

- Chapter 4: Determine whether toxic effects of high MNP loadings affect mitochondrial function, cytoskeletal function and test magnetically loaded cells to determine if a magnetic force will increase cell migration through a membrane.

This thesis advances the knowledge in magnetically targeted drug delivery by offering a synthesis process that allows high incorporation of magnetite into magnetic nanoparticles yielding significantly more magnetically responsive particles. It looks to show that the major endocytotic mechanism of particle uptake is force-dependent and the result is cells that are extremely highly loaded. Further clarification of MNP toxicity of such high loaded cells as well as how we can manipulate their movement under the influence of a magnetic field.

1.2 Superparamagnetic Nanoparticles

1.2.1 Nanoparticles

Nanoparticles have been in existence long before nanotechnology research began. A Roman piece of art known as the Lycurgus Cup has been in existence since the 4th Century AD and recent analysis has shown the presence of silver and gold nanoparticles on the surface of the cup[1]. Nanoparticles are small particulates with at least one dimension on the scale of one billionth of a meter. Nanoparticles can be further divided into fine nanoparticles, comprised of particles 1-100 nm and superfine nanoparticles, comprised of particles 100-1000 nm. Nanoparticles can currently be made of different materials, sizes and shapes and have various coatings, chemical and surface properties.

Currently, some of the most common nanoparticles are carbon nanotubes, nanoshells, quantum dots, spherical nanoparticles and nanorods [2].

1.2.2 Superparamagnetism

Superparamagnetism is a property only observed in small ferromagnetic particles. One of the unique properties of nanoparticles is that they behave very differently from bulk or thin film stocks. When particle size is reduced below 15-20 nm, particles no longer exhibit ferromagnetic behavior, indicating that once a magnetic field is removed, the particles do not exhibit permanent magnetization. Despite the lack of permanent magnetism, nanoparticles still exhibit strong paramagnetic properties with large magnetic susceptibilities, which is the materials magnetic response to an applied magnetic field.

The difference in electron spin alignment of nanoparticles is what makes them superparamagnetic as opposed to ferromagnetic. Ferromagnetic materials have unpaired electrons that align themselves spontaneously. Therefore, without the influence of an external magnetic field, they still show magnetization. This magnetization is present even upon removal from a magnetic field. A change in external magnetic field direction while initially opposed, eventually will lead ferromagnetic fields to switch directions, Figure 1.1 [3].

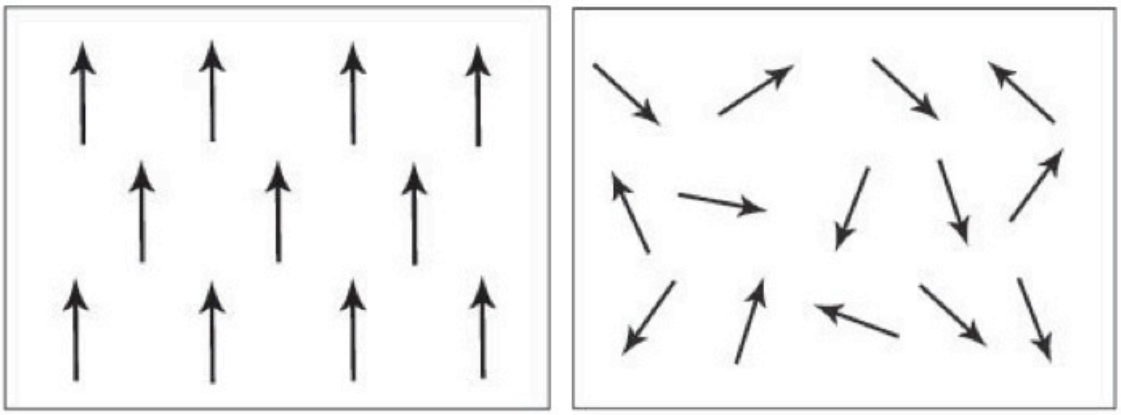

Figure 1.1: Ferromagnetism magnetic moments in a material are aligned parallel to one another under the influence of a magnetic field. These moments remain parallel when a magnetic field is not applied. Paramagnetism magnetic moments in a material are randomly oriented due to thermal fluctuations when there is no magnetic field. In an applied magnetic field, these moments will align parallel to the field so that the magnetization of the material is proportional to the applied field. [4]

When ferromagnetic materials reach particle dimensions smaller than a particular domain, they are no longer ferromagnetic and are called superparamagnetic [5]. In the case of paramagnetic particles, a magnetic field causes magnetic moments within the particles to align, causing them to have a magnetization, figure 1.1. However, unlike ferromagnetic materials, upon removal from the magnetic field, the magnetization returns back to zero.

What characterizes a particle as Superparamagnetism is a result of non-interacting, thermally fluctuating nanoparticle moments where the particle volume dependent effective anisotropy energy (KV) of each particle is easily overcome by the thermal energy (k_aT)[5]. The result, as stated before is nanoparticles with a high

saturation magnetization but magnetization (M)- field (H) curve that shows no hysteresis, remanence or coercivity, Figure 1.2.

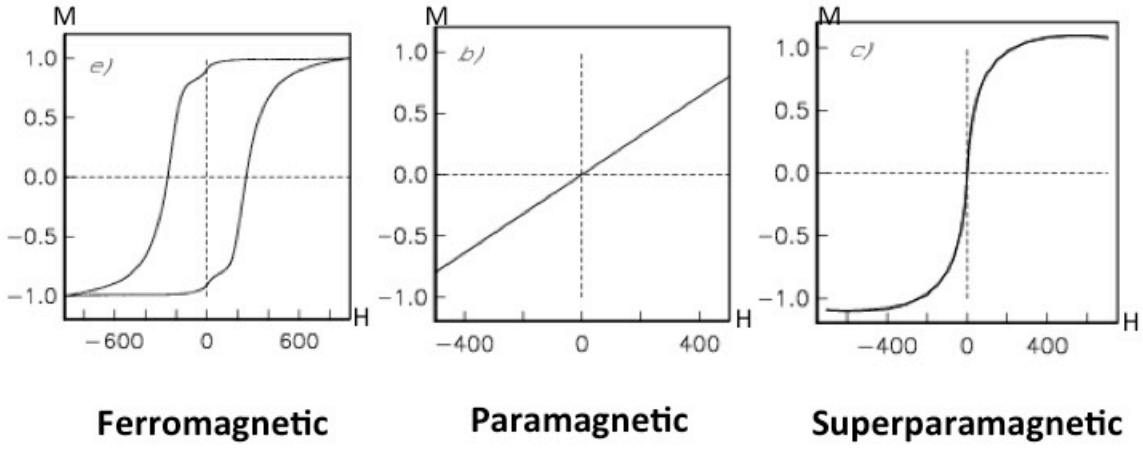

Figure 1.2: M-H curves of ferromagnetic material show hysteresis. Paramagnetic M-H curves show no hysteresis, but a long build up to saturation magnetization whereas superparamagnetic materials reach saturation magnetization quickly in comparison [6]

The difference between superparamagnetic as opposed to paramagnetic is the external field required to reach magnetization saturation. Superparamagnetic particles require minimal external field to reach magnetization saturation, whereas paramagnetic particles need the maximal external magnetic field strength to reach magnetization saturation, figure 1.2.

1.2.3 Superparamagnetic Nanoparticle Synthesis

Variations in synthesis methods lead to different size, shape and distribution of nanoparticles. The most important aspect of choosing a synthesis process is the ability to control the necessary nanoparticle characteristics for the intended application. Superparamagnetic nanoparticles can be synthesized via chemical methods (co-

precipitation, microemulsions, hydrothermal, thermal decomposition, sol-gel, polyol, sonochemical or electrochemical deposition), physical methods (flow injection, aerosol, pulsed laser ablation, laser induced pyrolysis or powder ball milling) or biological/bio-mineralization methods[7, 8]. Additional methods or alterations of current methods, in order to better control superparamagnetic nanoparticle characteristics, are being created daily as the field of nanotechnology grows.

Most of these methods fit into one of two categories: "top down" or "bottom up" approach. The top down approach involves taking a solid and breaking it down into smaller segments via milling, chemical methods or volatilization followed by condensation. The second approach, bottom up, involves synthesis of nanoparticles via condensation of materials in a gas phase or in solution, such as co-precipitation or emulsions[9].

The most common category used for superparamagnetic nanoparticle synthesis for biological applications is the bottom up approach. MRI based uses of MNPs use aqueous co-precipitation in the presence of the coating material as the synthesis method of choice[10]. Our research happens to use a modified version of this technique to create our MNPs, figure 1.3 [11-13].

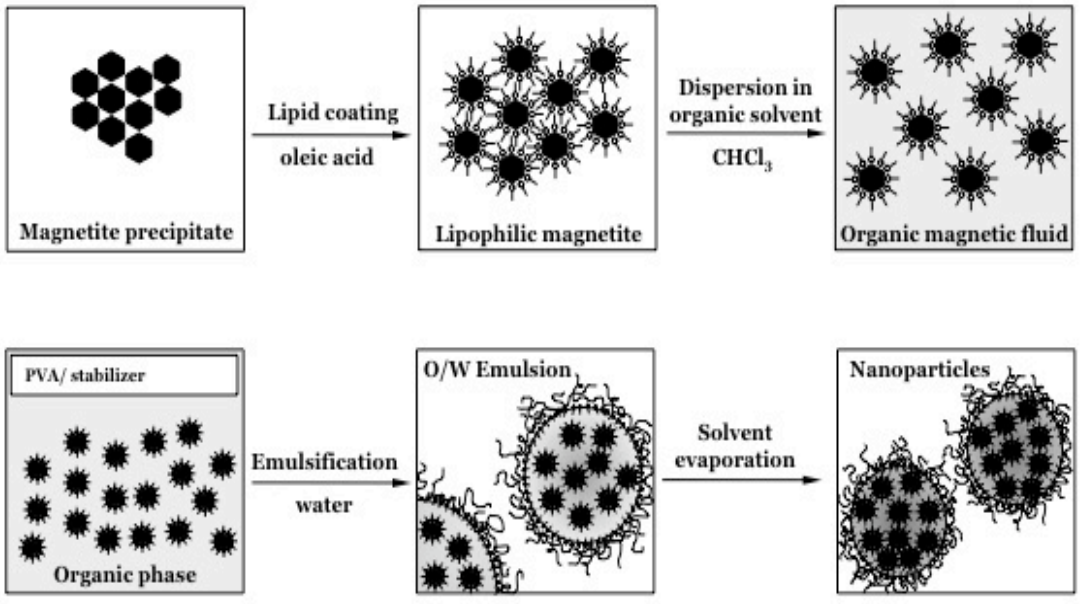

Figure 1.3: Modified Magnetic Nanoparticle Synthesis via a standard inverse microemulsion method.

Magnetite was formed following the chemical synthesis described:

$$2\ FeCl_3 \cdot 6\ H_2O + FeCl_2 \cdot 4\ H_2O + 8\ NaOH \rightarrow Fe_3O_4 + 8\ NaCl + 20\ H_2O \quad (1)$$

The resulting MNPs were coated with oleic acid as a stabilizer. A standard inverse microemulsion method was then used with PVA as a surfactant. One of the unique aspects of magnetic nanoparticles is that the percentage of magnetite within the nanoparticles can be altered [13]. Our research was unique in looking at MNPs with diameters of 250 nm varying magnetite concentrations and characterizing the resulting properties of the particles.

1.3 Applications of Superparamagnetic Nanoparticles in Biomedical Sciences and Medicine

Superparamagnetic nanoparticles such as the ones we have created have been used for biomedical applications and in medicine for more than thirty years [14]. The unique properties they display such as paramagnetism and inherent biocompatibility, due to the fact that they break down into iron and oxygen, make them attractive options for different functions in medicine. Some of their current and future uses in medicine are magnetic resonance imaging, hyperthermia, drug and gene delivery, cell separation and purification and tissue engineering [15].

1.3.1 Coating and Functionalization of Superparamagnetic Nanoparticles

Functionalization or coating magnetic nanoparticles is helpful in that it allows attachment of drugs, DNA or active binding sites as well as helps to protect the magnetite from degradation within the body [16]. Coatings of magnetic nanoparticles can be materials such as silver and gold or natural or synthetic polymers. Some commonly used natural polymers are dextran, albumin, alginate, chitosan, RGD and lipids. Examples of synthetic polymers are polyethylene glycol (PEG), polylactic co-glycolic acid (PLGA) and polyvinyl alcohol (PVA) [16]. These polymer coatings allow easier attachment of drug, DNA, fluorescent labels or active binding sites, due to the presence of a free end group or the ability to incorporate them into the matrix. The attachment of these therapeutic agents can be permanent (e.g. covalent bonding), or can be altered so that they are released with degradation of the polymer or MNP (e.g. encapsulation in particle).

For magnetic resonance imaging (MRI) purposes, dextran and PEG coatings on magnetic nanoparticles were found to be useful as they increased the longevity of

magnetite particle functioning circulation time in blood[17]. Similarly, MNPs for MRI, hyperthermia, drug delivery tissue engineering, and cell separation will often have monoclonal antibodies or peptides linked to the surface of the particle to detect cells of certain cancers[18].

1.3.2 Magnetic Nanoparticles in MRI

Magnetic nanoparticles, from 3-10 nm were first used in MRI as contrast agents for spleen and liver tissue imaging as a result of the particles tendency to accumulate reticuloendothelial system [19]. However, modern MRI techniques use contrast agents to improve signal intensity while differentiating diseased tissue, tumors, inflammation and microscopic blood vessels[20]. Traditional paramagnetic contrast agents for MRI are manganese (Mn^{2+}), iron (Fe^{3+}) or gadolinium (Gd^{3+})[20].

Iron particles offer some advantages of manganese or gadolinium commercially available contrast agents, firstly, in that iron nanoparticles have higher circulation times throughout the body.[21] Secondly, iron nanoparticles exhibit less toxicity than manganese and gadolinium particles, which have been shown to cause fetal toxicity in the cardiovascular system, central nervous system, lung and liver and cause serious kidney damage. This toxicity precludes the usage of manganese or gadolinium in patients with any pre-existing conditions that may have weakened any of these toxic-prone systems [22, 23]. Lastly, the ease at which we can functionalize magnetic nanoparticles also makes them more attractive in comparison to the other contrast agent types, as the particles can then perform as both diagnostics and therapeutics with the application of one dose.

1.3.3 Magnetic Nanoparticles in Hyperthermia

In addition to magnetic nanoparticle clinical uses in vivo, they are also currently being clinically investigated potential hyperthermia treatments in oncology. Traditional hyperthermia methods today are radiofrequency, microwave, ultrasound and whole body hyperthermia. For magnetic nanoparticle hyperthermia, the magnetic nanoparticles are exposed to an alternating field, which in turn cause the magnetic moment inside of the particle to oscillate; the energy caused from these oscillations is released in the form of heat. Temperature increases up to 56°C will cause thermalablation, demonstrated by necrosis, coagulation or carbonization of the surrounding tissue [24]. In hyperthermia, the tissues surrounding the nanoparticles are heated from 41-46°C[25, 26]. While this temperature increase in not sufficient to completely kill cancer cells, it does however make cancer tissues susceptible to treatment and allows healthy tissues to recover, whereas thermalablation would non-selectively kill both types of tissue. Therefore particles functionalized with drug treatments would be a benefit in magnetic hyperthermia, since the release of the drug would completely kill already weakened cancer cells[27].

Work first began on magnetic nanoparticle hyperthermia in lymph nodes with Gilchrist, et al. in the late 1950s [28]. Today, there are many pre-clinical trials in progress regarding magnetic nanoparticle hyperthermia [29] and the first clinical trial was performed in prostate cancers at the Charite´ University Medicine in Berlin, Germany in the early 2000s[30]. While hyperthermia is an attractive option, there are still issues such as homogeneity of heating throughout the tumor and the ability to reach deep areas of the tumor. While magnetic nanoparticle hyperthermia can potentially help to reach deep

areas of the tumor, more work is still necessary to determine how to get a homogeneous disbursement of magnetic nanoparticles in order to allow even heating throughout the tumor.

1.3.4 Magnetic Nanoparticles in Tissue Engineering

There have been very few published works that investigate how magnetic nanoparticles can be useful in tissue engineering applications, however, those that have been published show that there are many potentially useful purposes for their inclusion in standard tissue engineering procedures. Ito *et al*. was the first to use magnetic nanoparticles to create *in-vivo* simulated tissues consisting of various cell types [31]. This work used magnetic nanoparticles in magnetic cationic liposomes (MCLs) loaded into human aortic endothelial cells (HAECs) to create layers of tissue. HAECs that were not loaded with MCLs were seeded on a layer of rat hepatocytes in an attempt to get them to form an attached layer of cells, however, no attachment occurred. On the other hand, MCL loaded HAECs in the presence of a magnetic field did attach to the rat hepatocytes, forming a co-cultured tissue layer. Similarly, Perea *et al.* used clinically approved magnetically loaded human umbilical vein endothelial cells (HUVECs) in the presence of a magnetic field to form an endothelial cell lining on the surface of a vascular conduit (cite)[32].

Work at Drexel University shows similar results as shown previously. Buyukhatipoglu *et al*. showed that alginate and magnetically loaded porcine aortic endothelial cells were able to be successfully printed and the resulting three-dimensional (3-D) structure could be altered by magnetic fields that moved the nanoparticles and magnetically loaded cells[3, 33, 34]. The ability to move the magnetic nanoparticles

within the 3-D structure was important in realizing the potentials of moving bioactive factors throughout the system after printing, which would be important in helping to create 3-D printed tissues or organs. Similarly, work in the Polyak lab has recently begun in creating magnetic nanoparticle incorporated scaffolds that when combined with a magnetic field and magnetically loaded cells, helps to encourage cell seeding within the scaffold. The magnetic scaffolds when used in the presence of an AC field can also be used to deliver bioactive agents or stimulate growth as the contraction and expansion of the scaffold can be altered to release drug or stimulate growth in cells that are mechano-sensative (eg. Bone[35]).

While most of the above work investigates organization of cells to form tissues, other tissue engineering work shows how MNPs can be used to encourage cell differentiation. Kanczler *et al.*, showed that by tagging mechosensative receptors with magnetic nanoparticles on the cell membrane of human bone marrow stromal cells (HBMSCs), they were capable of activating differentiation in vitro and in vivo towards osteochondral lineage[36]. This work represents another promising function of magnetic nanoparticles in tissue engineering applications.

1.3.5 Magnetic Nanoparticles for Cell Separation and Purification

Magnetic nanoparticles have been used to separate cells, proteins and other biomolecules [37]. In magnetic separations, the MNPs are functionalized to attach to whatever material being separated and a magnetic field is applied, separating the desired material from the bulk suspension. Superparamagnetic nanoparticles are idea agents for biological separations since exposure to a magnetic field attracts them and they can then

be easily re-suspended once removed from that field, in contrast to liquid chromatography systems which are expensive and have extensive set up times.

1.3.6 Magnetic Nanoparticles in Gene and Drug Delivery

The ability of superparamagnetic nanoparticles to target and penetrate specific organs and cells contributes to their toxicity, however, under controlled situations, this functionality can be exploited for pharmacological treatment. Gene delivery occurs via viral vector delivery systems, or the increasingly used safer non-viral methods[38, 39]. Gene transfection, utilizing viral and non-viral vectors functionalized with surface proteins for cellular uptake and targeting ligands, exhibits slow accumulation which leads to small vector concentrations in the target tissues[40].

Magnetic nanoparticle assisted transfection, i.e. magnetofection, increases DNA vector accumulation within a cell in comparison to non-magnetically assisted methods. *In vitro* models show that magnetofection accelerates the transfection kinetics and the largest fraction of the dose is available in as little as ten minutes of incubation with cells, in comparison to the two and four hours it typically takes with non-magnetic protocols[41]. *In-vivo* models required targeting of desired tissue prior to tranfection and was completed by functionalization of the surface of the MNPs with the respective targeting ligands[41]. To test the feasibility and efficiency of magnetic non-viral vectors in comparison to viral vectors, Scherer,*et al.* used a rat and mice model, applying vectors to the ilea lumens or the stomach lumens, respectively along with a magnetic field. Scherer's group reported that magnetofection of non-viral vectors was equally as successful as its more toxic viral vector counterparts.

Magnetically targeted drug delivery typically focuses on cancer related treatments, since chemotherapy agents are not selective towards cancerous tissues and therefore deleterious to the healthy tissues as well[42]. The benefits of magnetically targeted drug delivery for cancer is that they allow these strong drugs to be delivered to only the cancer affected area, leaving the remainder of the tissues in the body unscathed from their toxic effects. Most importantly, smaller doses can be used if they are delivered right to the affected area.

Magnetically targeted drug delivery has been proven successful in small animal models [43, 44], however, the translation of these models into clinical settings, is difficult as a result of the size difference. Magnetic fields decrease exponentially with distance; therefore it takes a much stronger field to direct a MNP in the deep tissues of a human, versus the superficial location of a small mammal[45, 46]. One way to circumvent this issue is to create high gradient fields at the location for targeting. Forbes, *et al*. examined the targeting of magnetic nanoparticles to magnetic implants[45, 47-49]. By placing the magnetizable magnetic implant into a uniform magnetic field, it was able to increase the gradient of the magnetic force used to capture magnetic nanoparticles in flow. Similar work was done utilizing magnetically loaded cells captured with a magnetizable stent[50].

Overall, much of the work-completed shows that magnetically targeted drug delivery is a promising option that still has a few hurdles to overcome. Little research has been done on how magnetic nanoparticles can exit the vasculature of tumors and enter into the actual tumor tissues. Similarly, research is still needed to determine whether or not these magnetic nanoparticles can be manipulated to move through soft tissues in order to evenly distribute the therapeutic agent that they are delivering.

1.4 Magnetic Nanoparticle Motion

Most research published on magnetic nanoparticle motion investigates how magnetic nanoparticles flow through blood vessels and the magnetic forces necessary to remove particles from flow and attach them to either the vessel membrane or the magnetic implant [46, 51]. These published works are frequently mathematical models of the forces necessary to successfully quantify the magnetic field necessary to move this technology from *in-vivo* works on small animals to clinical trials.

In vitro studies on magnetic nanoparticles motion through cell culture layers or soft tissues are minimal, yet studies analyze model tissues such as alginate[52] , type 1 collagen[53] or agarose [54] to show that magnetic nanoparticles can in fact move through viscous materials. These studies determined that movements of MNPs in model tissues are dependent upon size, magnetic field and surface properties.

There have been few *in vivo* works on currently clinically feasible applications of magnetic nanoparticle movement through tissues, due to the high magnetic fields necessary to move MNPs through deeply set tissues in the human body. The only *in-vivo* works that can be potentially clinically relevant in the near future examining MNP movement through soft tissues is being done on MNP movement within the eyes and ears[44, 55, 56]. These works are more clinically relevant, because of the superficial nature of the necessary targeting, allowing easy transferability into a clinical setting.

In general, there are many questions that still need to be resolved about how magnetic nanoparticles move through tissues. The complex nature of the *in vivo* environment, as a result of interstitial pressures, blood flow, and potential uptake or

attachment of MNPs to non-targeted cell makes MNP movement characterization difficult. To break down some of the complexities, more modeling and *in vitro* work, like that done by Barnes *et al.* is necessary in order to more fully reveal how MNPs move through tissues and cells [57].

1.5 Magnetic Nanoparticle Endothelial Cell Uptake

Cells take up external materials by a process called endocytosis. There are many different types of endocytosis but most can be placed into one of two main categories: clathrin-mediated or clathrin-independent endocytosis. Clathrin-mediated endocytosis is characterized by the formation of morphologically distinct clathrin-coated vesicles on the cytoplasmic side of the membrane[58, 59]. Clatherin-independent forms of endocytosis are phagocytosis, pinocytosis and caveolae-mediated endocytosis. Phagocytosis is a form of "cell eating" while pinocytosis is a form of "cell drinking". Phagocytosis describes particle uptake by cells. It requires, and is initiated by, the attachment of the particle to the cell surface. Pinocytosis, however, is the uptake of a soluble or colloidal substance, and unlike phagocytosis is an ongoing process that is not typically susceptible to stimulation[60]. Caveolae-mediated endocytosis is characterized by the presence of caveolae, which are plasma membrane invaginations enriched with cholesterol and sphingolipids[59].

Typically nanoparticles and other materials get into contact with cells via Brownian motion, and that contact with the cell membrane initiates an endocytotic pathway. This process can be slow if there is a low concentration of low mass particles, however, magnetic nanoparticles exposed to a magnetic field cause a much faster initial introduction to the cell membrane[61]. While magnetic nanoparticles have proven to

increase gene transfection into a cell as a result of increased vector uptake, whether that uptake is the result of a faster introduction of uptake material to cells[62, 63] or a result of the magnetic force on the cells[64, 65] is greatly debated.

The main characteristic that determines which endocytotic mechanism a cell uses in uptake is particle size [66-69]. Clathrin-mediated endocytosis has been found to be the standard uptake mechanism for particles below 200 nm[68]. Whereas, caveolae-mediated endocytosis has been found to be the standard uptake mechanism for particles below 500 nm. Therefore, size differences do not automatically give the endocytotic mechanism, as shown in previous work that shows that 200nm nanoparticles were uptaken into the cell by both clathrin-mediated and the clatherin-independent caveolae-mediated endocytosis[62, 68].

In order to test the type of endocytosis that is being utilized by the cell for particle uptake, pharmacological inhibitors are often used. Common pharmacologic inhibitors of clathrin-mediated endocytosis are hypertoic sucrose, potassium depletion, cytosolic acidification, chlorpromazine, monodansylcadaverine and phenylarsine oxide. However, none of these chemical maneuvers selectively inhibit internalization via clathrin-coated pits with absolute selectivity. In particular, these inhibitors block uptake of fluid-phase markers and therefore cannot be used to decipher between clathrin-mediated endocytosis and macropinocytosis[59]. Inhibitors of caveolae-mediated endocytosis are statins, methyl-β-cyclodextrin, filipin and cholesterol oxidase[70, 71]. Again, use of these methods to block caveolae-mediated endocytosis also run the risk of damaging membrane integrity and therefore giving different uptake results[59]. Inhibitors of macropinocytosis and phagocytosis are sodium-proton exchange inhibitors such as

amiloride, f-actin depolymerizing drugs such as cytochalasin-D and inhibitors of phosphoinositide metabolism, such as PI3K[59, 71-73]. These inhibitors can potentially alter standard cell function so much that standard cellular endocytotic functions are altered. Overall to date, there are no popular inhibitors of different endocytotic pathways that possess certain specificity to the pathway of interest. However, these tools, in conjunction with other methodologies can help to shed light on cellular uptake mechanisms.

Another characteristic that determines whether or not magnetic nanoparticles are effectively endocytosed into a cell is the MNPs surface properties[74]. It has been shown that nanoparticles with higher (less negative) zeta potentials show greater uptake than those with lower (more negative) zeta potentials[72, 75-77]. Different polymer coatings can alter the surface charge of MNPs.

Lastly, it is important to note that the type of endocytosis of magnetic nanoparticles may vary from one cell type to another, despite there being no change in MNP surface properties or size. The different endocytosis mechanisms, lead to different MNP intracellular storage compartments. Therefore it is important to examine MNP uptake on the particular cell type you are looking to target before choosing the size, shape and surface properties of the synthesized nanoparticles.

1.6 Magnetic Nanoparticle Toxicity Mechanisms

Magnetic nanoparticles have been shown to have unique toxic effects on cells as a result of actin cytoskeletal disruption, mitochondrial damage, DNA damage and oxidative stress [21, 78-80]. Oddly enough, it has been shown that smaller nanoparticles, less than

100 nm exhibit stronger toxic effects than larger nanoparticles, up to one micron[81, 82] . This study focuses on the affects nanoparticles have on cytoskeletal disruption as well as mitochondrial toxicity.

1.6.1 Nanoparticle Induced Actin Cytoskeletal Disruption

Endocytosed magnetic nanoparticles are located within the cytoplasm of a cell, therefore their presence, especially in large concentrations, could potentially disrupt the cytoskeletal organization[83]. The cytoskeleton is responsible for maintaining cell shape, protecting the cell, enabling cellular motion and its roles in intracellular transport and cell devision[84]. The cells contain three main kinds of cytoskeletal filaments, namely microfilaments (actin filaments), intermediate filaments, and microtubules. The actin filaments are located beneath the cell membrane and are in charge of resisting tension and maintaining cell shape, participating in cell to cell or cell to matrix junctions and for forming cytoplasmic protuberances. Investigating any changes in actin filaments as a result of magnetic nanoparticle endocytosis is important since they are responsible for so many of the cells life functions.

There is minimal research regarding how magnetic nanoparticle incorporation into cells affects cytoskeletal organization and function. Wu *et al.* determined by imaging that cytoskeletal structures of human umbilical vascular endothelial cells (HUVECs) after loading with 35 nm iron oxide nanoparticles were greatly disrupted, as indicated by diminished vinculin spots and disorganized actin fibers and tubulin networks [85]. Similarly, their ability to form a vascular network, migrate and invade was inhibited significantly. Gupta *et al.,* found that 15 nm PEG coated magnetic nanoparticles were less cytotoxic to the cytoskeletal organization and cell adhesion in comparison to non-

coated magnetic nanoparticles of the same type *[86]*. They showed that microfilaments were well organized in thick bundles with stress fibers, while loaded cells with non-coated nanoparticles had actin fibers that were less defined and visibly disorganized. Soenen *et al.*, also saw that intracellular small iron oxide nanoparticles diminished cell proliferation, actin cytoskeletal organization as well as focal adhesion formation*[87]*.

Most of the work that has been completed on cytoskeletal organization and function as a result of MNP uptake is on MNPs less than 100 nm in diameter. Given that it has been shown that particles of this size have more detrimental affects in comparison to larger particles, it is necessary to determine whether the uptake of larger sized nanoparticles exhibit the same effects. It is also important to note that it is sometimes difficult to see cytoskeletal organization defects and therefore cytoskeletal function may detect damage earlier than can be seen with imaging methods.

1.6.2 Nanoparticle Induced Mitochondrial Depolarization

Mitochondrial health is a strong indicator of cell health and potential apoptosis. DNA damage, ischemia and oxidative stress are all examples of apoptotic signals that lead to cell death through mitochondrial pathways[88]. The mitochondrial pathway of apoptosis begins with the permeabilization of the mitochondrial membrane[89].

Xia *et al*, has shown that 60nm magnetic nanoparticle inclusion into five different cell types, macrophages, epithelial, endothelial, hepatocyte and pheochromocytomas showed toxicity at high loadings, but only a decrease in mitochondrial membrane potential, which indicates declining mitochondrial health, in macrophages and epithelial

cells[90]. Similarly, they showed that 200 nm MNP inclusions did not show any negative effects to the mitochondria.

The decline in mitochondrial membrane potential as a result of magnetic nanoparticle loading can be related to research that shows increase in reactive oxygen species (ROS) production by cells who have endocytosed magnetic nanoparticles[91-93]. Excess generation of ROS induces mitochondria membrane permeability, leading to a decline in membrane potential, triggering the apoptotic process[94, 95].

1.7 Organization of Dissertation

The aim of this thesis is to demonstrate that magnetic nanoparticles can be manipulated for potential drug delivery applications. We show this by moving magnetic nanoparticles through viscous gels with an applied AC magnetic field, showing a force dependent uptake of magnetic nanoparticles in endothelial cells and lastly demonstrating that particle loaded cells can be manipulated to migrate through a membrane at a higher rate than that of control cells. The thesis is organized into five chapters,

- Chapter 1 – The introduction chapter, covers the background of nanoparticles and superparamagnetic nanoparticles. Investigates the benefits of superparamagnetic nanoparticles as well as their application and relevance in clinical applications, in particular MRI, hyperthermia, tissue engineering, cell separation and drug/gene delivery. Lastly, it identifies work similar to ours such as magnetic nanoparticle manipulation, uptake and toxicity.
- Chapter 2 – Chapter two examines magnetic nanoparticle synthesis, characterization and movement through viscous gels. It shows a new magnetic

field set up that provides at alternating current magnetic field perpendicular to the static magnetic field and shows how this set-up increases the velocity of magnetic nanoparticle movement.

- Chapter 3 – Chapter three investigates the mechanism of uptake, in particular the role of the magnetic field in endocytotic uptake, as well as preliminary cell viability assays and quantifies the magnetic nanoparticles entrapped into a cell after uptake under the influence of a magnetic field.
- Chapter 4 – Chapter four studies more in depth the cell health of highly loaded endothelial cells by examining mitochondrial cell health and cytoskeletal arrangement, including confocal images. It also includes a feasibility study on using magnetically loaded cells as potential vectors for targeted drug delivery through tissues.
- Chapter 5 – Chapter 5 concludes the dissertation with a summary of the key findings and suggestions for future work.

Chapter 2: Time-varied magnetic field enhances transport of magnetic nanoparticles in viscous gel

2.1 Background

Magnetic nanoparticles (MNPs) are being extensively investigated in biomedicine as evidenced by the exponential growth in the number of publications dealing with these systems. In biotechnology the main applications of the MNPs are related to separation, detection and processing of bio-molecules. Their importance in medicine currently relates to their applications as imaging contrast agents in Magnetic Resonance Imaging (MRI) [96]. One of the most promising, yet clinically unrealized applications of MNPs in medicine is targeted delivery of various therapies to designated locations in the body[97]. These therapies may include hyperthermia in which the magnetic particles are selectively heated by application of a high frequency magnetic field, e.g. in thermal ablation/hyperthermia of tumors [30, 98], ionizing radiation [99, 100], and targeted delivery of specific drugs [101-107], gene vectors [63, 108-111], and cells [112-114]. The importance of targeted therapies stems from: (i) the reduction of the total quantity of drug or other therapeutic agent needed to attain a particular concentration in the vicinity of the target; and (ii) the reduction of the drug concentration at non-targeted sites [97, 115] minimizing severe side effects.

It has long been suggested that MNP targeting can be achieved through the use of magnetic field gradients, which apply a force on the magnetically responsive carriers and cause them to move to targeted locations. However, there are still serious gaps in our understanding of the mechanisms of MNP transport through soft tissues in a human body. Our lab and others have recently demonstrated the feasibility of the magnetic targeting approach through the vascular system, where MNPs or magnetically labeled cells were successfully localized to cardiovascular stents under static or flow conditions [46, 49, 114,

116]. The concept of using oscillating and static magnetic fields to enhance non-viral gene transfer *in vitro* has also been reported [16, 117]. Although these results are promising, MNPs often need to be transported not just through the circulatory system, or across cell membranes, but across blood vessel walls, the blood brain barrier or through other soft tissues. Forced transport of MNPs through soft tissues remains poorly understood [53, 57, 118-121]. Magnetic beads have been employed in rheological and magnetic actuation studies of cells following original investigations by Francis Crick, but these studies are not focused on active (external force controlled) transport of particles in tissues and cells [122, 123].

In the context of MNP transport, soft tissue is a multifaceted material that is more complex than blood, one of the most complex fluids,. Under the action of an external field gradient, MNPs will move through a viscous fluid at a constant rate dependent upon the fluid viscosity. However, in soft tissue, the MNPs reside in a complex material structure composed of liquids and solids. This material may exhibit a non-zero yield stress (the external stress below which the material responds elastically and above which it may respond as a viscous material) such that the MNPs may not move at all if the external magnetic force does not exceed a certain minimal value. The yield stress and viscous drag may depend strongly on the rate of variation of the magnetic forces and on MNPs characteristics, e.g., size, shape, degree of magnetic loading and surface properties. The mechanism of MNP transport across blood vessel walls and through soft tissue may vary depending on these characteristics. In order to successfully manipulate MNPs through soft tissues, it is important to determine the characteristics of the applied magnetic forces that produce the most controllable transport of the particles. The main

goal of the present study was to investigate the effect of a time-varying magnetic field superimposed with the static field gradient on MNPs mobility in viscous gel. Understanding these effects will enable development of means by which transport of MNPs through soft tissue can be controlled to a significant extent in a number of therapeutic approaches.

2.2 Materials and Methods

2.2.1 Materials

Poly(D,L-lactide) (average M_w: 75,000–120,000), ferric chloride hexahydrate, ferrous chloride tetrahydrate, sodium hydroxide, oleic acid, and polyvinyl alcohol (87-90% hydrolyzed, average M_w: 30,000-70,000) were obtained from Sigma-Aldrich (St. Louis, MO, USA). All solvents were purchased from Fisher Scientific (Pittsburgh, PA, USA) and were of HPLC grade. Deionized water used in all experimental procedures was obtained using a Milli-Q water purification system (Millipore, Bedford MA, USA). The viscous gel, Surgilube (15,000 cp) was obtained from (Altana Inc. NY, USA).

2.2.2 Magnetic Nanoparticle Formulation

Magnetite was obtained from ferric and ferrous chloride by alkaline precipitation as previously described elsewhere [108, 114, 124, 125]. In this study we investigated a novel aspect of nanoparticle formulation, the magnetite loading. Particularly we studied the effect of various magnetite loadings on MNP formation, magnetic properties and transport. For this purpose, various amounts of lipophilic magnetite were dispersed in 6 ml of chloroform, forming stable magnetic fluids further used for nanoparticle preparation. The amounts of iron salts and oleic acid used to obtain various loadings are

described in Table 2.1. Polylactide (PLA)-based magnetite-loaded nanoparticles (MNPs) were prepared by the emulsification-solvent evaporation method [11, 108, 114]. Typically, 200 mg of PLA was dissolved in 6 ml of magnetic fluid (containing various amounts of magnetite) to form an organic phase. The organic phase was emulsified in 15 ml of pre-chilled 1.5% (w/v) polyvinyl alcohol (PVA) by sonication, and the organic solvents were removed by evaporation under reduced pressure at 30°C. The particles obtained were passed through a 1.0 mm glass fiber prefilter (Millipore, Bredford, MA USA), dialyzed against 4 L of water with several water replacements for 24 h using a dialysis membrane with a 300,000 Da cut-off (Spectrum Laboratories, Inc., Rancho Dominguez, CA, USA) to remove unbound PVA, and lyophilized with 10% (w/v) trechalose as a cryoprotectant. Lyophilized MNPs were kept at +4°C and resuspended in deionized water before use.

Table 2.1. Amounts of the reagents used to obtain iron oxide loadings in a range of 10-50% (w/w).

Theoretical iron oxide loading (%)	$FeCl_3 \cdot 6H_2O$ (mg)	$FeCl_2 \cdot 4H_2O$ (mg)	1M NaOH (ml)	ddH_2O (ml)	Oleic acid, (mg)
10	65	24	1	9	100
20	130	48	1.9	8.1	150
30	195	72	2.9	7.1	150
40	260	96	3.8	6.2	200
50	325	120	4.8	5.2	200

2.2.3 MNP characterization

Particle size and zeta-potential measurements were performed using a Particle Size Analyzer (Zetasizer Nano-ZS90, Malvern, UK). The magnetic properties of MNPs were obtained from the hysteresis curves of 5 ml samples (corresponding to 125 mg) air-

dried on 4 mm diameter round coverglass slides measured by alternating gradient magnetometer (Princeton Instruments Corporation, Princeton, NJ, USA). The iron content of MNPs was determined spectrophotometrically (using Synergy 4 multimode plate reader, Biotek, USA) in 1 N hydrochloric acid (l=335 nm) against a standard curve after MNPs degradation with 1N aqueous sodium hydroxide (90°C, 30 min) and dissolution of the iron containing precipitate in the acid solution [108]. Transmission electron microscopy of MNPs samples was performed using JEM-1230 electron microscope (JEOL ltd, Japan). The samples of MNPs were diluted 1:10 with DI water and deposited on carbon-coated grids (Electron Microscopy Sciences, USA) with no use of contrast staining.

2.2.4 MNP velocity experiments

MNP velocity experiments were conducted in a translucent gel (15,000 cp) with uniform texture, free of bubbles and inclusions. This gel has been chosen as a commercially available material with a viscous texture that we could use as a feasibility study and a simplistic model to demonstrate the effects of various conditions on MNP transport through a viscous fluid. The gel was injected into a section of a disposable plastic pipette (4 mm in diameter and 10 mm in length) that served as a channel for the transport studies. A 3 ml aliquot of MNPs was placed into one end of the channel and allowed to settle on the gel's surface. The other end of the channel was placed flush against the permanent magnet such that the MNPs were located 10 mm away from the magnet. The distance that the MNPs traveled toward the magnet was measured in three minute intervals, by tracking the leading edge of the moving particles, and converted into MNPs velocities (mm/sec). The leading edge was tracked visually by using a magnifying

lens and a micro-ruler with 0.1 mm divisions. Given the assumption that error is ½ of the minor scale, the error associated with these readings would be 0.05mm. The experimental magnetic set up is shown in Figure 2.1.

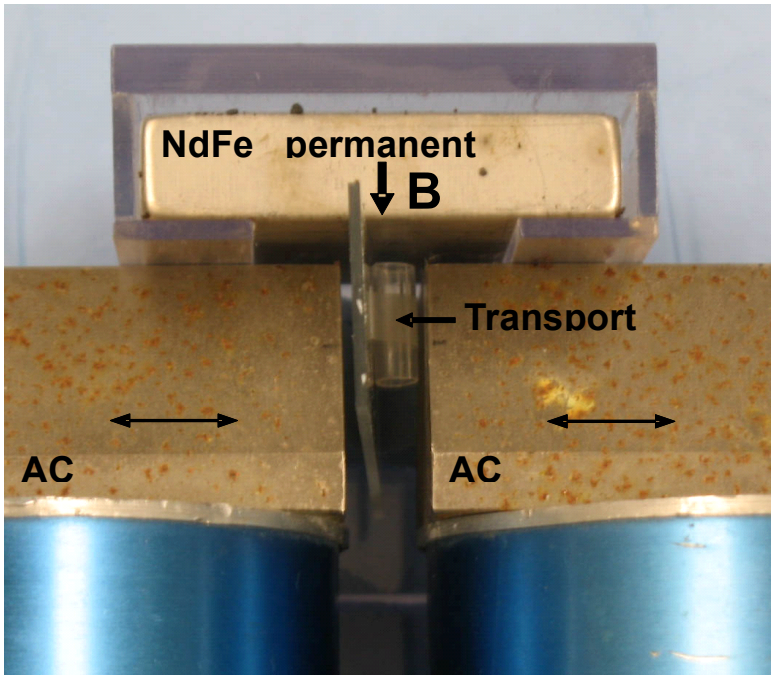

Figure 2.1. The experimental magnetic setup consisting of an AC field generator, a permanent NdFeB magnet and the transport channel positioned between cores of electromagnet and the permanent magnet.

To determine the AC field parameters that resulted in maximal increase in the MNPs velocity through the viscous gel, a series of optimization experiments using various AC field settings and frequencies were performed. In these experiments MNPs loaded with 30% (w/w) magnetite were used. The voltages on the AC power supply were set at 0.2-2.7 V. For each voltage, the frequency was tested at 50 and 100 Hz. The RMS (root-mean-square) AC field values were then measured for each voltage and frequency

using a hand-held Lakeshore 410 magnetometer (Lake Shore Cryotronics, Inc.). The velocity of the MNPs at each AC field setting was calculated, and the AC field that resulted in the maximal MNP velocities was used in subsequent magnetic transport efficiency experiments.

2.2.5 Magnetic Transport Efficiency

Static and AC field experiments (n=5) were conducted for each magnetite loading between 20-50% (w/w) using a 10 mm long channel (as described above). At the completion of the exposure time (30 min), the 2 mm of the channel closest to the permanent magnet was sliced off to separate the fraction of MNPs that completed motion from those that did not travel to completion (i.e., remained in the 8 mm segment). Since the MNPs do not move in a large clump but rather as a leading edge with a tail, in order for the tail to reach the completion point the leading edge would have had to leave the experimental channel. Therefore, we decided to collect the final 2 mm of motion to quantify the mean fraction of particles that were moving. Both segments of the channel were dried in a Petri dish for 24 hours. Then, the dry residues of gel samples containing the MNPs were transferred to Eppendorf tubes. The samples were re-suspended to a liquid form with 20 mL of DI water. Then the MNP-containing samples were incubated with 1M NaOH to digest PLA and release the magnetite (90^{o}C, 30 min). The released magnetite was separated by centrifugation and dissolved in 1M HCl (90^{o}C, 1hour). The amount of iron in both channel segments was determined spectrophotometrically (l=335 nm). The resulting value allowed us to estimate the fraction of particles based on their known composition. An initial reading was made of the iron content by analyzing the absorption at 335nm of total iron from a 3 ml sample of MNPs in order to normalize the

absorption readings of the MNPs that completed motion and those that did not. The fraction of MNPs that completed motion (originated from the 2 mm segment of the channel closest to the NdFeB permanent magnet) is presented as a percentage by comparing the MNPs that completed motion to that of the total initial MNPs dose.

2.2.6 Statistical analysis

Experimental data in plots were presented as means ± SD. The evaluation of which magnetic fields to use against the control (static field) was analyzed using Dunnett's test. A one-tailed, unequal variances *t*-test was then used to analyze the significance ($P<0.05$) of the velocities between the resulting experimental magnetic setups with varying AC frequencies.

2.3. Results

2.3.1 MNPs formulation and characteristics

Magnetic PLA-based nanoparticles were formulated by varying the inclusion of the magnetite within the PLA matrix in a range of 10 to 50% (w/w). Non-magnetic NPs were prepared as a control formulation. Various magnetite loadings did not cause any adverse effects on the stability of the emulsions or the formation of MNPs following the evaporation step. Stable oil-in-water emulsions were obtained for all formulations. During the evaporation step, no visible precipitates were observed. This evidence correlated well with the high magnetite entrapment yield that was estimated to be about 95% for all formulations. The MNPs hydrodynamic diameters ranged between 213 to 275 nm for different magnetite loadings averaging at 239±23 nm (by the dynamic light

scattering). No correlation was observed between the magnetite loading and MNPs size distribution (Table 2.2).

Table 2.2 Magnetic entrapment yield, size and surface charge characterization of MNPs.

Formulation description	Magnetic entrapment yield, %	Iron oxide loading, % (w/w)	Size, nm	Zeta potential, mV
0% iron oxide TL*	-	-	231	-5.75
10% iron oxide TL	94.1±1.8	9.7±1.0	244	-6.80
20% iron oxide TL	96.7±3.8	19.9±0.7	253	-5.70
30% iron oxide TL	94.9±8.6	29.3±2.3	213	-6.95
40% iron oxide TL	96.9±1.3	39.6±0.6	275	-7.43
50% iron oxide TL	94.6±0.6	48.8±0.4	219	-9.27

*TL=Theoretical Loading.

The MNPs size obtained by the Transmission Electron Microscopy (TEM) was in agreement with the light scattering data (Figure 2.2). Zeta potentials indicating the MNPs surface charge were slightly negative and varied between -5.75 and -9.27 mV (Table 2.2).

The resulting PVA-stabilized PLA-based magnetic nanoparticles of various magnetite loadings (10-50% (w/w)) exhibited a dose-dependent superparamagnetic behavior showing no significant hysteresis (Figure 2.3). The magnetic moment dependence on the magnetic field was nearly linear up to 1 kOe, reaching 65-70% of the saturation magnetization value for all magnetic formulations, whereas a comparatively low increment in magnetization was observed on further increasing the field to 5 kOe. The average normalized values of MNP magnetizations calculated at 1.0 and 5.0 kOe (saturation magnetization) were found to be 35±1 and 50±1 (emu/g) respectively.

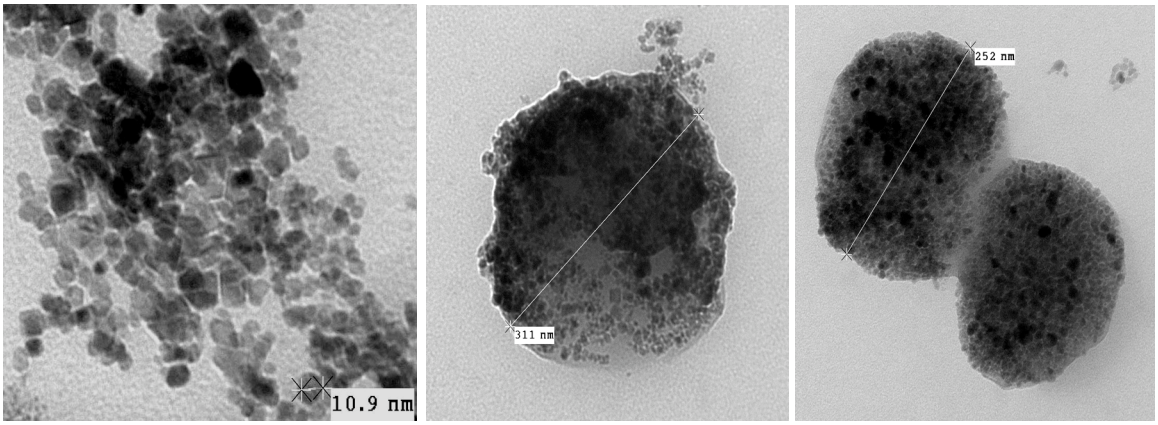

Figure 2.2. Transmission electron microscopy of (A) iron oxide crystals stabilized with oleic acid, (B) 20% and (C) 50% (w/w) iron oxide loaded polylactic (PLA)-based magnetic nanoparticles prepared by the emulsification-solvent evaporation method. The samples of MNPs were deposited on carbon grids and after drying visualized immediately without contrast staining.

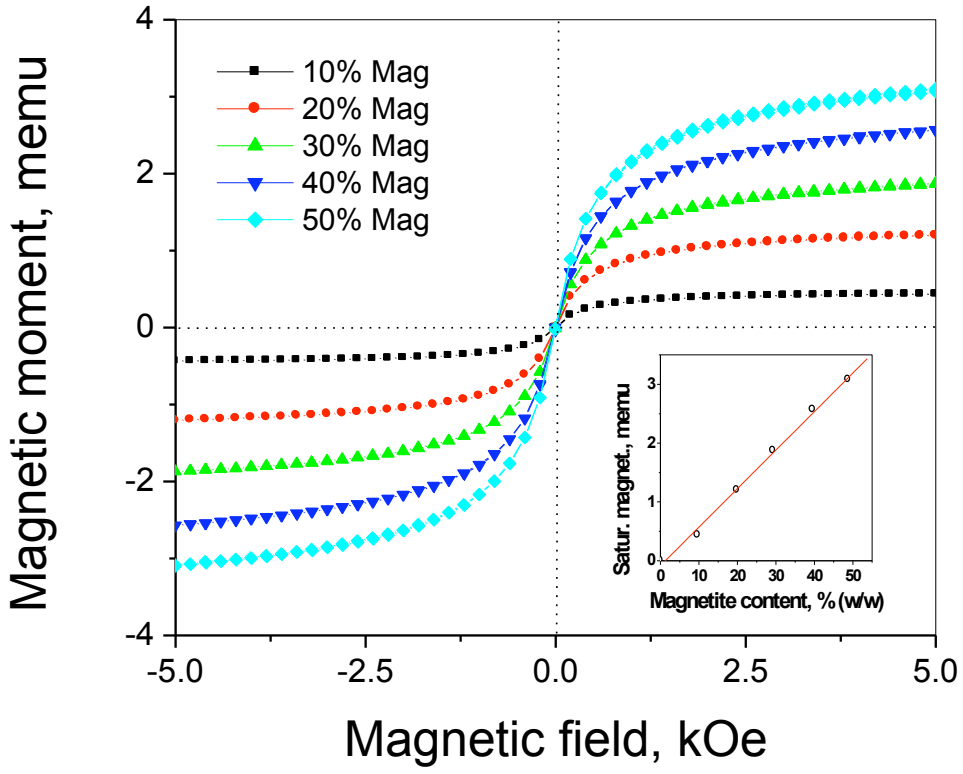

Figure 2.3. Magnetization curves of MNP formulations loaded with 10-50% (w/w) of iron oxide. Note the absence of remanence (superparamagnetism) exhibited by all MNP formulations. There is a linear correlation between the iron oxide content and the saturation magnetization values.

2.3.2 Generation of static and AC magnetic forces

To understand how magnetic forces are generated, it is important to know the dependence of the magnetic moments of PLA nanoparticles loaded with magnetite on the external magnetic field. The shape of the magnetization curve approximates the well-known Langevin function that can be derived theoretically for non-interacting superparamagnetic nanoparticles, which fill the core of the PLA polymeric sphere. The Langevin function is given by $L(\eta) = \coth\eta - 1/\eta$, where $\eta = M_s B/kT$ and M_s, *k, T* and *B* are particle's saturation magnetic moment, Boltzmann constant, absolute temperature and magnetic flux density, respectively. It is worth noting that for small values of the external magnetic flux density B, when $\eta = M_s B/kT << 1$, the Langevin function can be well approximated as a linear function of the field. However, when $\eta = M_s B/kT > 1$, the Langevin function begins an asymptotic approach to 1. This region of the magnetization characteristic is known as saturation.

The magnetic force on spherical particles is usually derived by treating them as magnetic point dipoles and is given by:

$$\vec{F} = \left(\vec{M} \cdot \nabla\right)\vec{B} \qquad (1)$$

where $\vec{M} = \vec{M}^{static} + \vec{M}^{AC}$ is the particle's magnetic moment and $\vec{B} = \vec{B}^{static} + \vec{B}^{AC}$ is the total magnetic field applied. The magnetic field generating set-up employed in these experiments and positioning of the sample within it are presented in Figure 1. We have chosen to employ a configuration where the static field at the location of the sample is

mostly perpendicular to the AC field produced by the electromagnet with laminated core (the laminated core is needed in order to minimize eddy current screening of the AC field). The static field generated by the permanent magnet (NdFeB) varies significantly along the magnet's and the sample axis (z-axis), creating fairly strong field gradients. The average z-field component at the sample location was measured to be around $B_z^{static} \approx 0.3$ Tesla (3 kOe), while z-field gradient along the z-direction was measured to be around $\frac{\partial B_z^{static}}{\partial z} \approx 10$Tesla/m. The location of the average z-field and gradient is presented in terms of the MNPs at their furthest distance from the magnet (10 mm), therefore the starting point. This then gives the lowest gradient field that they will experience throughout their period of motion. The gradient $\frac{\partial B_x^{static}}{\partial x}$ of the static field component directed across the electromagnet gap (x-axis) was somewhat larger (around 15 Tesla/m) along the direction of this field component (x-direction). It was observed that gradient of the z- field along its axis is far greater than its gradients $\frac{\partial B_z^{static}}{\partial x}$ and $\frac{\partial B_z^{static}}{\partial y}$ perpendicular to the z-axis. At the average value of the axial static field observed in these experiments, the particles' magnetic moments were nearly saturated (see Figure 3). Using the observations described above, the static magnetic force on the PLA nanoparticles can be obtained from (1) and is approximately given by:

$$F_z^{static} \approx M_s \frac{\partial B_z^{static}}{\partial z} \qquad (2)$$

Using the equation (2) the magnetic force in *z*-direction acting on particles located at the starting point of motion (10 mm away from the permanent magnet) was estimated to be

about 3fN. The AC force on the PLA nanoparticles arises mainly due to the AC component of the magnetic moment and due to the static field gradient (gradient of the AC field is confirmed to be much smaller than the static field gradient in our set-up). The strongest component of the AC force, therefore, in our set-up, is the one along the electromagnet gap (x-axis). This force is approximately given by:

$$F_x^{AC} = M_s \frac{B_x^{AC}}{B_z^{static}} \frac{\partial B_x^{static}}{\partial x} \qquad (3)$$

Taking into account that gradients $\frac{\partial B_z^{static}}{\partial z}$ and $\frac{\partial B_x^{static}}{\partial x}$ are about the same in magnitude, it becomes clear that the ratio of AC to static force magnitudes scales as $\frac{B_x^{AC}}{B_z^{static}}$. In our experiments this ratio was on the order of 0.01. Thus, the AC force employed in the preliminary experiments is estimated to be about 100 times weaker than the static force applied to the PLA nanoparticles and estimated as 0.03 fN. This analysis remains fairly accurate at relatively low frequencies (below about 100 kHz) where the magnetic moments can be assumed to respond nearly instantaneously to the external field.

2.3.3 Variations of AC magnetic field

Figure 2.4 shows the velocities of 30% (w/w) magnetic loading MNPs at various AC field values tested at 50 and 100 Hz frequencies, superimposed with the static field generated only by the permanent NdFeB magnet. The application of an AC field increases the velocity of the MNPs in viscous gel substantially as compared to the presence of a static field only. Under “no magnetic field” control condition the particles remain suspended in the initial deposition point showing no movement for at least 12

hours. Dunnett's test showed that with the exception of the lowest voltage at 100 Hz, all AC magnetic fields significantly increased the velocity of the MNPs ($P<0.05$). T-test comparisons between varying AC frequencies within experimental groups with the same power supply voltage showed no statistical differences. Therefore, further experiments were conducted using a RMS AC value of 16.4 Oe at a frequency of 50 Hz, as MNPs experienced the highest velocity under these conditions and the field requirements fit well within the range of our power supply.

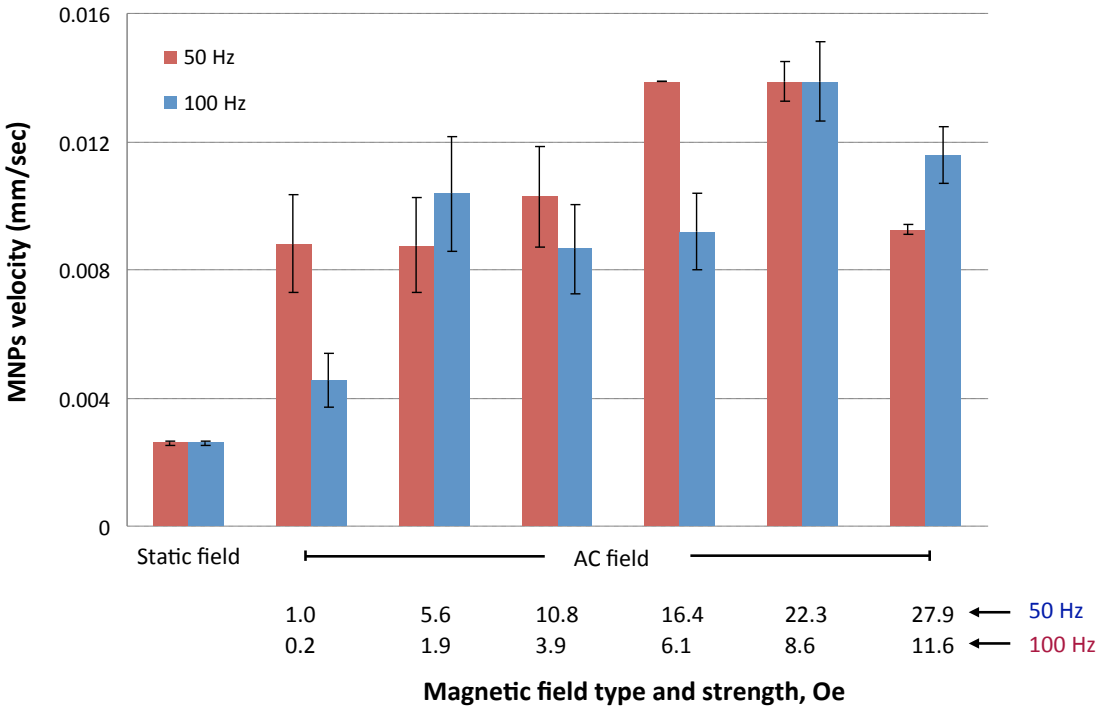

Figure 2.4. The velocities of 30% (w/w) MNPs at various AC field values tested at 50 and 100 Hz frequencies, superimposed with the static field generated only by the permanent magnet (n=3). All AC conditions were significantly different than static ($P<0.05$). All AC fields were statistically different from the static fields ($p<0.05$).

2.3.4 MNPs velocity as function of the magnetite loading and the MNPs transport efficiency

The transport of MNPs loaded with 20-50% (w/w) magnetite was compared at static field conditions versus static field superimposed with an AC field (termed later as an AC field condition for simplicity). The MNP transport efficiency is defined as a fraction of the MNPs that reached the 2 mm of the channel closest to the permanent magnet during 30 min. The transport of MNPs loaded with 20% (w/w) magnetite was very poor (<10% efficiency) and did not significantly differ between the static and an AC field conditions (Figure 2.5). At 30% (w/w) magnetite loading, the efficiency with an added AC field increased sharply to 60%, while the static remained unchanged. At 40% and 50% (w/w) magnetite loading, the magnetic transport efficiency with the AC field reached a plateau at 80%. The maximal enhancement of the magnetic transport efficiency (AC vs. static) is nearly 30-fold at 30% (w/w). At 40% and 50% (w/w) magnetite loading, the enhancement in magnetic transport efficiency by the AC field is less pronounced, yet the differences are statistically significant with $P<0.05$.

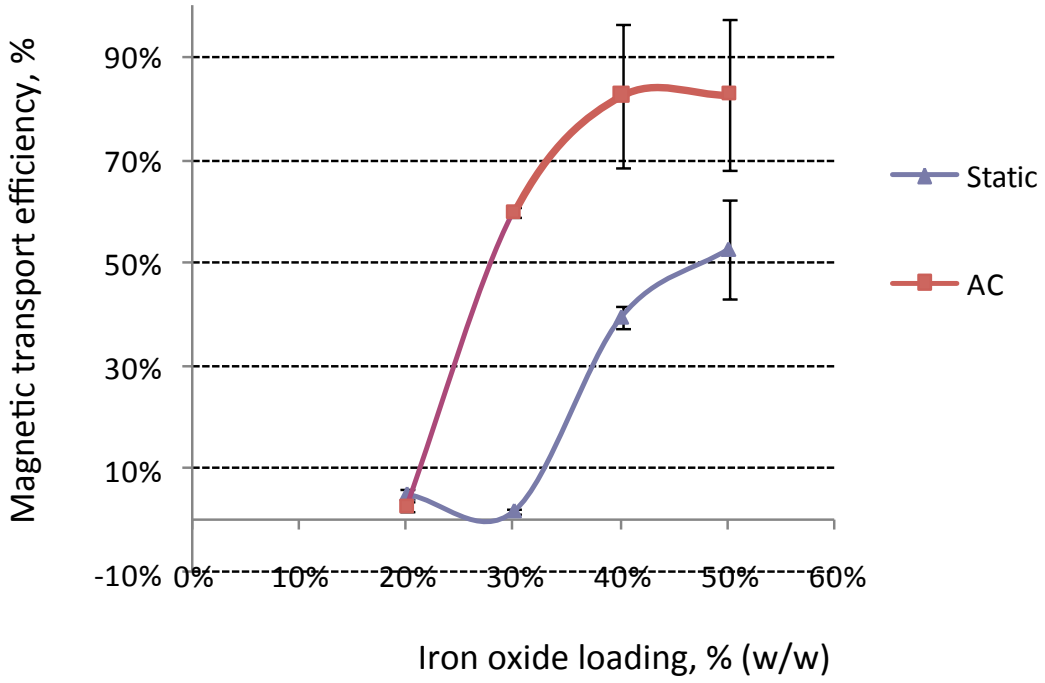

Figure 2.5. MNP transport efficiency as function of different magnetic field settings (static vs. AC) and iron oxide loadings, n=3. The AC field points are statistically different than the corresponding static points with $p<0.05$.

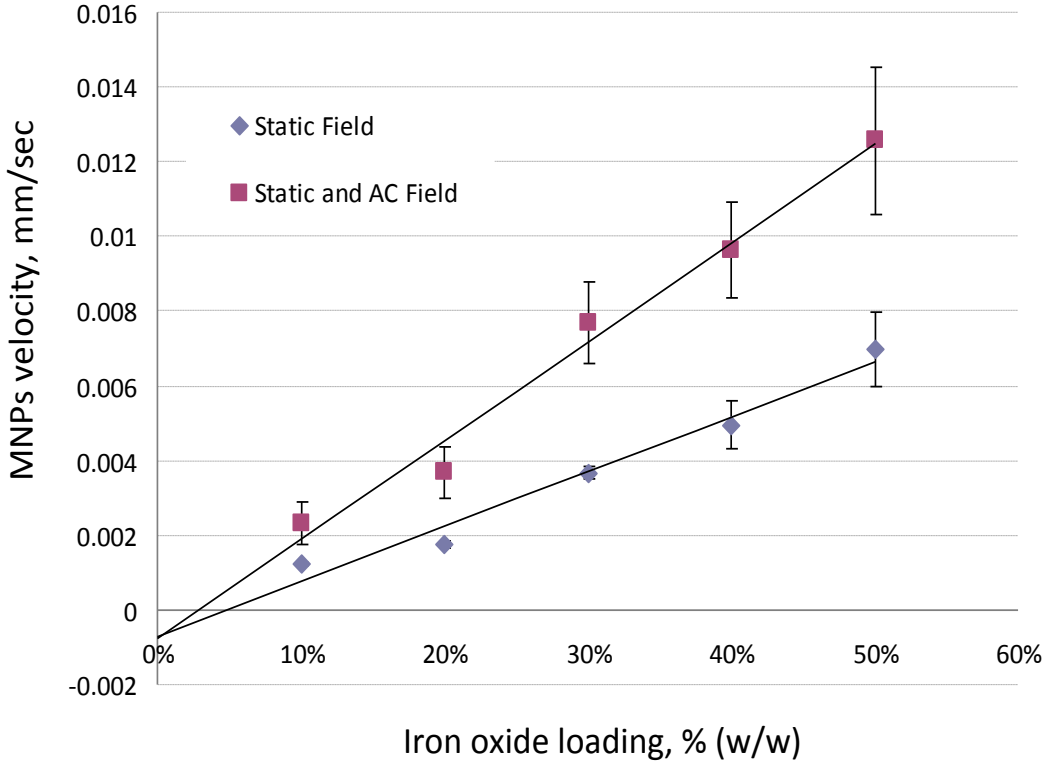

Figure 2.6. MNP velocity as function of iron oxide loading. An AC field was generated at RMS value of 16.4 Oe and frequency of 50 Hz, n=3. The static and AC fields combined yielded MNP velocities that were statistically different from their static field only counterparts ($p<0.05$).

To further examine the motion of particles and demonstrate the effect of the magnetite loading on the MNPs mobility, we measured the velocity of the MNPs loaded with 10-50% (w/w) magnetite at AC and static field conditions. Theoretically, MNPs loading should increase both the static and the AC forces equally. In these experiments an AC field was generated at RMS value of 16.4 Oe and a frequency of 50 Hz. The change in MNP displacement was recorded at 3-minute intervals, and the velocity of the particles was calculated. For all formulations, the velocity with the AC field was greater than with static field alone. A linear increment in the magnetite loading within MNPs resulted in a

linear increase in MNP velocity through the viscous gel as shown in Figure 2.6 for both AC and static fields; however, the slopes of the curves at both field conditions were significantly different (P = 0.03). Both fit lines had a small but nonzero x-intercept, indicating the magnetite content below which no motion would occur.

2.4. Discussion

2.4.1 MNPs formulation and characterizations

The initial aim of this research was to formulate a family of superparamagnetic nanoparticles loaded with various amounts of the iron oxide (magnetite) and evaluate the effects of various magnetite loadings on stability of the oil-in-water emulsions, MNPs size distribution and MNPs surface charge. The magnetite crystals obtained by alkaline precipitation [108, 124, 125] are not uniform and ranges between 5 to 20 nm (Figure 2.2 A). Coating the magnetite crystals with oleic acid provides steric stabilization and allows dispersion of the lipophilic magnetite in non-polar solvents (chloroform in this study). We formulated MNPs using an emulsification solvent evaporation method [11]. In this technique, the organic phase containing the polymer and the lipophilic magnetite (coated with oleic acid) is emulsified with an aqueous phase containing emulsion stabilizer to obtain stable oil-in-water (o/w) emulsion and the polymeric nanoparticles are formed after solvent evaporation [97]. The poly(lactic acid), PLA was chosen as a biodegradable and biocompatible polymer [126-129] to form stable solid-phase magnetic nanoparticles to be used in transport studies. Poly(vinyl alcohol), PVA has been preferentially used as colloidal stabilizer in many studies. PVA has been shown to be an excellent stabilizer to prepare biodegradable non-magnetic and magnetic nanoparticles using a variety of techniques [11, 130]. Furthermore it is one of the few stabilizers that prevents

nanoparticle aggregation during post-preparative steps (e.g., purification and freeze drying), enhancing the yield of dry nanoparticle product without addition of other adjuvants [11]. In our studies, stable oil-in-water emulsions were obtained for all magnetite loadings with 1.0 and 1.5% (w/v) PVA. The concentration of 1.5% (w/v) PVA was chosen to ensure the desired stability of the oil-in-water emulsions and therefore was further used in all final formulations. Due to its amphiphilic nature, PVA distributes only on the surface of PLA-based MNPs. The main organic component around the magnetite is PLA, while the fractions of oleic acid and PVA are minor relatively to the magnetite and PLA. The average size distribution of the PLA-based magnetic nanoparticles varied in 213-275 nm range (by the dynamic light scattering, Table 2.2). This result was in agreement with our TEM observations (MNPs average size 230-300 nm, Figure 2) and correlated well with the literature data reported for the non-magnetic nanoparticles stabilized with 0.5-2% PVA, homogenized by different techniques and obtained within a size range of 180-350 nm [11]. The inclusion of various amounts magnetite within the PLA matrix (up to 50% (w/w)) seemed to have no effect on the MNPs size (Table 2.2). However, MNPs exhibited magnetite dose-dependent superparamagnetic behavior (Figure 2.3). The nearly equivalent MNP size for the all magnetite loadings and increased magnetic responsiveness for particles of higher magnetite loadings suggest that the differences in magnetic responsiveness are due to different magnetite packing within the polymeric core. Indeed, our qualitative TEM data support this conclusion and show a denser packing of the magnetite crystals at 50% (w/w) comparing to 20% (w/w) loading (Figure 2.2 C and B). This observation also remarkably correlates with the experimentally quantified magnetite loadings as shown in the Table 2.2. Zeta potential, a

measure of surface charge, can influence particle stability, cellular uptake, intracellular trafficking as well as transport of MNPs through a complex media such as soft tissue. In some formulations, higher zeta-potential values, either positive or negative, are necessary to ensure colloidal stability and avoid aggregation of nanoparticles. However, the colloidal stability of nanoparticles can also be achieved by the sterric stabilization using non-charged polymers (PVA in this study). Zeta potential of studied formulations was slightly negative (in a range -5.75 to -9.27 mV, Table 2) and did not correlate with the magnetite loadings. Usually PLA has a certain amount of uncapped end carboxyl groups that result in a relatively high (above -30 mV) negative surface charge of the nanoparticles in neutral buffer [131]. However, when PLA nanoparticles are formulated with PVA as an emulsifier, the zeta potential becomes less negative (-6 to -10 mV) [132]. This occurs because PVA molecules are shielding the charged surface groups of PLA. The colloidal stabilization of MNPs in our case was mainly due to steric hindrances between PVA chains on the surface of neighboring MNPs rather than by charge due to low values of zeta potential of our formulations. Thus, MNPs formulated and used in this study can be seen as nearly neutral, colloidally stable particles that do not interact with themselves or with the viscous gel medium due to weak surface charges.

2.4.2 MNP transport studies

To evaluate the effect of an AC field on MNP transport we measured MNP average velocities at different AC and static field conditions. The addition of an AC field component significantly ($P<0.05$) increased velocity of the MNPs in viscous gel (Figure 2.4). The MNP maximum velocity was reached at 50 Hz frequency in an AC field range of 16-22 Oe. We did not observe a clear effect of varying AC frequencies on MNPs

velocity; however, in the field range of 16-22 Oe the 50 Hz frequency demonstrated a quantitatively superior MNPs velocity increase, and therefore the field of 16.4 Oe at 50 Hz was chosen as optimal. As a result all further MNP transport efficiency experiments were completed with the stated power supply settings. It is of note that initial experiments were conducted using frequencies in the range of 5-15 Hz. However, these experiments yielded no statistical differences from static field. Statistically different results from the static field were shown to be present at 50 Hz. Therefore, given this knowledge the power supply used in our setup to produce 50Hz electromagnetic fields had a maximum frequency of 100Hz. In order to keep experiments consistent, they were conducted using the minimum frequency that showed results and the maximum frequency we could produce on our setup. An expansion of these frequencies to a broader range is necessary to better map the effect of AC field frequency with MNP movement.

The transport efficiency experiment tests the ability to move MNPs long distances within a clinically feasible time frame. For the same field strength and gradient, the lower magnetite MNPs move more slowly (Figure 2.6), and this limits the range over which they can be captured by the magnetic field within a reasonable time frame. This is where the enhanced transport produced by the AC magnetic field component perpendicular to the direction of motion is most dramatically illustrated. We have not only increased magnetic particle velocity but we have also increased the fraction of MNPs that travel to the final destination, as shown in the MNPs transport efficiency results (Figure 2.5). The increase in MNPs transport efficiency varies according to the magnetite loading in the particles. MNPs loaded with 20% (w/w) magnetite show no difference in MNPs transport efficiency at both AC and static field conditions (Figure 2.5). MNPs with 30%, 40% and

50% (w/w) magnetite loadings experienced the statistically significant increase in transport efficiency with the addition of AC field component.

In order to determine the mechanism resulted in the improved magnetic transport efficiency, the velocity of the MNPs with respect to magnetite loading was plotted for both static and AC conditions as shown on Figure 2.6. These results show that an increased magnetite loading results in a higher velocity for both static and AC conditions, given the higher magnetic force obtained in the setup. However, we can also note that the slope of the static only condition is lower than that of the AC condition.

Our results imply that the reason that the AC field is having an effect on the velocity of the MNPs is because of a decrease in the effective local viscosity of the viscous fluid around the particles. The y-axis in Figure 2.6 shows the velocity of the particles which is related to the drag force on the MNPs. Since our experiments dealt with small spherical particles moving slowly through a viscous fluid, resulting in a low Reynolds number, the drag force, F_d, for spherical particles moving slowly through a viscous fluid is given by Stokes' Law:

$$F_d = -6\pi\eta r V \tag{4}$$

where, η is the fluid's viscosity and r is the Stokes radius of the particle. According to the equation (1), the magnetic force on the particle is proportional to the particle's magnetic moment and the gradient of the magnetic field applied. The magnetic moment of particles depends linearly on the percent of the magnetite loading (Figure 2.3). Thus, the percentages of the magnetite loadings (presented on the x-axis in Figure 2.6) are proportional to the magnetic forces acting on the particle due to the applied field. At low

Reynolds number, the magnetic force will be balanced by the drag force, so the slope of the lines in Figure 6 can be interpreted as being inversely proportional to the apparent viscosity of the medium (since r is constant). The increase in slope with the addition of the AC field can be explained by the magnetic forces resulting from the combination of static and AC field causing a decrease in localized gel properties immediately surrounding the particles. It is noteworthy to mention that possible AC field coupling to the particles resulting in an elevated temperature (magnetic fluid hyperthermia, MFH), which might enhance the diffusion of particles or lead to a gel's phase transition is highly unlikely due to a completely different operational frequency range applied in MFH (0.1-260 MHz) as compared to frequencies used in this studies [133-136]. While further investigation is needed to fully elucidate the mechanisms underlying the phenomena, it is believed that the oscillating AC magnetic field allows increased efficiency in particle movement because of localized shear thinning.

2.5 Conclusions

Biodegradable MNPs were formulated with variable loading of magnetite in a range of 10-50% (w/w). The inclusion of magnetite up to 50% (w/w) did not affect MNPs size distribution and surface properties. Magnetic susceptibility of the MNPs linearly correlated with the percentage of the magnetite loading. The application of an AC field significantly increased velocity of the MNPs in viscous gel reaching the maximum at a frequency of 50 Hz and AC field of 16-22 Oe as compared to a static field conditions. The results of this study show that the "oscillating" effect of an AC magnetic field greatly improves the ability to transport MNPs within soft media. While more investigation is needed to fully elucidate the mechanisms underlying the phenomena of the enhanced

MNPs transport, it appears that oscillating AC magnetic field reduces the effective viscous drag acting on carriers.

Chapter 3: Force dependent relationship for magnetically loading endothelial cells for targeted delivery

3.1 Background

Many groups have analyzed the endocytotic mechanisms used for nanoparticles to enter cells and MNP entry into cells has long been demonstrated to increase gene transfection in cells. However, MNP enhanced gene transfection papers identify the amount of transfection shown not the number of particles that are loading. The objective of this study is to examine how a static magnetic field influences MNP uptake into endothelial cells and how to quantify the loading of MNPs.

Whether for targeted drug delivery or tissue culture purposes, in order for movement of magnetically loaded cells to be most productive, it is best to load them with maximal amounts of magnetic nanoparticles, thereby increasing the magnetic responsiveness of the cell. However, the high loading of MNPs cannot affect cellular function, if the purpose is to deliver live, functioning cells. In this study we show that we can highly load endothelial cells without significantly impairing their function.

3.2 Materials and Methods

3.2.1 Materials

Poly(D,L-lactide) (average M_w: 75–120 kD), ferric chloride hexahydrate, ferrous chloride tetrahydrate, sodium hydroxide, oleic acid, and polyvinyl alcohol (87-90% hydrolyzed, average M_w: 30-70 kD), N-Hydroxysuccinimide (NHS), N,N'-Diisopropylcarbodiimide (DIC) were obtained from Sigma-Aldrich (St. Louis, MO, USA). Poly(D,L-lactide) 100DL 4A (acid end, M_w: 54 kD, M_n: 34 kD) was obtained from Lakeshore Biomaterials (Birmingham AL, USA). BODYPY®TR (588/617), Live/Dead Viability Cytotoxicity staining kit and Cell-Trace™ Calcein Green were purchased from Invitrogen™ (Carlsbad, CA, USA). All solvents were obtained from

Fisher Scientific (Pittsburgh, PA, USA) and were of HPLC grade. Deionized water used in all experimental procedures was obtained using a Milli-Q water purification system. Glass fiber 1.0 μm and 5.0 μm syringe driven filters were purchased from Millipore (Millipore, Bedford MA, USA). Phosphate buffered solution (PBS) and Dulbecco's modified eagle's medium (DMEM) supplemented with L-Glutamine, 4.5g/L Glucose and Sodium Pyruvate was from MediaTech (Manassas VA, USA), BenchMark^{TM} heat inactivated fetal bovine serum (FBS) was obtained from Gemini Bio-Products (West Sacramento, CA USA), Alamar Blue was purchased from AbD Seroteck (Kidlington, UK). Fluoroblok transwell inserts with 8μm pores were purchased from VWR (Radnor, PA). The LifeSep neodymium magnet fit for cell culture plates was purchased from Dexter Magnetic Technologies (Elk Grove Village, IL, USA). Glass bottom cell culture dishes for confocal imaging were purchased from MatTek Corporation (Ashland, MA, USA). For cholesterol depletion experiments and cytochalasin-D experiments, Methyl-B-cyclodextran was obtained from Sigma-Aldrich (St. Louis, MO, USA) and the Amplex Red Cholesterol Assay kit was obtained from Invitrogen (San Diego, CA, USA).

3.2.2 Magnetic Nanoparticle Synthesis

Magnetite was obtained from ferric and ferrous chloride by alkaline precipitation as previously described [137]. In this study, we examined the effect of various magnetite loadings within (poly)lactic acid (PLA) matrix on cellular uptake of magnetic PLA-based nanoparticles. For this purpose, various amounts of lipophilic magnetite (28, 83 and 195 mg) were dispersed in 6 ml of chloroform, forming stable magnetic fluids further used for magnetic nanoparticle preparation. The above amounts of magnetite are calculated based on the input amount of iron salts to result in 10%, 30% and 70% (w/w) theoretical

magnetite loadings [137]. In our earlier studies we found that the efficiency of encapsulation for 10% and 30% magnetite loading was ~95% [137, 138]and ~90% for 70% loading (in this study). Polylactide (PLA)-based magnetite-loaded nanoparticles (MNPs) were prepared by the emulsification-solvent evaporation method as described elsewhere [137, 138]. Fluorescent PLA-based magnetic particles were formulated by dissolution of 180 mg of non-labeled PLA and 20 mg of fluoresecently labeled (BODYPY®TR (588/617) PLA in 6 ml of magnetic fluid (containing various amounts of magnetite) to form an organic phase. The organic phase was emulsified in 15 ml of pre-chilled 1.5% (w/v) polyvinyl alcohol (PVA) by sonication, and the organic solvents were removed by evaporation under reduced pressure at 30°C. The particles obtained were passed through a 1.0 mm glass fiber and lyophilized with 10% (w/v) trechalose as a cryoprotectant. Lyophilized MNPs were kept at +4°C in 100 μL aliquots and re-suspended in deionized water before use.

Fluorescently labeled magnetic nanoparticles were also synthesized. Carboxyl end groups of PLA were coupled with amine-containing BODIPY® TR (588/617) cadaverine using carbodiimide chemistry in organic medium. The carboxyl group activation step was carried out in methylene chloride using NHS/DIC at a 1:1 molar ratio to obtain succinimidyl ester of PLA (PLA-Su). The ratio of NHS/DIC to PLA was kept around 300-fold of molar excess. The activated PLA-Su was precipitated three times from methylene chloride into cold methanol. In the next step, the PLA-Su was coupled with BODIPY® TR (588/617) cadaverine under argon atmosphere for 24h at basic conditions in methylene chloride supplemented with triethylamine. The excess of base

was neutralized with acetic anhydride and the fluorescently labeled PLA was precipitated three times from methylene chloride into cold methanol.

3.2.3 Magnetic Nanoparticle Uptake

Bovine Aortic Endothelial cells (BAEC) were seeded on clear-bottom 96-well plates at a density of 2.0×10^4cells per well by using DMEM supplemented with 10% FBS and grown until confluence. Dry aliquots of 10%, 30% and 70% (w/w) iron oxide-loaded PLA-based MNPs were re-suspended in 100 μL of deionized water and 20 μL of the nanoparticle suspension was diluted into 10 mL of 10% FBS supplemented DMEM. This MNP suspension was filtered through a Millipore syringe driven filter with 5.0 μm pores in order to separate any large non-reconstituted aggregates of MNPs. To synchronize cell cultures with respect to MNP uptake, the cells were incubated at 4°C for 30 min. Then MNPs were added to cells at different doses, and cell cultures were incubated at 37^{o}C on a magnetic separator (LifeSep 96F, Dexter Magnetic Technologies, IL, USA). The control (non-magnetic condition) cells were incubated off the magnet. Further, at predetermined time points of 2, 4, 6, 8, 10 and 24 hrs, cells were washed with PBS, and the amount of internalized MNPs was measured fluorimetrically (l_{em}/l_{ex} = 588/618 nm) using a Synergy™ 4 monochromator-based hybrid microplate reader (BioTek, VT, USA). The total dose of MNPs initially given to cells was measured at each time point before the washing step. Cell viability was determined after 12 hours of MNP uptake by using Calcein Green staining and the Alamar blue assay as described by the manufacturer.

3.2.4 Cholesterol and Cytochalasin-D Treated Magnetic Nanoparticle Uptake

BAEC cells were seeded in confluency in 96-well sterile cell culture treated plates. Cell culture media was aspirated and replaced with PBS containing 0 mM, 5 mM, 10 mM, 25mM or 50mM methyl-B-cyclodextran solution and incubated for 15 minutes in 37°C. Upon completion of the incubation, each well was rinsed three times with PBS. MNP uptake experiments were then performed as previously described with cells that were either not cholesterol depleted, or cholesterol depleted with 5 mM or 10 mM methyl-B-cyclodextran solutions. Cholesterol depletion was confirmed by utilizing the Invitrogen Amplex Red cholesterol assay to determine the amount of cholesterol present within the cell membrane. Treated and untreated cells were lysed using the included reaction buffer for 30 minutes after incubation with the respective amount of methyl-B-cylcodextran. The solution of lysed cells in buffer was then used in accordance with the directions included in the kit. Fluorescence of cholesterol remaining in each well was measured at 540 nm (excitation) and 590 nm (emission). For cytochalasin—D uptake experiments, cells were treated with 200 nM cytochalasin-D for fifteen minutes prior to uptake procedure.

3.2.5 Cell Viability

BAECs were grown to confluence in a 24-well plate. Cells were loaded for twelve hours with 10%, 30% and 70% MNPs in the influence of a magnetic field. Calcein green stock solution (4 mM) was added to 10 mL of PBS to get a final concentration of 2μM calcein-AM solution. 200 μL of this solution was added to each well and imaged with a fluorescent microscope.

To confirm the visual results and examine cell metabolism, Alamar Blue was utilized. BAECs were grown to confluence in a 96-well plate and loaded for twelve hours with 10%, 30% and 70% MNPs diluted to 100%, 75%, 50% and 25% of the initial 20 µl MNP per 10 ml of cell culture media. Cells were rinsed three times with PBS and cell culture media was replaced with 100 µl of a 10% solution of Alamar Blue In cell culture media. Fluorescence was read at an excitation and emission wavelengths of 560 nm and 590 nm respectively.

Lastly, in order to determine whether or not loaded cells were healthy enough to be trypsinized, spun down and re-seeded, 70% MNPs were loaded into cells for 24 hours. After loading, the cells were spun down and re-suspended and seeded 1:4 in a 24-well plate. Cells were then imaged.

3.2.6 MNP Quantification

In order to correlate the percent uptake of particles to the number of particles internalized per cell, magnetic nanoparticle cell suspensions were given to a confluent culture of bovine aortic endothelial cells, which were further exposed to a magnetic field for 12 hours. Then, the cells were rinsed three times with PBS, trypsinized and collected in Eppendorfs. Control cells (not loaded with magnetic particles) were counted in each well by using a hemocytometer and confirmed with Coulter counter to estimate the total cell density per well. Eppendorfs containing magnetically laden cells were then centrifuged and the remaining pellet was digested with RIPA_cell lysis buffer (Pierce Biotechnology, USA). After centrifugation step, the iron content was determined spectrophotometrically (using Synergy^{TM} 4 multimode plate reader, Biotek, USA and UV compatible 96- well plates, BD Bioscienses, USA) in 1N hydrochloric acid (l= 335 nm)

against a standard curve after MNP degradation with 1N aqueous sodium hydroxide (90°C, 30 min) and dissolution of the iron containing precipitate in the acid solution[12, 137, 138]. The iron content was correlated to the theoretical iron content in each particle in order to determine the approximate number of particles internalized per single cell.

3.2.7 Statistical Analysis

Experimental data presented in figures demonstrated the mean ± standard deviation. One-tailed, unequal variance *t*-tests were used to analyze the significance of MNP uptake of various MNP loaded and unloaded cells. The differences were termed significant at $p<0.05$. All statistics were performed via Graph Pad Prism software (Graph Pad Software Inc., USA).

3.3 Results

3.3.1 Magnetic Nanoparticle Synthesis

Magnetic nanoparticles were synthesized with magnetite concentrations of 10%, 30% and 70%. The MNPs hydrodynamic diameters ranged between 213 to 275 nm for different magnetite loadings averaging at 239±23 nm (by the dynamic light scattering). Size distribution was unaffected by varying magnetite entrapment. Zeta potentials indicating the MNPs surface charge were slightly negative and varied between -5.75 and -9.27 mV. The resulting PVA-stabilized PLA-based magnetic nanoparticles of various magnetite loadings (10-70% (w/w)) exhibited superparamagnetic behavior with no significant hysteresis, as previously described in Chapter 2.

3.3.2 Magnetic Nanoparticle Uptake

The uptake of PLA-based magnetic nanoparticles loaded with 10%, 30% and 70% (w/w) iron oxide (magnetite) was quantitatively determined by measuring fluorescence of internalized MNP fraction to conclude whether variation in magnetite contents within particles would affect MNPs uptake into cells when the MNPs and cells were exposed to a static magnetic field. For simplicity reasons we will call MNP formulations of different magnetite loads as 10, 30 and 70% loaded magnetic nanoparticles. It is noteworthy to mention that higher loads of iron oxide resulted in fluorescence quenching of the labeled PLA. However, since the fluorescence of taken up fraction of MNPs at each time point was normalized to the total fluorescence of each MNP type, the quenching did not affect the calculation of the MNP internalization extent. Figure 1A shows that the uptake of 70% loaded MNP into cells occurred with a quite fast initial rate of ~20%$_{uptake}$/hour for the first four hours almost reaching a saturation (~0.6%$_{uptake}$/hour) after four hours resulting in a ~80% of uptake of the given MNP dose. The initial uptake rates for 30% and 10% loaded particles were found to be comparable at about 10.5%$_{uptake}$/hour and 8.7%$_{uptake}$/hour respectively (based on the first eight hours) and were significantly (statistics) slower relatively to 70% loaded MNPs. At ten hours, 30% loaded MNPs reached similar uptake percentage to that of 70% loaded MNPs. experience similar uptake percentages and continue at the same rate for the rest of the observation period, reaching a maximum uptake of 91% and 87% respectively after 24hours, while uptake of 10% loaded MNPs remains well below 30% and 70% loaded MNPs from 6 hours on (statistics), reaching a maximum uptake of ~60% after the 24 hour observation period (Figure 3.1).

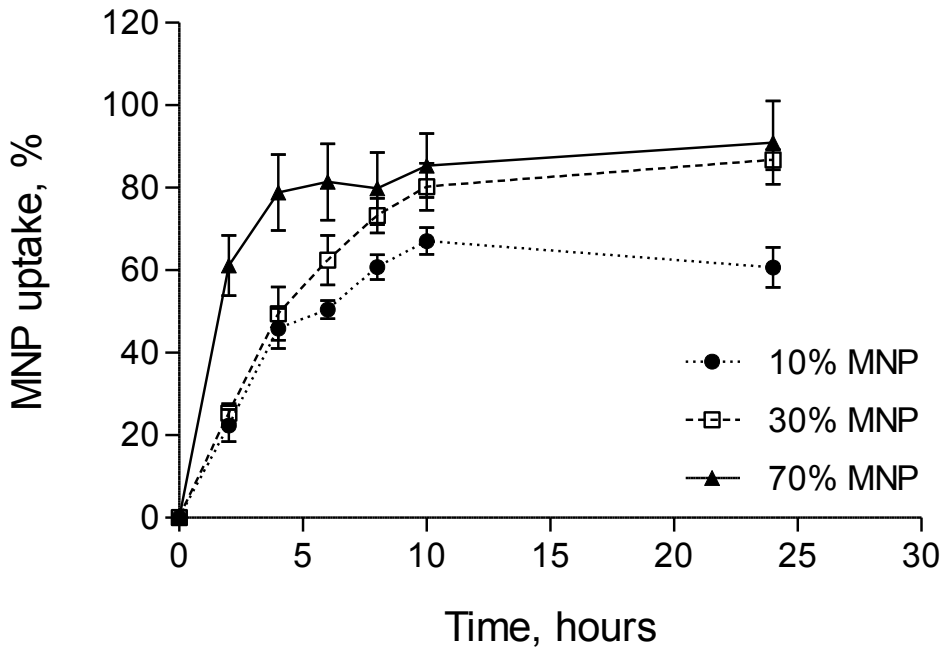

Figure 3.1: The kinetics of 10%, 30% and 70% (w/w) MNP uptake by Bovine Aortic Endothelial Cells (BAEC) in culture as a function of incubation time and a magnetic field of 500 G "On" by using a fixed magnet applied directly to the underside of the cell culture plates.

3.3.2.A MNP Uptake on and off magnet

To determine if this uptake is force dependent, magnetic nanoparticle uptake with the influence of the magnet was compared to uptake of particles without a magnetic field present over the initial 24 hour timeperiod, since they show the greatest differences in trend. The magnetic force can either drive the MNPs into the cell, affect initial interctions between the cell membrane and the MNP or facilitate some receptor binding events. When magnetic nanoparticles are taken into the cell without the aid of an external field, magnetic nanoparticle uptake significantly decreases for all magnetite loadings, Figure 3.2. The control MNP uptake experiment without exposure to a magnetic field resulted in a significantly (statistics) smaller internalization of MNPs

within cells for particles of all iron oxide loadings (Figure 3.2). We observed a direct correlation between the initial uptake rates and magnetite loadings resulting in maximal internalization of MNPs at about 31%, 25% and 11% for the 70%, 30% and 10% loaded MNPs respectively.

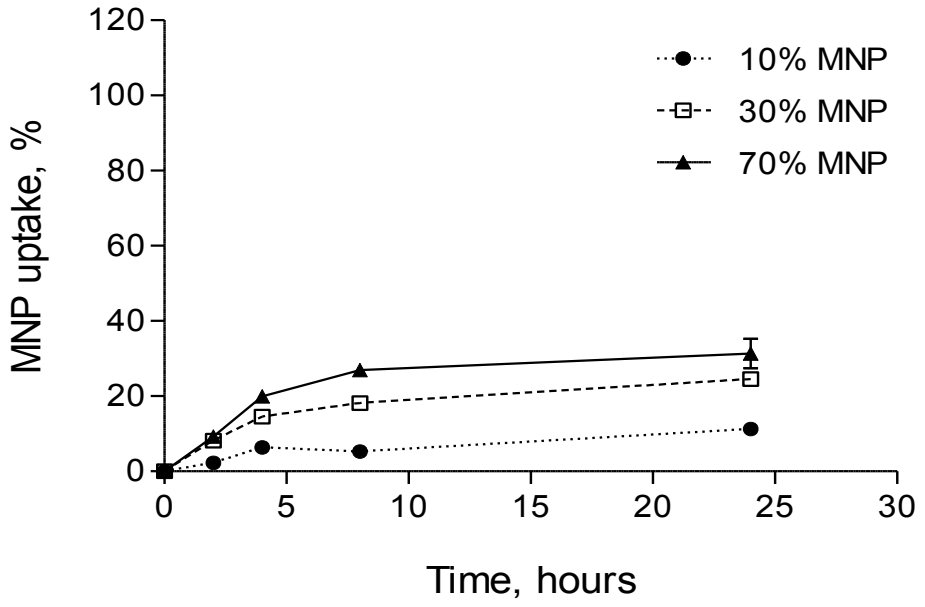

Figure 3.2: The kinetics of 10%, 30% and 70% (w/w) MNP uptake by Bovine Aortic Endothelial Cells (BAEC) in culture as a function of incubation time and magnetic field off.

3.3.2.B MNP Uptake with initial magnetic field exposure

To address the question of whether or not the increase in magnetic nanoparticle uptake is only force dependent process, but is also influenced by the availability of MNPs on the cellular surface, we performed uptake experiments with exposure of cells and particles to the magnet for only the first hour, while the rest of the experimental period was carried out "off" the magnetic field. The results of this experiment show that after the cells are removed from a magnet, MNP uptake

plateaus, indicating an exclusively force dependent mechanism in particle internalization, Figure 3.3.

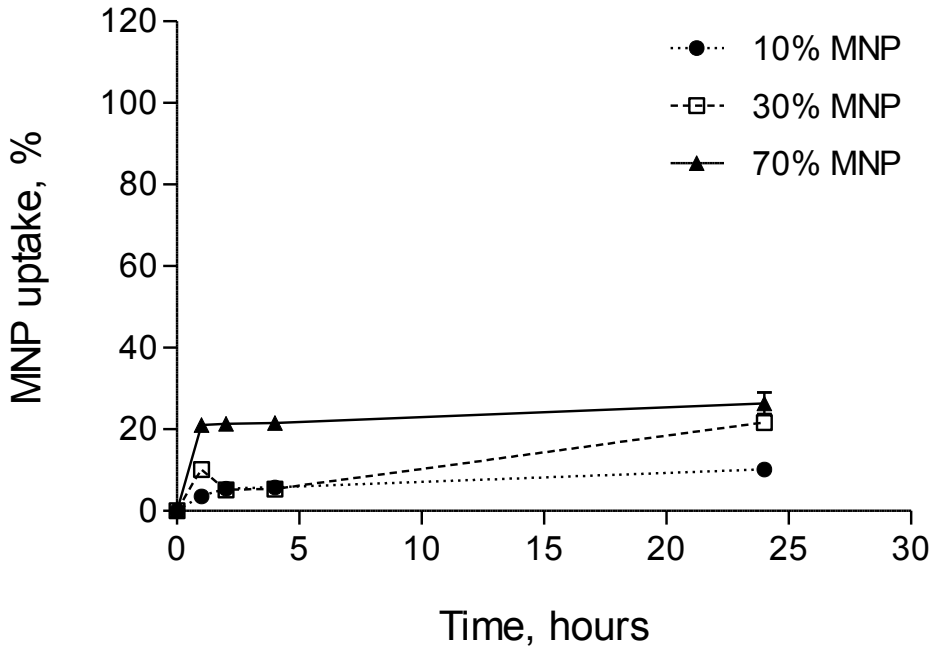

Figure 3.3: The kinetics of 10%, 30% and 70% (w/w) MNP uptake by Bovine Aortic Endothelial Cells (BAEC) in culture as a function of incubation time and magnetic field on for 1 hour then "off".

3.3.3 Cholesterol Depleted Magnetic Nanoparticle Uptake

Cholesterol depletion of BAECs was performed to confirm that MNP uptake was not via a caveolae-mediated endocytotic mechanism. In order to deplete the cholesterol in the membrane associated with forming caveolae, methyl-B-cyclodextran in three different concentrations was used to maximize cholesterol depletion in the membrane while causing minimal cell damage. Invitrogen's amplex red cholesterol depletion assay was used to determine the amount of cholesterol. After treating cells with 5mM, 10 mM

and 25 mM and 50 mM of methyl-b-cyclodextran for 15 minutes we were able to deplete the cholesterol within the cells by up to 97%, Figure 3.4.

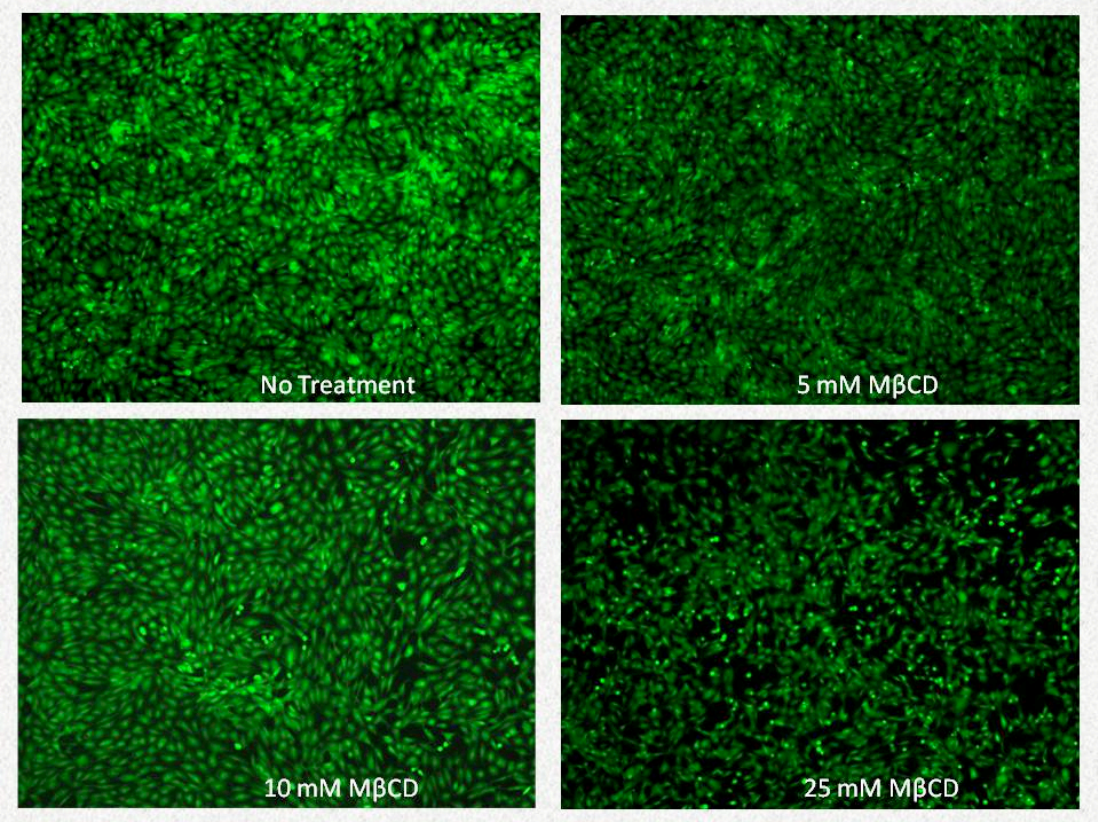

MβCD Dose	% Cholesterol Depletion
5 mM	17%
10 mM	21%
25 mM	42%
50 mM	97%

Figure 3.4. top) Calcein Green staining of no treatment, 5mM, 10mM 25mM methyl-B-cyclodextran treated cells bottom) Methyl-B-Cyclodextran was used to deplete cholesterol in cellular membrane of BAEC cells. Cholesterol depletion was able to remove up to 97% of the cholesterol. However, that amount of cholesterol killed all cells. 5 mM to 25 mM were healthier doses to the cell

Live-dead staining of cells was performed by using calcein green and imaging the cells under a fluorescent microscope. Calcein green imaging, Figure 2.4, shows that 50

mM completely kills all cells exposed to the incubation and 25 mM are significantly less viable, therefore, there were eliminated subsequent experiments.. Magnetic nanoparticle uptake with 70% MNPs was then completed utilizing the remaining methyl-b-cyclodextran dosages. Uptake experiments showed no correlation between cholesterol depletion and magnetic nanoparticle uptake Figure 2.5.

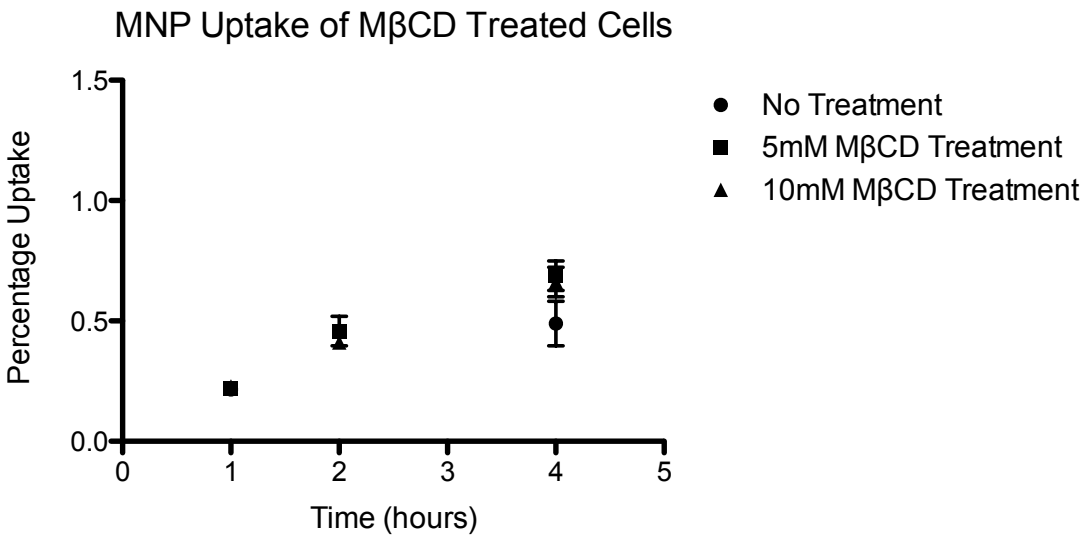

Figure 3.5: Magnetic nanoparticle cellular uptake increased with cellular membrane cholesterol depletion after 4 hours.

3.3.4 Cytochalasin-D Effects on MNP Uptake

Cytochalasin- D was used to inhibit actin polymerization in endothelial cells. By inhibiting actin polymerization, the cells can no longer actively uptake MNPs due to the importance of the cells cytoskeleton in the process. When treating BAECs, caution was used to not over treat BAEC cells with cytochalasin D. Cells were treated with 200nM of cytochalasin-D. This dose was enough to see slight deformation of cells, but not so much

to initiate cell detachment or death. Cytochalasin-D treatment significantly impaired the ability for BAECs to uptake MNPs both with and without a magnetic influence, Figure 2.6. BAECs treated with cytochalasin-D with no magnetic field experienced the no change, three times less uptake and two and a half times less uptake respectively for 10%, 30% and 70% MNPs compared to their non-treated counterparts. Cells treated with cytochalasin-D and exposure to a magnetic field experienced fifteen, four and three and a half times less for 10%, 30% and 70% MNPs in comparison to their non-treated counterparts.

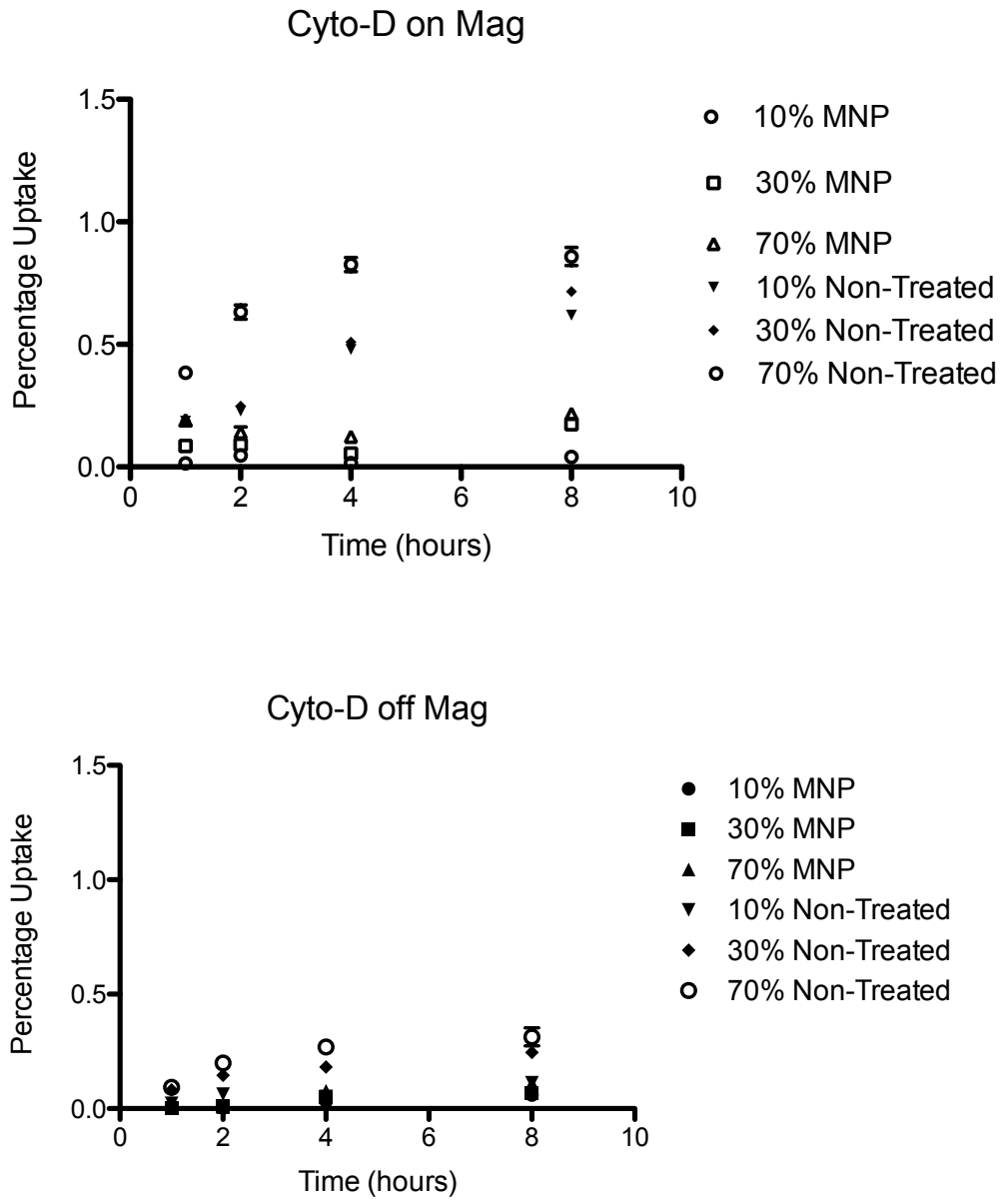

Figure 3.6: top) 10%, 30% and 70% MNP uptake of cells treated with 200nM of cytochalasin-D under the influence of a magnetic field. Bottom) 10%, 30% and 70% MNP uptake of cells treated with 200nM of cytochalasin-D without the influence of a magnetic field. There is a clear significant difference ($p<0.001$) between non-treated cells and cytochalasin-D treated cells both on and off the magnet.

3.3.5 Calcein Green Staining After Loading

Live cell staining was performed using CellTrace™ calcein green AM reagent. In live cells the nonfluorescent CellTrace calcein green AM is converted to a green-fluorescent calcein after intracellular esterases remove the acetoxymethyl (AM) esters. The magnetic nanoparticles were internalized within the cells on a magnet for twelve hours. Live cells were stained green (488/530 nm), while magnetic nanoparticles exhibited red fluorescence (588/617 nm). Figure 2.7 shows no significant differences in cell viability for all magnetite loadings comparing to the control cells not treated with MNPs.

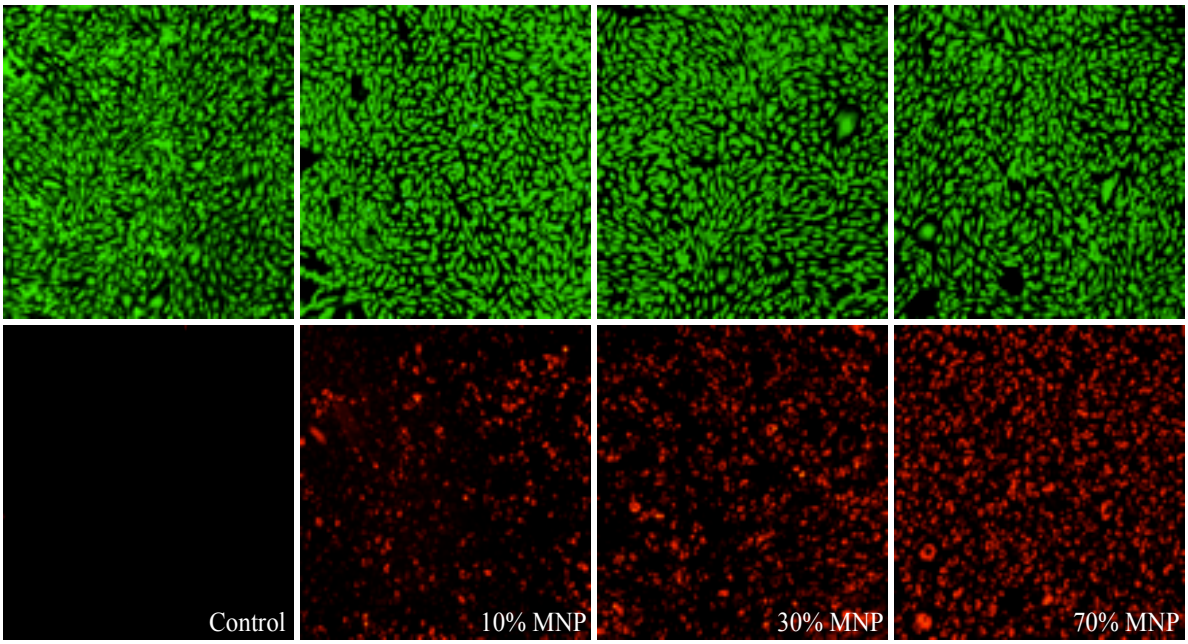

Figure 3.7: Micrographs of Bovine Aortic Endothelial Cells (BAECs) in green and red fluorescent channels qualitatively showing the relative amount of 10%, 30% and 70% magnetite loaded MNPs internalized within cells at 12 hour time point. Control cells were not treated with MNPs. Green fluorescent micrographs show healthy cells as assessed by calcein green staining. (Magnification:x100.)

3.3.6 Alamar Blue of Cells after Loading

To further examine MNP compatibility within cells, we utilized the Alamar Blue assay 48 hours after the conclusion of magnetic nanoparticle incubation. The MNP uptake was conducted for 12 hours using various dilutions of MNPs. Figure 2.8 shows that a maximum of 15% in fluorescence variation relatively to control cells was measured for particles of all loadings at different dilutions. The maximal dose used in these experiments showed 89±7% survival for 10% loaded MNPs, 86±1% survival for 30% loaded MNP and 85±10% for 70% loaded MNP.

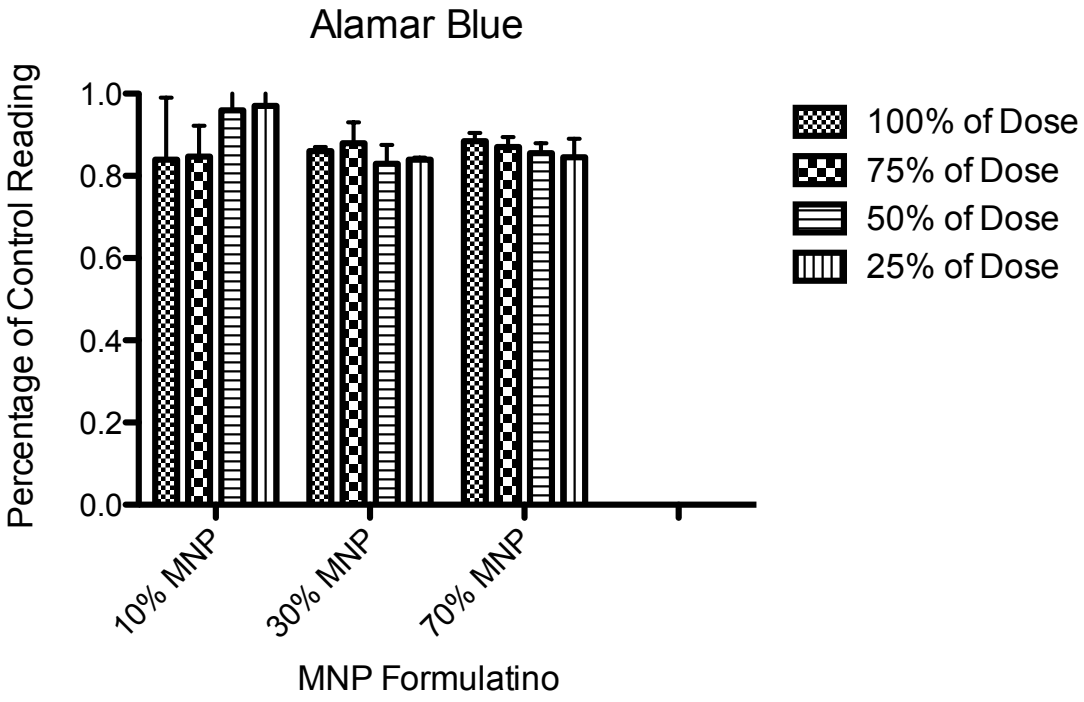

Figure 3.8: Alamar Blue assay for Bovine Aortic Endothelial cells (BAEC) loaded for 12 hours with 10%, 30% and 70% MNPs and various dilutions. The Alamar Blue assay was performed 48 hours post loading with MNPs. Cell survival is presented as a fraction relatively to control, unloaded cells.

3.3.7 Ability to Re-plate cells after loading

After 12 hours, the cells were imaged with a light-microscope. Figure 2.9, shows that MNP loaded cells could be re-seeded and attach as healthy cells would.

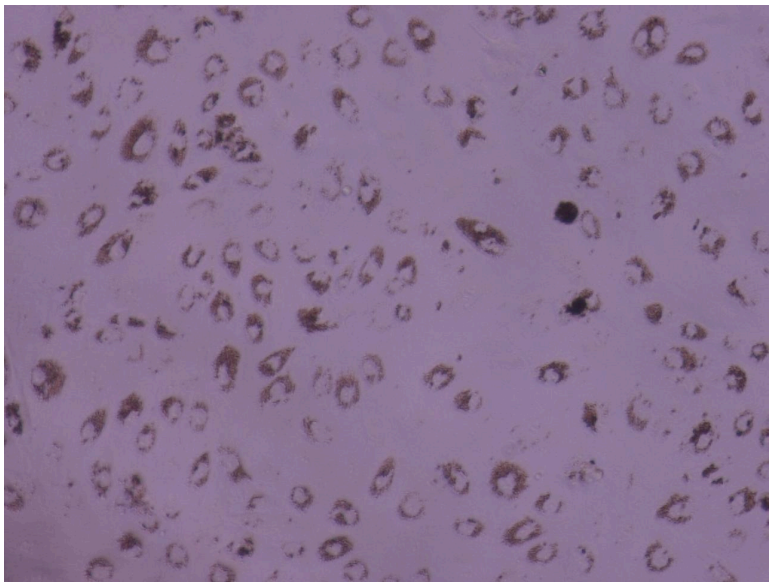

Figure 3.9: 70% MNP loaded for 12 hours into bovine aortic endothelial cells after trypsinization and re-seeding

3.3.8 Magnetic Particle Quantification

The amount of magnetite uptake into cells was found by spectrophotometry measuring specific absorption of iron at 335 nm as previously described in the literature [137]. The amount of magnetite internalized within the cells that were loaded with 10%, 30% and 70% MNPs was found to be 10.0±5.0 ng/cell, 19.0±6.0 ng/cell and 50.0±10.0 ng/cell respectively. These numbers were used along with theoretical calculations based on MNP geometry (assuming an average MNP diameter of 300 nm,[137, 138]) to determine the number of magnetic nanoparticles incorporated into a single cell. Cells loaded with 10%, 30% and 70% MNPs for 12 hours were found to have accumulated approximately 10,000 MNPs/cell, 16,000 MNPs/cell and 35,000 MNPs/cell respectively.

Therefore, MNPs incorporation into a single cell took up approximately 3%, 5% and 12% of the cell's total volume respectively.

3.4 Discussion

The aim of this study was to evaluate the effects of magnetic forces acting on cells with respect to the MNP internalization kinetics and mechanism. To understand whether the MNP uptake into cells is a force dependent process. Additional questions of interest here are how cells tolerate high doses of MNPs and whether the high MNP loads would affect BAECs. This information is of high relevance for magnetically-mediated cell targeting applications where the responsiveness of MNPs is an important parameter to allow efficient targeting. On the other hand the cytocompatibility of MNPs with cells is also a very important prerequisite in magnetic cell targeting applications because targeted cells are expected to provide a therapeutic effect at the target site, either by restoration of a physiologically normal cellular layer (stent applications or cardiac tissue applications), secreting regulatory factors or "drugs" utilizing cellular machinery mechanisms.

3.4.1 Magnetic Nanoparticle Synthesis

To understand how magnetic forces affect MNP uptake kinetics and internalization mechanism, we formulated magnetic nanoparticles of distinctive theoretical magnetite loads of 10%, 30% and 70% (w/w). In our earlier studies we found that for 10% and 30% magnetite loaded particles the efficiency of incorporation was about 95% (MacDonald, Johnson). In this study, we found that for 70% magnetite loaded particles the efficiency of incorporation was about 90%. These high magnetite incorporation efficiencies indicate on an adequate level of magnetic material loading

matching well the expected theoretical vales. Particles of all loads exhibited a mean hydrodynamic diameter in a range 250-310 nm, which indicates that magnetite loadings did not affect particle size.

With regards to zeta potential, each of these magnetite loadings had a negative zeta potential of -6.8 mV, -6.95 mV and -9.27 mV for 10%, 30% and 70% loadings. Highly negatively charged MNPs would typically not be well incorporated into cells due to the negatively charged endothelial cell membrane, however, our MNPs exhibit low negative zeta potentials. Our MNPs exhibit standard superparamagnetic properties, as shown in chapter two.

3.4.2 Magnetic Nanoparticle Uptake

We expect that the force exerted on an endothelial cell by a MNP exposed to a magnetic field will increase as iron oxide concentration within the particle increase. Our results show that 250-310 nm MNPs internalize within endothelial cells at different rates, depending on the magnetite incorporation per particle (Figure 3.1). This indicates that the uptake mechanism used by the cell is force dependent. Our results also indicate that MNPs are also taken into the cell without the influence of a magnetic field, therefore, it was important to examine if the magnetic field actually stimulates uptake because of the force it is applying on a cell, or whether it just allows the MNPs to reach a surface of the cell at a faster rate. To examine this phenomenon, we conducted an experiment where MNPs given to cells were exposed to a magnet for only one hour (a sufficient time to sediment >90% of MNPs). We found that before removal of the magnet (1 hour time point), the MNP uptake rates were similar to those seen in previous experiments,

however, after the removal of the magnet, MNP uptake was stalled and the uptake rate plateaued for the remainder of the observation period. This result also supports that MNP uptake is force dependent process and not an effect of the magnetic field allowing MNPs quicker access to the cell-surface. No further increase in MNP uptake after removal of the magnet at a 1 hour time point shows that internalization of a fraction of MNPs (21%, 10% and 4% uptake for 70%, 30% and 10% loaded particles respectively, Figure 3.3) cause cells to reach saturation with no further ability to internalize more particles. These levels of uptake correlate well with the final uptake extents in the non-magnetic uptake experiment (Figure 3.2). This result show that without the magnetic field cellular ability to internalize particles is limited, however when magnetic field is applied, the magnetic forces will cause MNPs penetrate the cell allowing almost full MNP dose internalization.

3.4.3 Treated Cells Magnetic Nanoparticle Uptake

We expect that the force exerted on an endothelial cell by a MNP exposed to a magnetic field will increase as iron oxide concentration within the particle increase. Our results show that 250-310 nm MNPs internalize within endothelial cells at different rates, depending on the magnetite incorporation per particle (Figure 3.1). This indicates that the uptake mechanism used by the cell is force dependent. Our results also indicate that MNPs are also taken into the cell without the influence of a magnetic field, therefore, it was important to examine if the magnetic field actually stimulates uptake because of the force it is applying on a cell, or whether it just allows the MNPs to reach a surface of the cell at a faster rate. To examine this phenomenon, we conducted an experiment where MNPs given to cells were exposed to a magnet for only one hour (a sufficient time to sediment >90% of MNPs). We found that before removal of the magnet (1 hour time

point), the MNP uptake rates were similar to those seen in previous experiments, however, after the removal of the magnet, MNP uptake was stalled and the uptake rate

Previous research examining endocytosis of nanoparticles, magnetic or otherwise, points to clathrin-mediated endocytosis for particles less than 200 nm in diameter and caveolae-mediated endocytosis as the most probable candidate for endocytosis of particles greater than 200 nm in diameter. Our particles are larger than those that we would expect to see internalized via clathrin-mediated pathways, therefore, methyl-β-cyclodextran, a common caveolae-mediated endocytosis inhibitor was used during MNP uptake to deplete the BAEC cell membrane of cholesterol. Since caveolae are enriched with cholesterol, theoretically, depleting the membrane of cholesterol would in turn minimize the number of caveolae present in the membrane; therefore, reducing the number of MNPs a cell is able to take in. Our results however, show that cholesterol depletion of the cells does not affect MNP uptake into cells, suggesting that MNP uptake into endothelial cells is not a caveolae-mediated process.

Cytochalasin-D affects the actin polymerization in the cytoskeleton of endothelial cells by binding to the ends of microfilaments, which in turn prevents assembly and disassembly of actin monomers. As a result, it inhibits the binding phase in phagocytosis. When our cells were treated with Cytochalasin-D MNP uptake was severely inhibited with and without the influence of a magnetic field. This suggests that MNP uptake is in fact a force-mediated active process. We would suspect that the cytochalasin-D would cause a weakening in the stiffness of the cellular membrane, therefore, allowing MNPS to penetrate much easier. However, we find that cytochalasin-D actually inhibits MNP

uptake, indicating that the uptake process is not only an active process but also dependent upon the force the MNP induces on the membrane.

It is important to note that altering either cholesterol or actin filaments in an endothelial cell can seriously alter the standard endocytotic mechanisms of a cell. Therefore, the suggestions made in regards to the mechanism of uptake of these particles must be further examined. At this point in time, there are no clear methods to block the endocytotic pathways that we are examining for particle uptake of our size that do not alter standard cell function.

3.4.4 Calcein Green Imaging of Loaded Cells

To determine the health status of MNP-loaded cells, images of BAEC fully-loaded with MNPs exhibit the same cell density and morphology as control cells not loaded with particles. Fluorescent images of the MNPs internalized within cells after 12 hours correspond well with the fluorescent uptake data found in the uptake experiments and calcein green staining shows no detrimental effects to the cell.

3.4.5 Alamar Blue Fluorescence of Loaded Cells

Alamar Blue fluorescence of loaded cells with varying dilutions of the standard 20 μl MNP per 10 ml of cell culture media was examined in comparison to control cells. Cells loaded with 10% MNPs diluted to 25% and 50% showed viability above 90% in comparison to control. All other MNP loadings and dilutions showed viability 85% in comparison to control. Overall, Alamar Blue results were in agreement with Calcein Green images of the cells. This indicates that 48 hours post uptake process cells preserve their healthy state showing a very marginal decrease in number of viable cells.

3.4.6 Ability to Reseed after Loading

While preliminary viability tests indicate relatively healthy cells, an important characteristic of magnetically loaded endothelial cells for drug delivery or targeting would be the ability to load them and utilize them as one would standard cells. That means that the ability to trypsinize and reseed or release into the body is necessary. To be certain that we can treat MNP loaded cells as we would non-loaded cells, we trypsinized, spun down re-suspended and reseeded MNP loaded endothelial cells to be certain that the high MNP loading of 70% MNPs after 12 hours did not affect their ability to survive the vigorous process. Our results show that these MNPs successfully survive the standard re-suspension and re-seeding process.

3.4.7 Magnetic Nanoparticle Quantification

To find the approximate number of magnetic nanoparticles present in a single cell, we utilized the known mean diameter of MNPs as well as iron content information obtained after loading in conjunction with the theoretical values we would obtain from the chemical equations and protocol of MNP formulation. We found that after 12 hours of loading, MNPs comprised approximately 3%, 5% and 12% of the entire endothelial cells volume. This value can be considered a lower level limit given a few assumptions made throughout the quantification process. MNPs were loaded in 96-well plates, however, given the nature of the LifeSep magnetic plate, particles were loaded mainly through the centerline of the well. Therefore, the cells on the outside edges were not loaded nearly as highly as those in the center. The iron content found in those center cells was spread out amongst all of the cells in the well, therefore, giving us a slightly lower value than what might be expected.

3.5 Conclusion

The aim of this study was to evaluate the effects of magnetic forces acting on cells with respect to the MNP internalization kinetics and mechanism. To understand whether the MNP uptake into cells is a force dependent process? Additional questions of interest here are how cells tolerate high doses of MNPs and whether the high MNP loads would interfere with cellular functions? This information is of high relevance for magnetically-mediated cell targeting applications where the responsiveness of MNPs is an important parameter to allow efficient targeting. On the other hand the cytocompatibility of MNPs with cells is also a very important prerequisite in magnetic cell targeting applications because targeted cells are expected to provide a therapeutic effect at the target site, either by restoration of a physiologically normal cellular layer (stent applications) or tissue (cardiac tissue applications? other ideas), secreting regulatory factors or "drugs" utilizing cellular machinery mechanisms (ref for gene therapy). To understand how magnetic forces affect MNP uptake kinetics and internalization mechanism, we formulated magnetic nanoparticles of distinctive theoretical magnetite loads of 10%, 30% and 70% (w/w). In our earlier studies we found that for 10% and 30% magnetite loaded particles the efficiency of incorporation was about 95% (MacDonald, Johnson). In this study, we found that for 70% magnetite loaded particles the efficiency of incorporation was about 90%. These high magnetite incorporation efficiencies indicate on an adequate level of magnetic material loading matching well the expected theoretical vales. Particles of all loads exhibited a mean hydrodynamic diameter in a range 250-310 nm, which indicates that magnetite loadings did not affect particle size.

We expect that the force exerted on an endothelial cell by a MNP exposed to a magnetic field will increase as iron oxide concentration within the particle increase. Our results show that 250-310 nm MNPs internalize within endothelial cells at different rates, depending on the magnetite incorporation per particle (Figure 1A). This indicates that the uptake mechanism used by the cell is force dependent. Our results also indicate that MNPs are also taken into the cell without the influence of a magnetic field, therefore, it was important to examine if the magnetic field actually stimulates uptake because of the force it is applying on a cell, or whether it just allows the MNPs to reach a surface of the cell at a faster rate. To examine this phenomenon, we conducted an experiment where MNPs given to cells were exposed to a magnet for only one hour (a sufficient time to sediment >90% of MNPs). We found that before removal of the magnet (1 hour time point), the MNP uptake rates were similar to those seen in previous experiments, however, after the removal of the magnet, MNP uptake was stalled and the uptake rate plateaued for the remainder of the observation period. This result also supports that MNP uptake is force dependent process and not an effect of the magnetic field allowing MNPs quicker access to the cell-surface. No further increase in MNP uptake after removal of the magnet at a 1 hour time point shows that internalization of a fraction of MNPs (21%, 10% and 4% uptake for 70%, 30% and 10% loaded particles respectively, Figure 1C) cause cells to reach saturation with no further ability to internalize more particles. These levels of uptake correlate well with the final uptake extents in the non-magnetic uptake experiment (Figure 1B). This result show that without the magnetic field cellular ability to internalize particles is limited, however when magnetic field is applied, the magnetic

forces will cause MNPs penetrate the cell allowing almost full MNP dose internalization.

To determine the health status of MNP-loaded cells, images of BAEC fully-loaded with MNPs exhibit the same cell density and morphology as control cells not loaded with particles. Fluorescent images of the MNPs internalized within cells after 12 hours correspond well with the fluorescent uptake data found in the uptake experiments and calcein green staining shows no detrimental effects to the cell. Alamar Blue fluorescence of loaded cells with varying dilutions of the standard 20 μl MNP per 10 ml of cell culture media was examined in comparison to control cells. Cells loaded with 10% MNPs diluted to 25% and 50% showed viability above 90% in comparison to control. All other MNP loadings and dilutions showed viability 85% in comparison to control. Overall, Alamar Blue results were in agreement with Calcein Green images of the cells. This indicates that 48 hours post uptake process cells preserve their healthy state showing a very marginal decrease in number of viable cells.

While preliminary viability tests indicate relatively healthy cells, an important characteristic of magnetically loaded endothelial cells for drug delivery or targeting would be the ability to load them and utilize them as one would standard cells. That means that the ability to trypsinize and reseed or release into the body is necessary. To be certain that we can treat MNP loaded cells as we would non-loaded cells, we trypsinized, spun down re-suspended and reseeded MNP loaded endothelial cells to be certain that the high MNP loading of 70% MNPs after 12 hours did not affect their ability

to survive the vigorous process. Our results show that these MNPs successfully survive the standard re-suspension and re-seeding process.

To find the approximate number of magnetic nanoparticles present in a single cell, we utilized the known mean diameter of MNPs as well as iron content information obtained after loading in conjunction with the theoretical values we would obtain from the chemical equations and protocol of MNP formulation. We found that after 12 hours of loading, MNPs comprised approximately 3%, 5% and 12% of the entire endothelial cells volume. This value can be considered a lower level limit given a few assumptions made throughout the quantification process. MNPs were loaded in 96-well plates, however, given the nature of the LifeSep magnetic plate, particles were loaded mainly through the center line of the well. Therefore, the cells on the outside edges were not loaded nearly as highly as those in the center. The iron content found in those center cells was spread out amongst all of the cells in the well, therefore, giving us a slightly lower value than what might be expected.

Chapter 4: Magnetically loaded endothelial cells for targeted drug delivery applications

4.1 Background

Magnetic nanoparticles (MNPs) are continuously examined as part of biotechnologies growing interest in nanotechnology[139, 140]. Currently, MNPs have been shown to be useful in gene delivery, imaging and diagnostics ([12, 140-143]), with the main application being their use as contrast agents in Magnetic Resonance Imaging (MRI)[14]. Aside from these standard purposes, nanoparticles are an attractive option for drug delivery, due to the ease of surface functionalization and biocompatibility [24, 141, 144, 145].

Given the ease at which we can load magnetic nanoparticles, cells loaded with MNPs as vectors for targeted drug delivery can potentially eliminate the difficulties of circumventing the immune system of the human body. Previous work has shown that MNP loaded endothelial cells are promising vectors for targeted delivery to cardiovascular stents[45-50]. In our work we show the feasibility of using these MNP loaded cells to increase transport through non-fluid model systems of the human body, utilizing a 3-D migration system.

Furthermore, our research investigates whether high loading of MNPs alters the function of the endothelial cells. Our studies examine cytoskeletal function upon high loading of these cells. The ability to keep the natural function of the cells intact with high loading allows us to obtain highly magnetic responsive bodies that can be utilized in targeted cell delivery for drug delivery or tissue culture functions.

4.2 Materials and Methods

4.2.1 Confocal Imaging

Bovine aortic endothelial cells were seeded in 35 mm glass bottom dishes (MatTek Corp, Ashland, MA, USA). 10%, 30%, 70% and control solutions were prepared as discussed in chapter two, with 20 μL of the fluorescent MNP suspension in 10 ml of 10% FBS DMEM. Four dishes were used for each magnetite concentration MNP solution. 2 ml of each solution was placed in the glass bottom dish and the dishes were placed on the LifeSep magnet. For each of the control, 10%, 30% and 70%, the dishes were rinsed three times prior to visualization of the uptake using Drexel University's Olympus FluoView FV1000 confocal laser scanning inverted confocal microscope.

4.2.2 Mitochondria Imaging

Mitotracker Green and Mitotracker Orange were obtained from Invitrogen (San Diego, CA, USA). Bovine Aortic Endothelial cells were seeded in 35 mm glass bottom dishes. MNP solutions were added and incubated on a magnet for 12 hours. Mitotracker Green and Mitotracker Orange were dissolved in HEPES buffer with final concentrations of 70 nM and 25 nM respectively. 2 ml of the combined Mitotracker stains were added to each glass bottom dish, covered with foil, and incubated at room temperature for 30 minutes. Confocal images were taken.

Mitochondria titrations were completed utilizing carbonyl cyanide *m*-chlorophenyl hydrazine (CCCP). BAECs loaded with MNPS for 12 hours were then treated with Mitotracker Orange and Mitotracker Green. Confocal images were taken every 2

seconds over a 5 minutes time period. Two separate doses of CCCP were added, the first dose of 0.2 μM at 100 seconds and the second dose of 0.4 μM at 200 seconds. Intensity of Mitochondria Orange was monitored over the 5 minute time period.

4.2.3 Actin Imaging

We utilized a standard transfection protocol using GenDrill (BamaGen Biosciences, Gaithersburg, MD, USA) to image actin filaments in our BAEC cells. BAEC cells were grown to confluence in a 35mm glass bottom dish. MNP solutions of 10%, 30% and 70% MNPs were added and allowed to incubate for 12 hours. To begin the transfection process, we diluted 1 μg of DNA (equivalent to 2.5 μl of β-actin) in 100 μl of serum-free cell culture media. 3μl of GenDrill was diluted into 100 μl of serum free cell culture media. The GenDrill solution added to DNA mixture and vortexed. This solution was incubated at room temperature for 15 minutes. To each plate of control and MNP loaded cells, 500 μl of serum free cell culture media was used and 200 μl of the transfection mixture was added drop wise. The BAEC cells along with transfection mixture and serum-free media were incubated for five hours at 37°C. At the completion of the incubation, 1 ml of cell culture media supplemented with 10% FBS was added to the plates and cells were incubated at 37°C for 24 hours. Cells were then imaged using the confocal microscope.

4.2.4 Cytoskeletal Function – 2-D Migration

Bovine aortic endothelial cells were seeded on gridded cover slips from Electron Microscopy Sciences (Hatfield, PA, USA) with the aid of a cloning ring (VWR, Radnor, PA, USA). The cloning ring was placed in the center of the gridded cover slip and cells were seeded in the interior of the cloning cylinder. Cells were allowed to reach

confluence and then the cell culture media inside the cloning cylinder was replaced with 100 μL of magnetic nanoparticle suspension. A cylindrical neodymium magnet was placed underneath of each well to load magnetic nanoparticles within cells. After 12 hours of cell loading on the magnet, the cloning ring was removed and cells were rinsed three times with PBS before beginning the migration assay. Migration of the cells was measured by using light microscopy with the gridded coverslip to measure the distance cells traveled over a 45 hour time period.

4.2.5 Model Targeting – 3-D Migration

Fluoroblok transwell inserts were coated with 100μg/ml type-I collagen from Sigma-Aldrich (St. Louis, MO, USA) and allowed to set for one hour and then rinsed with PBS. BAEC cells were loaded for 12 hours with 70% (w/w) magnetite containing MNPs. Control (not leaded) cells and magnetically loaded cells were then trypsinized and seeded in 5% FBS supplemented DMEM in the apical chamber of a 24-well Fluoroblok transwell insert at 100,000 cells/well. The basal section of the transwell insert contained either 5% or 10% FBS supplemented DMEM in order to induce cell migration through the collagen coated membrane. Control cells and magnetically loaded cells were then allowed to migrate in each condition and either in a control condition or one with a static magnetic field from a neodymium magnet. After 12 hours of migration, the basal section of the well was aspirated and Calcein Green was applied to stain cells. Fluorescent images were then taken to determine the extent of migration that occurred in each well. Further magnified images were taken at four random locations in order to quantify the number of cells that had migrated through the membrane.

4.2.6 Statistical Analysis

As stated before, experimental data presented in figures demonstrated the mean ± standard deviation. One-tailed, unequal variance *t*-tests were used to analyze the significance of migration distances and quantities of loaded and unloaded cells. A linear regression was used to demonstrate the rate of migration (in 2D experiment) of control and MNP loaded cells and determine whether the rates of uptake were significantly different. In 3D migration experiment two-way ANOVA was run for comparisons of multiple groups. In all tests, the differences were termed significant at $p < 0.05$ and the degree of significance is given in figures when appropriate (*, $p<0.05$; ** $p<0.01$; *** $p<0.001$). A segmented linear regression was used to compare the mitochondrial analysis with CCCP. All statistics were performed via Graph Pad Prism (Graph Pad Software Inc., USA).

4.3 Results

4.3.1 Confocal Imaging

MNP formulations of 10%, 30% and 70% were loaded into cells for 12 hours under the influence of a magnetic field for 1 hour, 4 hours and 10 hours. Magnetic nanoparticle uptake into BAEC cells was confirmed via confocal imaging, Figure 4.1. These images show the density of loading of MNPs. The z-stack of loaded cells shows MNP incorporation within the cell. Earlier time points, after one hour, showed uptake in Chapter 2. To confirm that MNPs were within the cell at these time points and not just associated with the membrane, confocal slices were examined. MNPs were proven to be within the cell for all time points and particle formulations with the exception of 10% after 1 hour, Figure 4.2

.

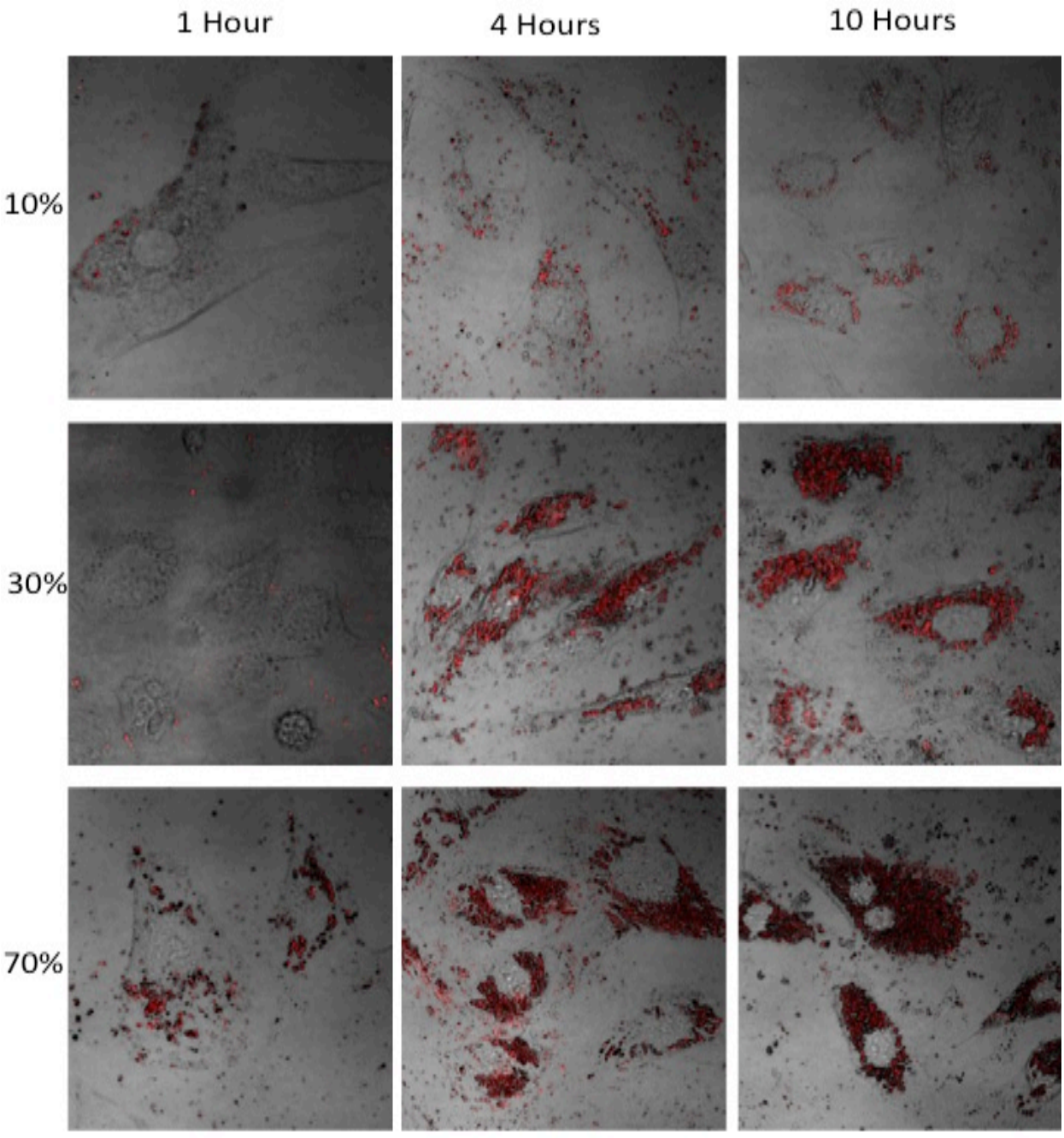

Figure 4.1: Confocal images of MNP uptake. 10%, 30% and 70% MNPs incubated for 1, 4 and 10 hours respectively. Images represent Z-stack.

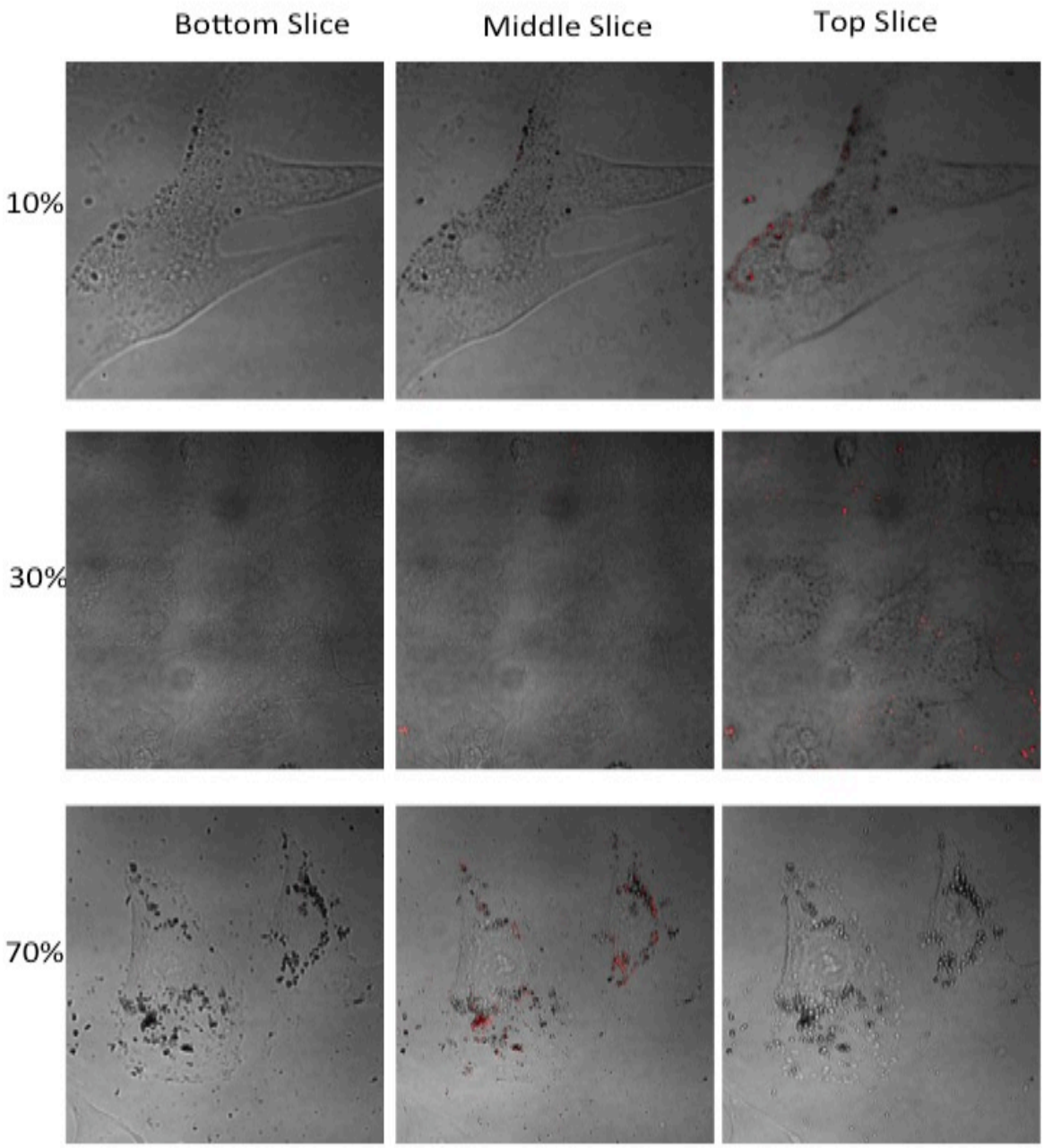

Figure 4.2: Magnetic Nanoparticle uptake for 10%, 30% and 70% MNPs after one hour. Shows top, middle and bottom slices of the z-stack. MNPs not located in the center or bottom slices of the z-stack are assumed to be associated with the membrane and not yet fully internalized by the endothelial cells.

4.3.2 Mitochondria Imaging

Mitotracker Green and Orange were used to fluorescently label high membrane potential mitochondria (orange) and all other mitochondria (green) of control and 10%, 30% and 70% MNP loaded cells incubated for twelve hours prior to being imaged via confocal microscope. After examining the initial images of our MNP loaded cells, that MNP loading on cells appeared to increase the number of actively respiring mitochondria in the cell in comparison to the Mitotracker-Green to Orange ration seen in control cells, Figure 4.3

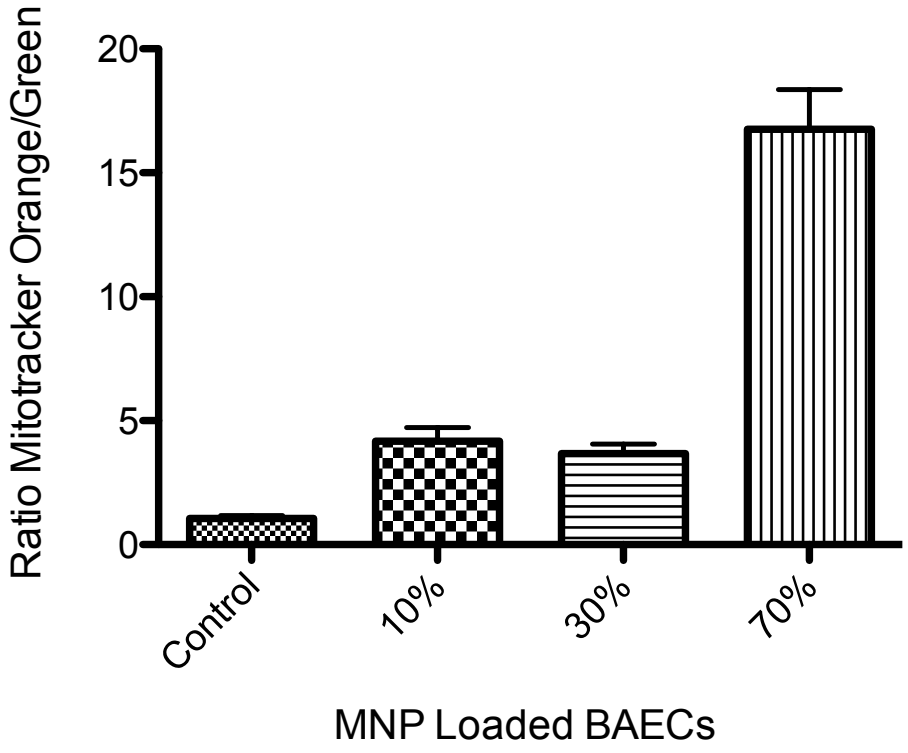

Figure 4.3: MNP uptake into cells increased the number of actively respiring mitochondria with respect to the mass. The ratio of Mitotracker red (actively respiring)/Mitotracker green (present but not actively respiring mitochondria) increases with the addition of MNPs into BAEC cells. All loaded BAEC (n=5) were statistically different from the control ($p<0.05$).

To examine whether or not these were negative effects on the cell, titrations with CCCP, a mitochondrial membrane depolarizer was used to show negatively affected mitochondria. Images were taken after CCCP doses of 0.6 µM and 1.4 µM were used to uncouple the mitochondrial membrane, Figure 4.4

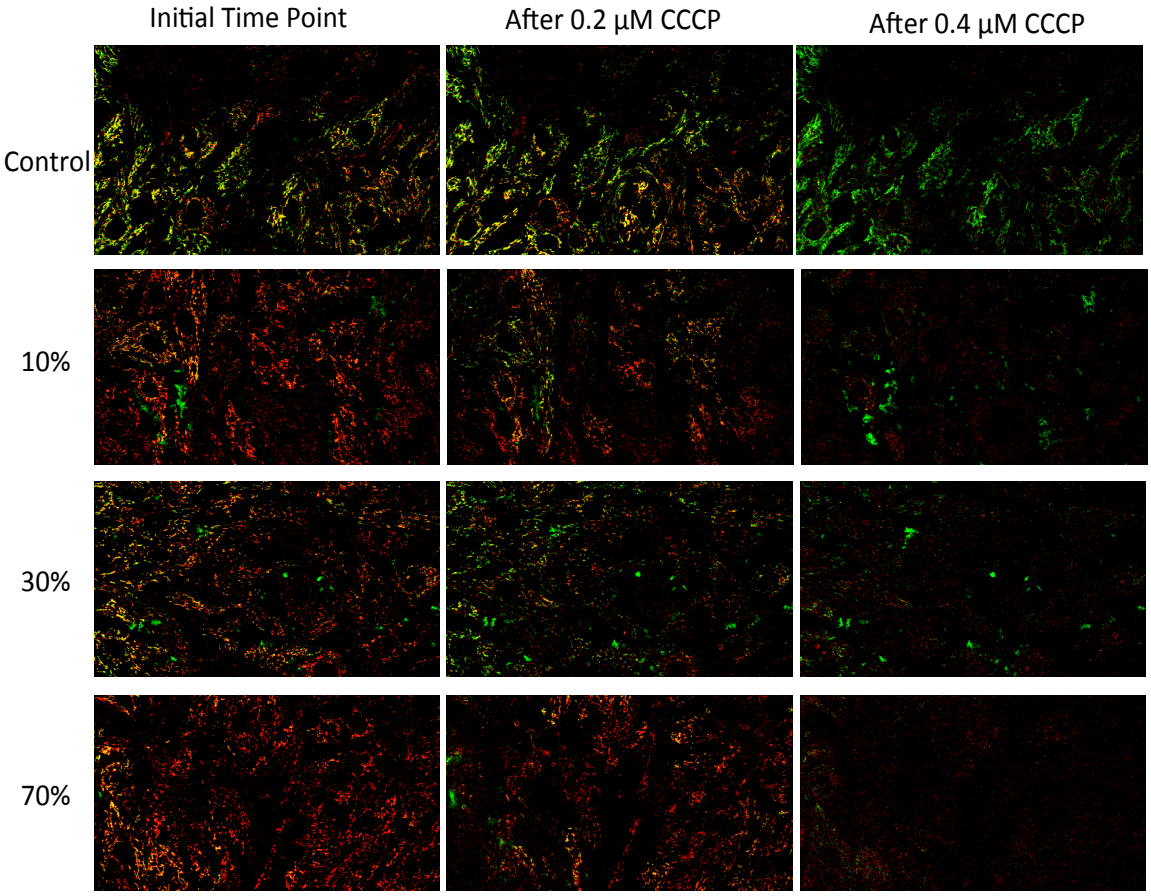

Figure 4.4: Bovine aortic endothelial cells loaded with 10%, 30% or 70% MNPs for 12 hours. Cells were stained with Mitotracker-Orange to label high membrane potential mitochondria and Mitotracker-Green to label the remaining mitochondria. Shows the presence of each type of mitochondria and how the loaded cells are affected when exposed to a 0.5µM followed by 1.4 µM dose of CCCP, a mitochondrial membrane uncoupler.

Fluorescent Intensity of Mitotracker orange in each cell in the confocal frame was measured over time during the addition of CCCP, Figure 4.5. Each time a CCCP dose was added the fluorescent intensity of the Mitotracker dropped, indicating depolarization of the mitochondrial membrane and thus a decrease in the mitochondria's ability to actively respire.

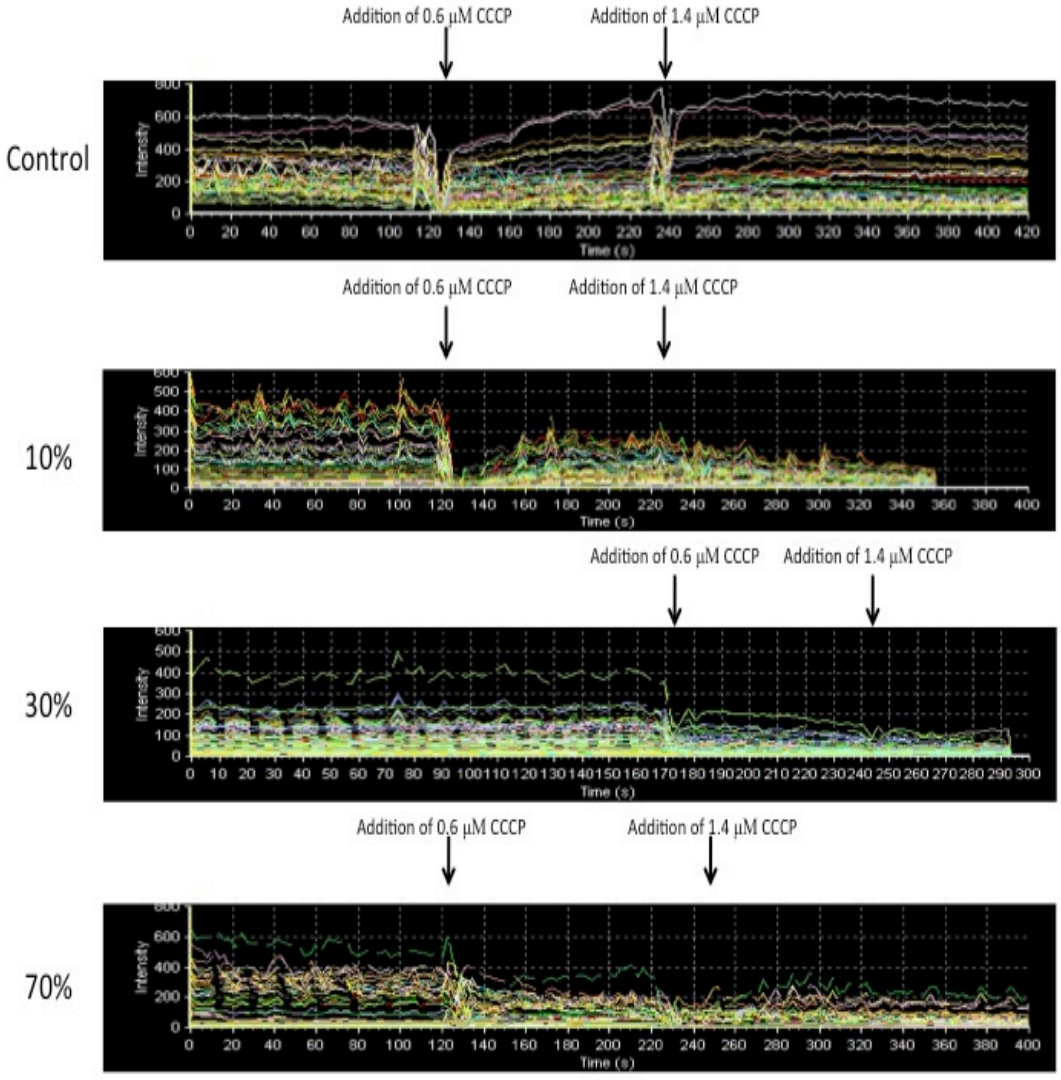

Figure 4.5: Mitotracker-orange intensity profiles over time of control and MNP BAEC cells loaded with 10%, 30% and 70% MNPs for 12 hours in response to two doses of CCCP a 0.2 µM and 0.4 µM dose after 100 and 200 seconds respectively.

The intensity values for each cell and each time point were normalized to the initial intensity. These values were plotted using a 2nd order smoothing, following the Savistsky-Golay smoothing principles, Figure 4.6. A segmented linear regression was used to compare the lines after the dose of CCCP was added at t = 100 seconds. The segmented linear regression showed that the decrease in mitotracker-red intensity was similar for the control and 30% MNP loaded cells ($p>0.05$) and similar for 10% and 70% MNP loaded cells ($p>0.05$). However, when comparing loaded cells to control cells, only 30% loaded MNPs mitochondrial response acted similarly to control cells.

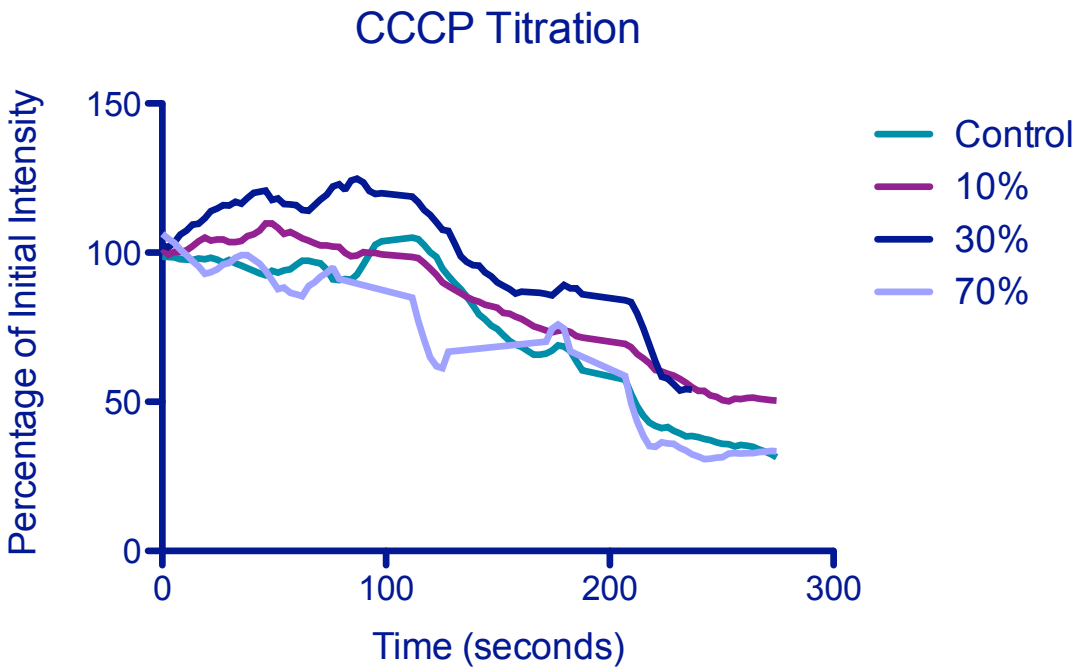

Figure 4.6: Titration curve of control cells and MNP loaded cells after titrating with CCCP concentrations. The first dose of 0.6 µM CCCP was added at 100 seconds, while the second dose of 1.4 µM was added at 200 seconds.

4.3.3 Actin Imaging

BAECs were transfected with DNA to have fluorescently labeled actin filaments. MNPs were loaded for 12 hours on a magnet prior and then imaged under the fluorescent scope. Images show that actin filaments do not seem to be damaged, but merely parted so that MNP aggregates can take up space, Figure 4.7. However, it is important to note that this analysis is subjective in nature so further studies will be completed to further demonstrate actin function.

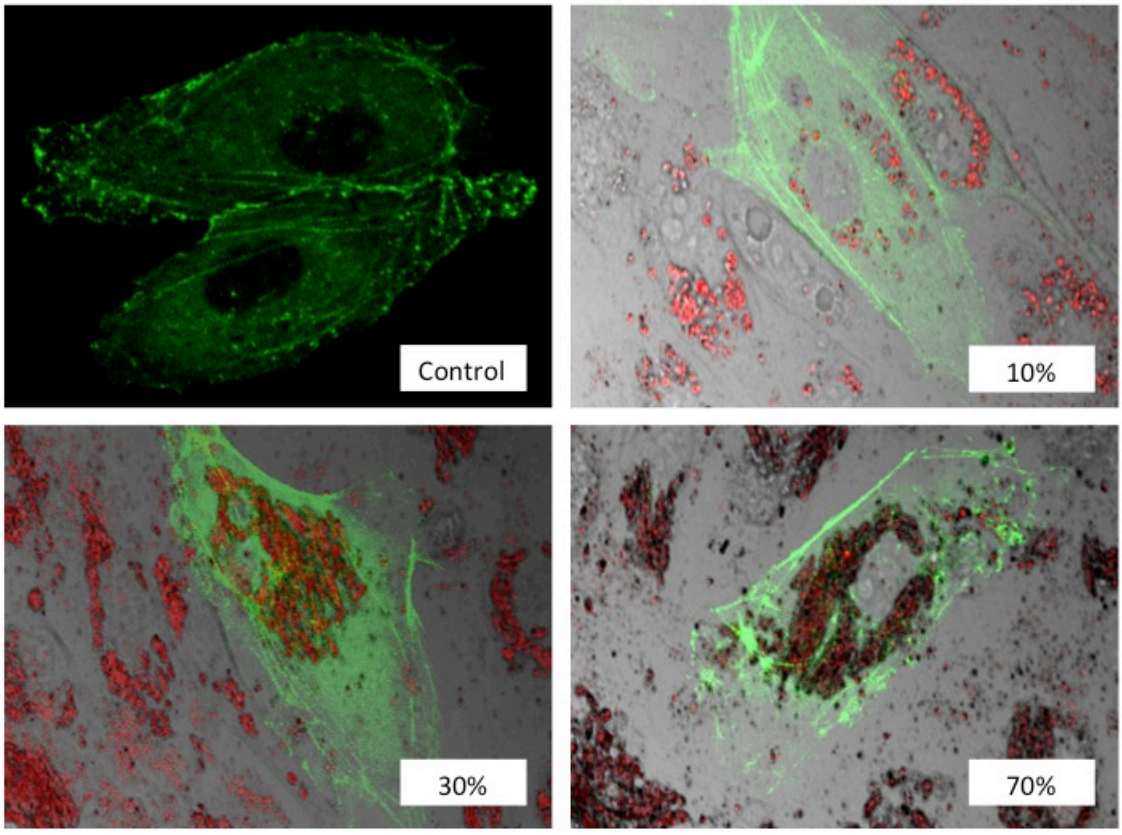

Figure 4.7: Transfected DNA into BAEC cells led to fluorescent actin filaments. Actin filaments of Control, 10%, 30% and 70% loaded MNPs were stained and show similar morphologies in comparison to control cells.

4.3.4 Cytoskeletal Function – 2-D Migration

Migration studies were performed without the influence of magnetic field as a re-assurance that the magnetic nanoparticles were not affecting the cytoskeletal functions. Migration distance was statistically different ($p < 0.001$) from the control for cells loaded for twelve hours with 10% or 70% MNPs Figure 4.8. However, the difference was not inhibitory. An increase in MNP loadings led to an increase in migration distance with the exception of 30% MNP loaded cells ,which exhibited a similar migration distance as that of control cells. Images of the migration distance were taken via light microscope and image analysis was used to quantify the distance traveled by the furthest cell, Figure 4.9.

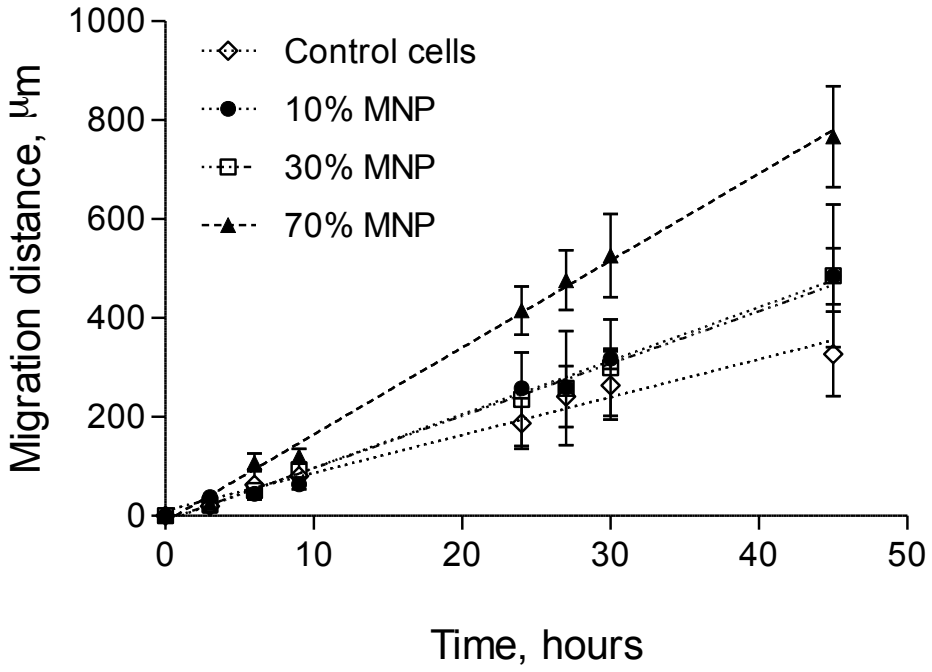

Figure 4.8: BAEC cells were loaded with 70% MNPs for 12 hours before being placed into a Transwell insert for 3-D migration. Migration was performed under the influence of a static magnetic field and without the influence of a magnetic field for loaded cells

and the migration was compared to control, unloaded cell migration. Migration was monitored for 12 hours and 24 hours to compare with a change in FBS as a positive control. In comparison to control cell migration, both 10% and 70% MNP loadings were statistically different ($p<0.001$). However, migration of 30% loaded BAEC was similar to that of control cell migration ($p>0.05$).

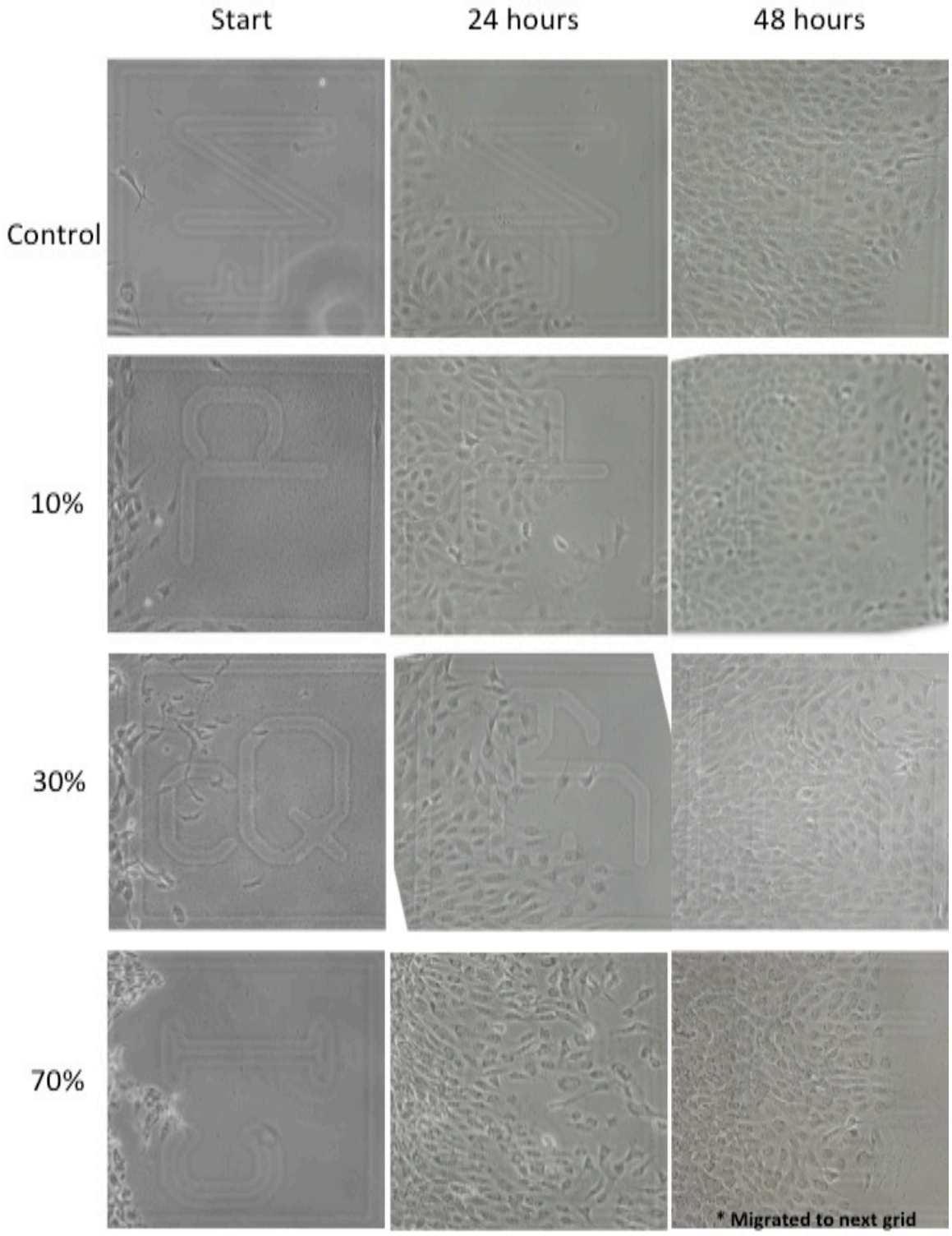

Figure 4.9: BAEC migration assays. Control cells and 10%, 30% and 70% MNP loaded migrations. Note that the 48-hour migration image of the 70% loaded cells proceeded to the next grid.

4.3.5 Model Targeting – 3-D Migration

70% MNP loading into cells was used since these particles exhibited the largest magnetic gradient and maximal loading that we could get in the time period, therefore leading to a more intense magnetic response. The magnetic field placed below the transwell membrane (Figure 4.10a) allowed us to image from the bottom only the cells that had migrated through the Fluoroblok wells that block the fluorescence of cells located on top of the membrane. 3-D migration showed that magnetically loaded cells exposed to a magnetic field migrated at an increase rate in comparison to control cells exposed to a FBS concentration difference. This can be seen in calcein green imaging, Figure 4.10b**,** and also image analysis of the number of cells that migrate through, Figure 4.11**.**

Magnetically loaded cells migrated significantly faster when under the infuence of a magnetic field as seen in the images and confirmed with image analysis and cell counts. Examining five frames of reference magnetically loaded cells exposed to a magnet showed 2.5 times more migration than that of control cells after 24 hours. FBS concentration differences were used as a positive control and magnetic nanoparticles exposed to a magnet without a FBS change also showed more migration in comparison to control cells with an FBS concentration change. Lastly, magnetically loaded cells not exposed to a magnetic field exhibited results statistically similar ($p>0.2$) to control cells.

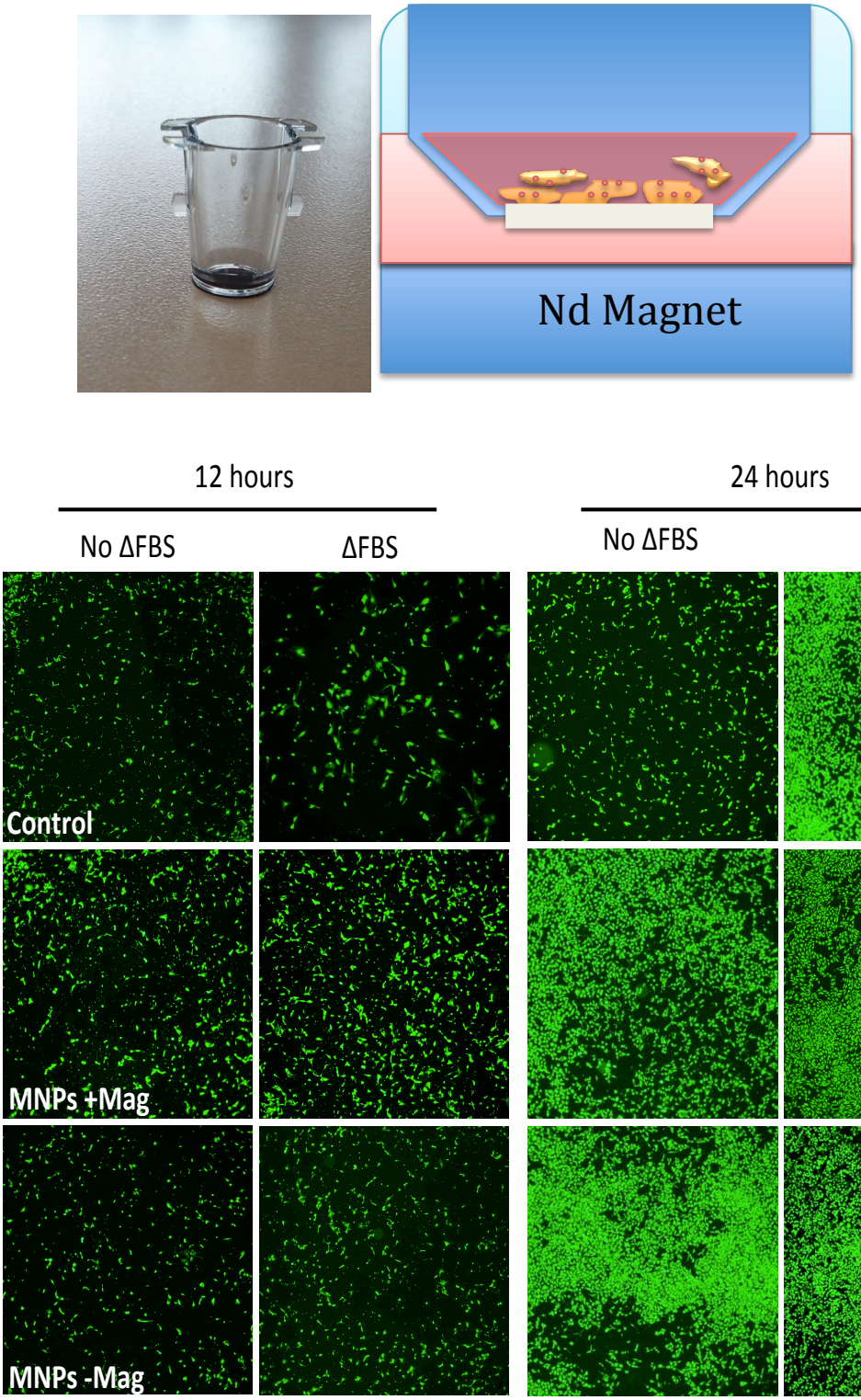

Figure 4.10: a) BAEC cells were loaded with 70% MNPs for 12 hours before being placed into a Transwell insert for 3-D migration. Image of setup is shown. Migration was performed under the influence of a static magnetic field and without the influence of

a magnetic field for loaded cells and the migration was compared to control, unloaded cell migration. 4.10 b) Migration was monitored for 12 hours and 24 hours to compare with a change in FBS as a positive control.

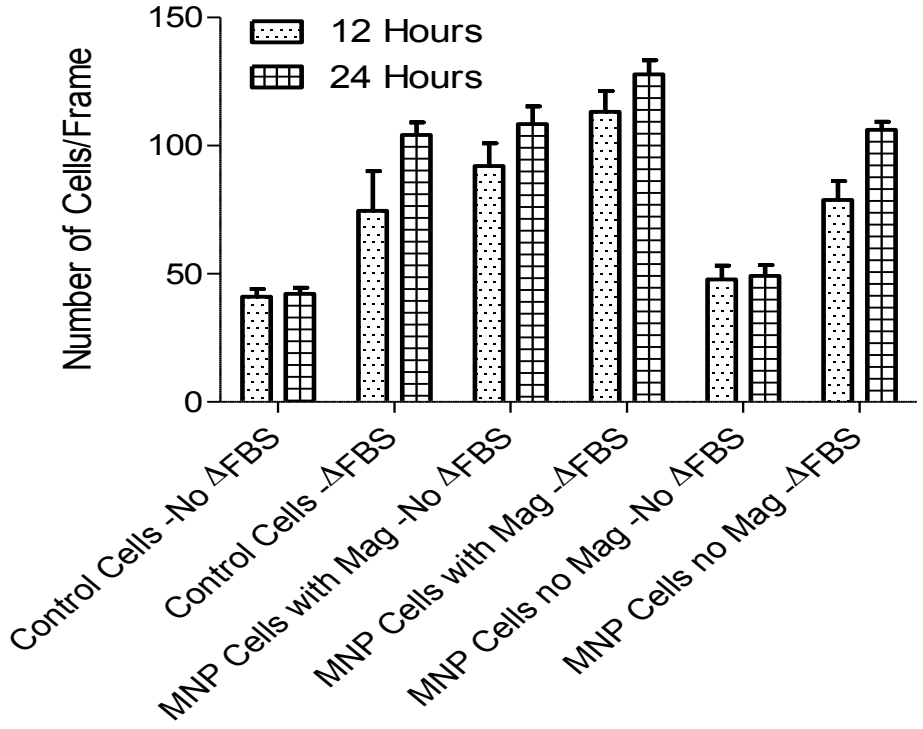

Figure 4.11: BAEC cells loaded with70% MNPs for 12 hours showed an increased migration under the influence of a magnetic field through an 8 μm pore Transwell membrane. The positive migratory control was differing FBS concentrations in the apical versus basal compartments of the Transwell set up. When comparing the above values we find that there is a significant difference ($p<0.001$) between magnetically loaded cells with our without a FBS gradient on a magnet in comparison to control cells without a FBS gradient. The addition of the magnetic field to loaded cells with our without a FBS gradient provides similar ($P>0.05$) migration values as that of control cells with an FBS change.

4.4 Discussion

4.4.1 Confocal Imaging

Confocal imaging was performed to determine if particle volume calculations from Chapter two were correlated with the image results and to determine the location of MNPs within endothelial cells. After 1 hour of loading, images demonstrate an interesting phenomenon for 10% and 30% MNPs. For these MNP formulations uptake is minimal. So minimal, that upon further investigation, MNPs are not in fact incorporated into the cell, but associated with the cell membrane.

At 4 hour and 10-hour time points for 10% and 30% and all 70% time points, magnetic nanoparticles exhibited perinuclear accumulation within the cell and are aggregated into small pockets within the cell. MNP loading for 4 hours and 10 hours in 30% and 70% MNPs is so extensive that MNP loading fills the cell from the perinuclear area to the cell membrane.

4.4.2 Mitochondria Imaging

Mitochondria health is important to a cells well being, given that they are responsible for cellular respiration and ATP production. Without healthy mitochondria, the cell will die. After confocal images showed BAECs highly loaded with MNPs, it was determined that a look at mitochondria health was important to show that the cells were not “suffocating”. In order to examine the health of the mitochondria we looked at mitochondrial membrane potential, $\Delta\Psi$, with the help of two fluorescent probes, Mitotracker-Green and Mitotracker-Orange. Mitotracker-Orange, reflects mitochondrial oxidative capacity and only penetrates into mitochondria with high $\Delta\Psi$. Mitotracker-

Green penetrates into all mitochondria, including those with low ΔΨ, and is therefore often used as a measure of total mitochondria within a cell. We looked at the ratio of the fluorescent intensities of Mitotracker Orange to Mitotracker Green as a metabolic index representing the proportion of actively respiring mitochondria in the total mitochondrial mass.

Our results showed that an after 12-hours of MNP loading into BAECs, the ratio of high membrane potential mitochondria to low membrane potential mitochondria is extremely high, in comparison to control cells where the ratio is approximately one, indicating that all mitochondria in the cell are operating at full capacity in attempt to respire as a result of high MNP loading.

In order to be certain that mitochondria were still actively functioning, CCCP was used as a negative control to show how the fluorescent intensity of the Mitotracker orange would be affected the presence of a mitochondrial membrane-uncoupling agent. CCCP was used to measure the sensitivity of depolarization of the mitochondrial membrane. Our images showed that for control, 10%, 30% and 70% MNP loaded cells, ΔΨ, was decreased after an initial dose of 0.6 μM CCCP, but was then restored after some time, suggesting that neither collapse of ΔΨ or depolarization of the mitochondria occurred. A linear regression of this segment of the graph showed that there was no significant difference between loaded and non-loaded cells ($p>0.05$). However, after the second dose of 1.4 μM CCCP, there was a steep decrease in ΔΨ, indicating loss of mitochondrial membrane potential and an increase in mitochondrial membrane permeability. This can be confirmed in the confocal images after that dose that no longer show fluorescently labeled mitochondria. When comparing the differences in rate of

decrease in mitotracker red intensity, it was observed that Control cells and 30% MNP loaded cells acted similarly ($p>0.05$) while 10% and 70% MNPs acted similarly ($p>0.05$), with the control cells and 30% MNP loaded cells reacting more strongly to the CCCP than that of the 10% and 70% loaded cells. After an initial dose of 0.6 μM CCCP mitochondria responded to the stimuli and did not recover enough before the final 1.4 μM CCCP dose that caused complete depolarization. While all control and loaded cells eventually showed signs of complete depolarization the control and 30% MNP cells responded at a much faster rate than that of 10% and 70% loaded cells. These results indicate that while the mitochondria of the loaded BAECs are still functioning, since we do see a response to CCCP aided uncoupling, there does not seem to be an correlation to MNP loadings and mitochondrial response.

4.4.3 Actin Imaging

Cytoskeletal microfilaments such as actin are important in cellular attachment and shape, therefore, we used transfection to stain β-actin in control and 12 hour 10%, 30% and 70% MNP loaded cells to determine if MNP loading had an affect on microfilament organization. While not much work has been done in regards to MNP uptake effects on cytoskeletal organization, prior work has demonstrated that ultra-small MNP loading decreases microfilament organization within a cell [85, 86]. However, our results indicate that in comparison to control cells, 10% and 30% loaded cells after 12 hours did not show any altered cell morphology or difference in cytoskeletal organization. 70% loaded cells however, did show slightly rounder cell morphology with fewer cytoplasmic extensions in comparison to controls. However, these effects can be assumed to be minimal, as they did not alter the cells ability to remain attached to the plate that they

were seeded in. The difference in our results and prior work showing severely altered microfilament organization lies in the size difference in particles used. It has previously been indicated that MNPs of smaller sizes are more toxic to cells than those of larger sizes. Given the difficulty in seeing the difference in actin organization in control and loaded cells, migration assays were performed in order to confirm whether or not cytoskeletal functionality was altered.

4.4.4 Cytoskeletal Function – 2-D Migration

It was expected that the high loading of MNPs exhibited after 12 hours of MNP uptake into BAECs would affect the ability for cells to migrate over a flat surface; however, our results showed that MNP uptake into cells significantly increased cell migration for 10% ($p < 0.0001$), 30% ($p < 0.0001$) and 70% ($p < 0.0001$) in comparison to control. The increase in migration rate with MNP loading can potentially be described in a few ways, with further research necessary to fully elucidate the actual mechanism. Previous work has suggested that MNP incorporation into endothelial cells causes intercellular gaps to form [93]. Given that BAEC growth and migration is contact inhibited, an increase in intercellular gap distance, by either shrinkage of the cell or some other method would signal for the cell to grow and/or migrate, despite the cell number being similar to that of control cells. Our loaded cells do exhibit a slight shrinkage that is only noticeable under the microscope that could be the cause of the observed increase in migration of cells. Similarly, another potential theory for the enhanced migration is shown in research that reports MNP uptake of similar size as ours indicates a decrease in intercellular gap junction communication, which would again affect the contact inhibited nature of our BAECs [146]. This work suggests that stress kinases and β-catenin levels

modulate the alterations in intercellular gap junction communication. This implies that the exposure of cells to MNPs induces a stress response that ends with a down regulation of intercellular signaling. Overall, these are two theories as to why uptake of MNPs into BAECs causes an increase in migration; however, further investigation is needed to determine whether these cellular responses are chronic or they are alleviated once cellular MNP concentration is diluted after cell division.

4.4.5 Model Targeting – 3-D Migration

Three-Dimensional migration experiments have been conducted using a standard Boyden Chamber Assay of MNP loaded cells in the past [85]. Similarly, MNP loaded cells have been targeted *in vitro* to tissues for cell attachment [147] and even to implants[47, 50] however, MNP-loaded cells as targeted cell delivery/targeting vectors can be even more promising if we can characterize and manipulate their movement through tissues. As a first step in order to eliminate the idiosyncrasies of transport through soft tissues, it is necessary to determine how MNP-loaded endothelial cells can navigate through a membrane with or without an applied magnetic field. Our 3-D migration experiments of MNP-loaded endothelial cells through a transwell membrane show that not only are maximally loaded 70% MNP loaded cells capable of migrating, but there is a significant ($p<0.001$) increase in migration of MNP-loaded endothelial cells under the influence of a magnetic field to the point that MNP loaded cells exposed to a magnet without an FBS gradient have the same migration amount as non-loaded cells with a FBS gradient.

Control cells were seeded on the Transwell membrane with either a directional gradient in FBS concentration or no gradient in FBS concentration. Control cells with a

directional gradient in FBS were the positive control and exhibited an increase in migration ($p<0.001$) of two and two and a half times in comparison to control cells ,whose apical and basal chambers were comprised of cell culture media of the same concentration of FBS for both 12 and 24 hour time points respectively. MNP loaded endothelial cells exposed to a magnet without an FBS gradient exhibited the same ($p=0.57$) migratory patterns as those of control cells with an FBS gradient. This result suggests that the magnetic force does in fact encourage a migratory response in MNP-loaded cells.

MNP-loaded BAECs not exposed to a magnetic field responded the same ($p=0.188$) as control cells both with and without a concentration gradient of FBS, indicate that the magnetic field was causing the effect and not just the presence of the MNPs. To be certain that these were migratory affects and not affects of increased proliferation as a result of MNP loading, alamar blue was conducted at 12 hour and 24 hour timepoints. Alamar blue at the 24 hour timepoints indicated that there were approximately 125,000 cells/transwell for wells that did not show a concentration gradient and approximately 135,000 for cells that did show a concentration gradient. These values both correlate with the 0.5 population doublings/day that is suggested for bovine aortic endothelial cells. There was not however an increase between magnetically loaded and non-magnetically loaded cells, indicating that the increase in migration was not an affect of an increase in proliferation. Overall, these results are promising indicators that magnetically loaded cells can be adequate targeted therapy delivery vectors in soft tissues.

4.5 Conclusion

Biodegradable MNPs were formulated with variable loading of magnetite in a range of 10-70% (w/w) and loaded into bovine aortic endothelial cells under the influence of a magnetic field. Confocal images show that 10% and 30% MNPs incubated with bovine aortic endothelial cells after one hour are not in fact internalized but merely associated with the endothelial cell membrane. On the contrary, images of 30% and 70% MNP loaded cells display endothelial cells that are highly loaded during maximal incubation times. An analysis of cytoskeletal organization, microfilament function and mitochondrial health were performed, and we found no severe indications that these loadings were detrimental to cell health.

These few, yet important characteristics of cell health, along with previous Alamar blue and calcein green studies demonstrate relatively healthy endothelial cells, despite the massive MNP loadings. Furthermore, while more investigation is needed to fully elucidate the effect of MNPs on sub-cellular organelle functions, it appears that MNP loadings do not affect the mitochondrial, cell division or migratory functional levels of the BAEC. The ability to have maximal MNP loading allows the cells to be more magnetically responsive which increases their attractiveness as potential targeted drug delivery vectors, in addition to their innate biocompatibility

It was expected that the high loading of MNPs exhibited after 12 hours of MNP uptake into BAECs would affect the ability for cells to migrate over a flat surface, however, our results showed that MNP uptake into cells significantly increased cell migration for 10% ($p < 0.0001$), 30% ($p < 0.0001$) and 70% ($p < 0.0001$) in comparison to control. The increase in migration rate with MNP loading can potentially be described in

a few ways, with further research necessary to fully elucidate the actual mechanism. Previous work has suggested that MNP incorporation into endothelial cells causes intercellular gaps to form [93]. Given that BAEC growth and migration is contact inhibited, an increase in intercellular gap distance, by either shrinkage of the cell or some other method would signal for the cell to grow and/or migrate, despite the cell number being similar to that of control cells. Our loaded cells do exhibit a slight shrinkage that is only noticeable under the microscope that could be the cause of the observed increase in migration of cells. Similarly, another potential theory for the enhanced migration is shown in research that reports MNP uptake of similar size as ours indicates a decrease in intercellular gap junction communication, which would again affect the contact inhibited nature of our BAECs (Ale-Agha, Albrecht et al. 2010). This work suggests that stress kinases and β-catenin levels modulate the alterations in intercellular gap junction communication. This implies that the exposure of cells to MNPs induces a stress response that ends with a down regulation of intercellular signaling. Overall, these are two theories as to why uptake of MNPs into BAECs causes an increase in migration, however, further investigation is needed to determine whether these cellular responses are chronic or they are alleviated once cellular MNP concentration is diluted after cell division.

Three-Dimensional migration experiments have been conducted using a standard Boyden Chamber Assay of MNP loaded cells in the past [85]. Similarly, MNP loaded cells have been targeted *in vitro* to tissues for cell attachment[147] and even to implants [47, 50] however, MNP-loaded cells as targeted cell delivery/targeting vectors can be even more promising if we can characterize and manipulate their movement through

tissues. As a first step in order to eliminate the idiosyncrasies of transport through soft tissues, it is necessary to determine how MNP-loaded endothelial cells can navigate through a membrane with or without an applied magnetic field. Our 3-D migration experiments of MNP-loaded endothelial cells through a transwell membrane show that not only are maximally loaded 70% MNP loaded cells capable of migrating, but there is a significant ($p<0.001$) increase in migration of MNP-loaded endothelial cells under the influence of a magnetic field.

Control cells were seeded on the Transwell membrane with either a directional gradient in FBS concentration or no gradient in FBS concentration. Control cells with a directional gradient in FBS were the positive control and exhibited an increase in migration ($p<0.001$) of two and two and a half times in comparison to control cells that whose apical and basal chambers were comprised of cell culture media of the same concentration of FBS for both 12 and 24 hour time points respectively. MNP loaded endothelial cells exposed to a magnet without an FBS radient exhibited the same ($p=0.57$) migratory patterns as those of control cells with an FBS gradient. This result suggests that the magnetic force does in fact encourage a migratory response in MNP-loaded cells. MNP-loaded BAECs not exposed to a magnetic field responded the same ($p=0.188$) as control cells both with and without a concentration gradient of FBS, indicate that the magnetic field was causing the effect and not just the presence of the MNPs. To be certain that these were migratory affects and not affects of increased proliferation as a result of MNP loading, alamar blue was conducted at 12 hour and 24 hour timepoints. Alamar blue at the 24 hour timepoints indicated that there were approximately 125,000 cells/transwell for wells that did not show a concentration

gradient and approximately 135,000 for cells that did show a concentration gradient. These values both correlate with the 0.5 population doublings/day that is suggested for bovine aortic endothelial cells. There was not however an increase between magnetically loaded and non-magnetically loaded cells, indicating that the increase in migration was not an affect of an increase in proliferation. Overall, these results are promising indicators that magnetically loaded cells can be adequate targeted therapy delivery vectors in soft tissues.

.

Chapter 5: Conclusions and Future Work

5.1 Magnetic Nanoparticle Synthesis and Movement

5.1.1 Summary of Principle Findings

Our study showed that it was possible to incorporate up to 70% (w/w) iron oxide into biodegradable magnetic nanoparticles without affecting MNP size distribution or surface properties. By doing so we were able to increase the magnetic susceptibility of the MNPs. The increase in magnetic saturation was linearly correlated with the percentage of the iron oxide loading.

Our study used a model system with viscous fluid to analyze how magnetic nanoparticles of various loadings would move through viscous fluid with the addition of an alternating magnetic field perpendicular to a gradient field provided by a permanent magnet. The theory was that the magnetic nanoparticles would move faster with this small "shaking" field since it helped them to overcome the initial static force. Our study showed that the time-varying magnetic field superimposed onto the permanent gradient field is in fact a promising approach to enhance transport of magnetic carriers in soft media.

5.1.2. Implications of the Current Study

In recent years, much research has been completed on how magnetic nanoparticles can help with drug delivery and therapeutic treatments. While many of these studies have examined the aspects of MNPs formulation, characterization and drug release, actual work on how to target, deliver or transport the particles to the treatment area has been lacking. Thus it is important to understand the fundamental mechanisms by which MNPs can be actively transported through biological tissues under the action of a

magnetic field. MNPs can be carriers of various treatment modalities such as drugs, genes, radioactivity, and hyperthermia. Improved insight into the MNPs transport and actively-controlled soft tissue penetration is essential for improving the efficacy of current therapeutic methods for cancer, transport of drugs through Blood Brain Barrier (BBB), wound healing, cardiovascular disease, and many other pressing medical problems to which nanoparticulate drug delivery approach is applicable.

Even if locomotion of carriers is difficult to achieve, the use of a time-varying uniform magnetic field superimposed onto the permanent gradient field may dramatically improve transport of carriers through soft tissues and their delivery to the target. The present study shows that, when applied correctly, time varying magnetic field could create oscillating force on the carriers which will reduce effective yield stresses which prevent the carriers from moving and, possibly, decrease effective viscous drag in tissues. Alternatively, the magnetic targeting can be enhanced by changing the effective resistance of the biological tissues, for example, by using magnetic carriers with proteolytic surface functionalization to increase carrier's mobility through the extracellular matrix, as was shown *in vitro* [118] or through the inertial cavitation created by ultrasound, as has been shown in transdermal drug delivery [148, 149].

Our results on the effects of a time-varying uniform magnetic field superimposed on the permanent gradient field on the transport of MNPs demonstrate the potential of this approach to achieve more effective and controllable delivery of therapeutic agents or therapeutic effects. Hopefully this will lead to exploitation of the potential ability of this methodology to improve the delivery of the therapeutic agents/effects *in vivo* and in future clinical settings.

5.2 Magnetic Nanoparticle Uptake

5.2.1 Summary of Principle Findings

Our results showed that there was a significant increase in uptake of magnetic nanoparticles under the influence of a magnetic field. Indicating a force-dependent mechanism of uptake. MNP exposure to a magnetic field for one hour allows complete sedimentation of the nanoparticles to the cell surface, however, removal of the field results in a plateau in the amount of MNP uptake over a 12 hour period. This shows that the increase in uptake when exposed to the magnet is not a result of faster initiation to the cell's membrane. In non-treated cells, MNPs were loaded into cells and incorporated up to 15% of the cells volume. Preliminary toxicity studies utilizing calcein green and alamar blue show that the cells are not significantly affected by these high loadings.

While our results indicate that there is certainly a force related mechanism of uptake, the exact mechanism is still unknown. Previous studies demonstrate that cholesterol depletion is a way to block caveolae-mediated endocytosis. MNP uptake after cholesterol depletion results in no change in MNP uptake. On the contrary, cytochalasin –D treatment of cells, historically used to block phagocytosis, blocks almost all uptake of MNPs. These results suggest that our particles are in fact taken up via a phagocytotic mechanism that is enhanced with the magnetic forces presented on the cell membrane. As with all endocytotic studies, altering a cells normal function, similar to what we do in these studies via cholesterol depletion or inhibition of actin polymerization, can modify how a cell would normally process

particles. Therefore further research and newer technologies are needed to determine with greater certainty the uptake mechanism.

5.2.2 Implications of the Current Study

Cellular uptake studies involving particles typically fall into one of two categories: non-magnetic nanoparticle endocytotic pathway studies or magnetic nanoparticle transfection studies. This study combines these two ideas by examining the effect a magnetic field has on how bovine aortic endothelial cells uptake MNPs. Similarly, the uptake of these MNPs in previous studies looks at cellular health with MNP concentrations much lower than we show in our study.

The ability to load high concentrations of MNPs into a cell with low toxicity effects allows us to have a drug delivery vector that is much more magnetically responsive and therefore easier to target. Similarly, the large concentrations are beneficial in hyperthermia applications, as there is more magnetic material located in the targeted area. Overall, our study is novel in that it shows that endothelial cells survive after 24 hours with high loadings of high magnetite concentration nanoparticles.

5.3 Loaded Endothelial Cells for Magnetic Targeting

5.3.1 Summary of Principle Findings

Confocal imaging of loaded cells showed endothelial cells that were highly loaded with MNPs. These images made it difficult to believe that the cells were still functioning and not “suffocating”. Analysis of the mitochondrial membrane potentials showed that despite an increase in actively respiring mitochondria, the

mitochondrial response to additional damages was similar in control cells and MNP loaded cells, indicating that there was no severe damage done by the presence of MNPs.

Similarly, despite high loadings of MNPs shown in confocal images, actin filaments were visualized and did not show any major deformities. Analysis of cytoskeletal function by trypsinization and re-seeding indicated that the cells ability to attach was not affected. Similarly, migration assays indicate that MNP loaded cells are not only still capable of migrating, but do so at a faster velocity than that of the control cells. Lastly, we were able to show that we can manipulate the movement of magnetically loaded endothelial cells through a membrane in the presence of a magnetic gradient provided by a permanent magnet.

5.3.2 Implications of the Current Study

Currently, there are multiple approaches to targeted therapies being researched that involve the use of magnetic micro/nanoparticles. Their high biocompatibility as a result of magnetite's composition and the ability to position the magnetite in biocompatible polymer coatings such as PLA and PLGA [14, 24] makes them a potential resource for cancer treatment and gene delivery. Magnetic targeting utilizes an external magnetic field in combination with MNPs to allow delivery of particles to the desired target area and fixation to a local site while the medication is released and acts locally [24]. This technique allows for decreased dosage of chemical therapies that may otherwise cause deleterious systemic effects.

This method has been demonstrated successfully in treatments for cardiovascular diseases, as the simplistic nature of the vasculature leads to a straightforward model. The success of this treatment has contributed to the optimistic views on magnetic drug targeting in other areas of the body. While studies outside of the cardiovascular system are few, there has been some success shown in *in-vitro* models of mobilizing MNPs through simulated soft tissues [53, 57, 120, 121]. Our work is a first step in showing that magnetically loaded cells are promising vectors for targeted drug delivery through soft tissues. We take the success of our colleagues and take it a step further by showing that loaded MNPs into cells not only does not affect cellular function but that we can also manipulate the movement of these cells through a simulated "tissue model".

The other benefit of our system is toxicity. It has been shown that larger scale nanoparticles (>200nm) have a less toxic effect on the human body, therefore loaded cells with nanoparticles would have a significantly less toxic effect, since the body sees the cell and not the nanoparticles themselves. The loaded cells do not allow MNPs to float freely throughout the body and the MNP concentration is diluted each time the cell divides. Therefore, the body eliminates them more gradually.

5.4 Future Work

There are a number of potential studies that can result from this work. Magnetic targeting is still a hot topic in biomedical engineering and the ability to show successful targeting is a very publishable body of research, possibly even more so than functionalization of magnetic nanoparticles. This work lays the groundwork for further tests of MNP loaded cell delivery.

Our work is unique in that the MNP concentrations we expose the cells to results in equally high magnetic loadings with minimal negative effects. Therefore, further transport studies of these cells should be conducted to show if the indication that loaded cells have higher magnetic susceptibilities translates to a better-targeted delivery option than MNPs on their own. A similar study to the 3-D migration we performed can be completed with a FluoroBlok tumor invasion assy. This assay involves the same setup we used with the addition of a BD matrigel matrix on the apical part of the chamber. Using this system would be the next step in mimicking a tissue type that magnetically targeted drug delivery is looking to treat.

Another interesting study that could be completed if the correct alternating coil could be produced would be to complete the magnetically loaded cell manipulation studies with the addition of the "vibrating" field present perpendicular to the direction of movement. One would assume that a soft-tissue is a matrix like structure that does now allow a straight path of travel for the MNP loaded cell. The path that a loaded cell would have to follow would most likely be a zigzag pattern. The "vibrating field" methodology that showed promise in Chapter 2 could more effectively guide the loaded cells through the intercellular pathways and cell junctions of a soft tissue.

Works Cited

1. Freestone, I., et al., *The Lycurgus Cup - A Roman Nanotechnology.* Gold Bulletin, 2007. 40(4): p. 270-277.

2. Buzea, C., I.I. Pacheco, and K. Robbie, *Nanomaterials and nanoparticles: Sources and toxicity.* Biointerphases, 2007. 2(4): p. MR17-MR69.

3. Buyukhatipoglu, K., *Bioprinted superparamagnetic nanoparticles for tissue engineering applications: synthesis, cytotoxicity assessment, novel hybrid printing system*, in *Mechanical Engineering*2009, Drexel University: Philadelphia, PA.

4. Metallurgy, D.-D.o.M.S.a., *Ferromagnetic Materials*, 2008, University of Cambridge.

5. Hariharan, S. and J. Gass, *Superparamagnetism and magneto-caloric effect (MCE) in functional magnetic nanostructures.* Rev.Adv.Mater.Sci, 2005. 10: p. 398-402.

6. Tauxe, L., *Paleomagnetic Principles and Practice*, 1998, Book News, Inc: Portland, Oregon.

7. Mahmoudi, M., et al., *Superparamagnetic Iron Oxide Nanoparticles: Synthesis, Surface Engineering, Cytotoxicity and Biomedical Applications*2011.

8. Gubin, S., et al., *Magnetic nanoparticles: preparation, structure and properties.* Russian Chemical Reviews, 2005. 74(6): p. 489-520.

9. Gopalakrishnan, J. and A.R. Barron, *Introduction to Nanoparticle Synthesis.* Chemical Materials, 1995. 7.

10. Sun, C., J.S.H. Lee, and M. Zhang, *Magnetic nanoparticles in MR imaging and drug delivery.* Advanced Drug Delivery Reviews, 2008. 60(11): p. 1252-1265.

11. Quintanar-Guerrero, D., et al., *Preparation techniques and mechanisms of formation of biodegradable nanoparticles from preformed polymers.* Drug Dev Ind Pharm, 1998. 24(12): p. 1113-28.

12. Chorny, M., et al., *Magnetically Responsive Biodegradable Nanoparticles Enhance Adenoviral Gene Transfer in Cultured Smooth Muscle and Endothelial Cells.* Molecular Pharmaceutics, 2009. 6(5): p. 1380-1387.

13. Gong, T., et al., *Preparation of monodispered hybrid nanospheres with high magnetite content from uniform Fe304 clusters.* Colloids and Surfaces a-Physicochemical and Engineering Aspects, 2009. 339(1): p. 232-239.

14. Gupta, A.K. and M. Gupta, *Synthesis and surface engineering of iron oxide nanoparticles for biomedical applications.* Biomaterials, 2005. 26: p. 3995-4021.

15. Hofmann-Amtenbrink, M., B. von Rechenberg, and H. Hofmann, *Superparamagnetic nanoparticles for biomedical applications.* Transworld Research Network, 2009. 37(2): p. 120-149.

16. McBain, S., H.H. Yiu, and J. Dobson, *Magnetic nanoparticles for drug and gene delivery.* International Journal of Nanomedicine, 2008. 3(2): p. 169-180.

17. Weissleder, R., et al., *Long-circulating iron oxides for MR imaging.* Advanced Drug Delivery Reviews, 1995. 16: p. 321-334.

18. Ramanujan, R., C. Tan, and H. Rumpel, *MRI in Nanotechnology: Nanomagnetic probes for biomaging*, in *Looking into Living Things through MRI*, R. Chaughule and S. Ranade, Editors. 2006, Prism Publications.

19. Ito, A., et al., *Medical application of functionalized magnetic nanoparticles.* J Biosci Bioeng, 2005. 100(1): p. 1-11.

20. Rohrer, M., et al., *Comparison of magnetic properties of MRI contrast media solutions at different magnetic field strengths.* Investigational Radiology, 2005. 40(11): p. 715-724.

21. Gupta, A.K. and M. Gupta, *Cytotoxicity suppression and cellular uptake enhancement of surface modified magnetic nanoparticles.* Biomaterials, 2005. 26(13): p. 1565-1573.

22. Moran, G.R., et al., *An investigation of the toxicity of gadolinium based MRI contrast agents.* Proc. Intl. Soc. Mag. Reson. Med, 2002. 10.

23. Hasebroock, K.M. and N.J. Serkova, *Toxicity of MRI and CT contrast agents.* Expert Opinion on Drug Metabolism and Toxicity, 2009. 5(4): p. 403-416.

24. Neuberger, T., et al., *Superparamagnetic nanoparticles for biomedical applications: Possibilities and limitations of a new drug delivery system.* Journal of Magnetism and Magnetic Materials, 2005. 193: p. 483-496.

25. Jordan, A., R. Wust, and H. Faehling, eds. *Scientific and Clinical Applications of Magnetic Carriers*. 1997, Plenum Press: New York.

26. Jordan, A., et al., *Magnetic fluid hyperthermia (MFH): Cancer treatment with AC magnetic field induced excitation of biocompatible superparamagnetic nanoparticles.* Journal of Magnetism and Magnetic Materials, 1998. 201: p. 413-419.

27. Lee, J., et al., *Hyperthermia Induced Magnetic Nanoparticles Improves the Effectiveness of the Anticancer Drug cis-Diamminedichloroplatinum.* Journal of Nanoscience and Nanotechnology, 2011. 11(5): p. 4153-4157.

28. Gilchrist, R., et al., *Selective Induction heating of lymph nodes.* Annals of Surgery, 1957. 146: p. 596-606.

29. Silva, A.C., et al., *Application of hyperthermia induced by superparamagnetic iron oxide nanoparticles in glioma treatment.* International Journal of Nanomedicine, 2011. 6: p. 591-603.

30. Johannsen, M., et al., *Clinical hyperthermia of prostate cancer using magnetic nanoparticles: Presentation of a new interstitial technique.* International Journal of Hyperthermia, 2005: p. 1-11.

31. Dunina-Barkovskaya, A.Y., *Phagocytosis - Three in one: Endocytosis, exocytosis, adhesion.* Biologicheskie Membrany, 2004. 21(4): p. 243-270.

32. Perea, H., *Vascular tissue engineering with magnetic nanoparticles: seeing deeper.* Journal of Tissue Engineering and Regenerative Medicine, 2007. 1(4): p. 318.

33. Buyukhatipoglu, K., et al., *Bioprinted Nanoparticles for Tissue Engineering Applications.* Tissue Engineering Part C-Methods, 2010. 16(4): p. 631-642.

34. Buyukhatipoglu, K., W. Jo, and A.M. Clyne, *The role of printing parameters and scaffold biopolymer properties in the efficacy of a new hybrid nano-bioprinting system.* Biofabrication, 2009. 1(3).

35. Cartmell, S.H., et al., *Development of magnetic particle techniques for long-term culture of bone cells with intermittent mechanical activation.* IEEE Transactions Nanobiosciences, 2002. 1(2): p. 92-97.

36. Kanczler, J.M., et al., *Controlled Differentiation of Human Bone Marrow Stromal Cells Using Magnetic Nanoparticle Technology.* Tissue Engineering Part A, 2010. 16(10): p. 3241-3250.

37. Laurent, S., et al., *Magnetic Iron Oxide Nanoparticles: Synthesis, Stabilization, Vectorization, Physiochemical Characterizations, and Biological Applications.* Chem. Rev., 2008. 108: p. 2064-2110.

38. Pouton, C.W. and L.W. Seymour, *Key issues in non-viral gene delivery.* Advanced Drug Delivery Reviews, 1998. 34: p. 3-19.

39. Crystal, R., *The gene as the drug.* Nature Medicine, 1995. 1(1): p. 15-17.

40. Roy, I., M.K. Stachowiak, and E. Bergey, *Nonviral gene transfection nanoparticles: function and applications in the brain.* Nanomedicine: Nanotechnology, Biology and Medicine, 2008. 4(287-97).

41. Scherer, F., et al., *Magnetofection: enhancing and targeting gene delivery by magnetic force in vitro and in vivo.* Gene Therapy, 2002. 9(2): p. 102-109.

42. Alexiou, C., W. Arnold, and R. Klein, *Locoregional cancer treatment with magnetic drug targeting.* Cancer Research, 2000. 60: p. 6641-6648.

43. Shinkai, M., *Functional Magnetic Particles for Medical Application.* Journal of Bioscience and Bioengineering, 2002. 94(6): p. 606-613.

44. Dormer, K.J., et al., *Magnetically-targeted, technetium 99m-labeled nanoparticles to the inner ear.* Journal of Biomedical Nanotechnology, 2008. 4(2): p. 174-184.

45. Forbes, Z.G., et al., *An approach to targeted drug delivery based on uniform magnetic fields.* Ieee Transactions on Magnetics, 2003. 39(5): p. 3372-3377.

46. Yellen, B.B., et al., *Targeted drug delivery to magnetic implants for therapeutic applications.* J Magn Magn Mater, 2005. 293: p. 647-54.

47. Forbes, Z.G., et al., *Improving the efficacy of cellular therapy by magnetic cell targeting.* Cytotherapy, 2006. 8.

48. Forbes, Z.G., et al., *In vivo evaluation of a magnetic stent based drug delivery system.* Journal of the American College of Surgeons, 2006. 203(3): p. S102-S103.

49. Forbes, Z.G., et al., *Validation of high gradient magnetic field based drug delivery to magnetizable implants under flow.* Ieee Transactions on Biomedical Engineering, 2008. 55(2): p. 643-649.

50. Polyak, B., et al., *High field gradient targeting of magnetic nanoparticle-loaded endothelial cells to the surfaces of steel stents.* PNAS, 2001. 105(2): p. 698-703.

51. Nacev, A., et al., *Magnetic nanoparticle transport within flowing blood and into surrounding tissue.* Nanomedicine, 2010. 5(9): p. 1459-1466.

52. Salloum, M., et al., *Controlling nanoparticle delivery in magnetic nanoparticle hyperthermia for cancer treatment: Experimental study in agarose gel.* International Journal of Hyperthermia, 2008. 24(4): p. 337-345.

53. Kalambur, V.S., et al., *In vitro characterization of movement, heating and visualization of magnetic nanoparticles for biomedical applications.* Nanotechnology, 2005. 16: p. 1221-1233.

54. Holligan, D., G. Gillies, and J. Dailey, *Magnetic guidance of ferrofluidic nanoparticles in an in vitro model of intraocular retinal repair.* Nanotechnology, 2003. 14(661).

55. Raju, H., et al., *Evaluation of magnetic micro- and nanoparticle toxicity to ocular tissues.* PLoS One, 2011. 6(5).

56. Gao, X., et al., *Magnetic Assisted Transport of PLGA Nanoparticles Through Human Round Window Membrane Model.* J. Nanotechnol. Eng. Med, 2010. 1(3).

57. Barnes, A.L., et al., *Magnetic characterization of superparamagnetic nanoparticles pulled through model membranes.* BioMagnetic Research and Technology, 2007. 5(1).

58. Atala, A., et al., *Injectable alginate seeded with chondrocytes as a potential treatment for vesicoureteral reflux.* J Urol, 1993. 150(2 Pt 2): p. 745-7.

59. Ivanov, A.I., ed. *Exocytosis and Endocytosis*. Methods in Molecular Biology, ed. J.M. Walker. Vol. 440. Humana Press: Rochester, NY.

60. Pratten, M. and J.B. Lloyd, *Pinocytosis and phagocytosis: the effect of size of a particulate substrate on its mode of capture by rate peritoneal macrophages cultured in vitro.* Biochimica et Biophysica Acta, 1986. 881: p. 307-313.

61. Prijic, S., et al., *Increased cellular uptake of biocompatible superparamagnetic ron oxide nanoparticles into malignant cells by an external magnetic field.* J Membr Bio, 2010. 236(167-179).

62. Huth, S., et al., *Insights into the mechanism of magnetofection using PEI-based magnetofectins for gene transfer.* J Gene Med, 2004. 6: p. 923-936.

63. Plank, C., *The magnetofection method: Using magnetic force to enhance gene delivery.* Biological Chemistry, 2003. 384(5): p. 737.

64. Vasir, J.K. and V. Labhasetwar, *Quantification of the force of nanoparticle-cell membrane interactions and its influence on intracellular trafficking of nanoparticles.* Biomaterials, 2008. 29(31): p. 4244-4252.

65. Bausch, A., et al., *Local measurements of viscoelastic parameters of adherent cell surfaces by magnetic bead microrheometry.* Biophysical Journal, 198. 75: p. 2038-2049.

66. Zhang, S., et al., *Size-dependent endocytosis of nanoparticles.* Advanced Materials, 2009. 21: p. 419-424.

67. Thorek, D.L.J. and A. Tsourkas, *Size, charge and concentration dependent uptake of iron oxide particles by non-phagocytic cells.* Biomaterials, 2008. 29(26): p. 3583-3590.

68. Rejman, J., et al., *Size-dependent internalization of particles via the pathways of clathrin- and caveolae-mediated endocytosis.* Biochem J, 2004. 377(Pt 1): p. 159-69.

69. Chithrani, B., A. Ghazani, and W. Chan, *Determining the size and shape dependence of gold nanoparticle uptake into mammalian cells.* Nano Letters, 2006. 6(4): p. 662-668.

70. Fazlollahi, F., et al., *Polystyrene nanoparticle trafficking across MDCK-II.* Nanomedicine: Nanotechnology, Biology and Medicine, 2011.

71. Qaddoumi, M.G., et al., *Clathrin and caveolin-1 expression in primary pigmented rabbit conjunctival epithelial cells: Role in PLGA nanoparticle endocytosis.* Molecular Vision, 2003. 9(68-69): p. 559-568.

72. Chung, T.H., et al., *The effect of surface charge on the uptake and biological function of mesoporous silica nanoparticles 3T3-L1 cells and human mesenchymal stem cells.* Biomaterials, 2007. 28: p. 2959-2966.

73. Nakamura, K., et al., *Regional intestinal absorption of FITC-dextran 4,400 with nanoparticles based on beta-sitosterol beta-D-glucoside in rats.* Journal of Pharmaceutical Sciences, 2003. 92(2): p. 311-318.

74. Zhang, Y., N. Kohler, and M. Zhang, *Surface modification of superparamagnetic magnetite nanoparticles and their intracellular uptake.* Biomaterials, 2001. 23(71553-1561).

75. Chen, L., et al., *The role of surface charge on the uptake and biocompatibility of hydroxyapatite nanoparticles with osteoblast cells.* Nanotechnology, 2010. 22.

76. Tan, K., et al., *Nanosized bioceramic particles could function as efficient gene delivery vehicles with target specificity for the spleen.* Gene Therapy, 2007. 14: p. 828-835.

77. Motskin, M., et al., *Hydroxyapatite nano and microparticles: correlation of particle properties with cytotoxicity and biostability.* Biomaterials, 2009. 30: p. 3307-3317.

78. Kang, J.S., Y.N. Yum, and S.N. Park, *Cytotoxicity and DNA Damage Induced by Magnetic Nanoparticle Silica in L5178Y Cell.* Biomolecules and Therapeutics 2011. 19(2): p. 261-266.

79. Shubayev, V.I., T.R. Pisanic II, and S. Jin, *Magnetic nanoparticles for theragnostics.* Advanced Drug Delivery Reviews, 2009. 61(6): p. 467-477.

80. Hsiao, J., et al., *Magnetic nanoparticle labeling of mesenchymal stem cells without transfection agent: cellular behaviour and capability of detection with clinical 1.5 T magnetic resonance at the single cell level.* Magn Reson Med, 2007. 58(4): p. 717-724.

81. Karlsson, H.L., et al., *Size-dependent toxicity of metal oxide particles - A comparison between nano- and micrometer size.* Toxicology Letters, 2008. 188(2): p. 112-118.

82. Ying, E. and H. Hwang, *In vitro evaluation of the cytotoxicity of iron oxide nanoparticles with different coatings and different sizes in A3 human T lymphocytes.* Sci Total Environ, 2010. 408(20): p. 4475-4481.

83. Frixione, E., *Recurring View on the Structure and Function of the Cytoskeleton: A 300-Year Epic.* Cell Motility and the Cytoskeleton, 2000. 46(1): p. 73-94.

84. Lodish, H., et al., *Molecular Cell Biology*. 5th ed2003, New York City, NY: W.H. Freeman and Company.

85. Wu, X., et al., *Toxic effects of iron oxide nanoparticles on human umbilical vein endothelial cells.* International Journal of Nanomedicine, 2010. 5: p. 385-399.

86. Curtis, A.S.G. and A.K. Gupta, *Surface modified superparamagnetic nanoparticles for drug delivery: Interactions with human fibroblasts in culture.* Journal of Materials Science: Materials in Medicine, 2004. 15: p. 493-496.

87. Soenen, S., et al., *High intracellular iron oxide nanoparticle concentrations affect cellular cytoskeleton and focal adhesion kinase-mediated signaling.* Small, 2010. 6(7): p. 832-842.

88. Marchetti, P., et al., *Mitochondrial permeability transition is a central coordinating event of apoptosis.* J. Exp. Med, 1996. 184: p. 1155-1160.

89. Green, D., R and G. Kroemer, *The pathophysiology of mitochondrial cell death.* Science, 2004. 305(5684): p. 626-629.

90. Xia, T., et al., *Cationic polystyrene nanopsphere toxicity depends on cell-specific endocytic and mitochondrial injury pathways.* Acs Nano, 2008. 2(1): p. 85-96.

91. Park, E.-J., et al., *Oxidative stress and apoptosis induced by titanium dioxide nanoparticles in cultured BEAS-2B cells.* Toxicology Letters, 2008. 180: p. 222-229.

92. Buyukhatipoglu, K. and A.M. Clyne, *Superparamagnetic iron oxide nanoparticles change endothelial cell morphology and mechanics via reactive oxygen species formation.* Journal of Biomedical Materials Research Part A, 2011. 96A(1): p. 186-195.

93. Apopa, P.L., et al., *Iron oxide nanoparticles induce human microvascular endothelial cell permeability through reactive oxygen species production and microtubule remodeling.* Particle and Fibre Toxicology, 2009. 6(1).

94. Valko, M., et al., *Free radicals, metals and antioxidants in oxidative stress-induced cancer.* Chem. Biol. Interact., 2006. 160: p. 1-40.

95. Jezek, P. and L. Hlavata, *Mitochondria in homeostasis of reactive oxygen species in cell, tissues and organism.* Int. J. Biochem.Cell Biol., 2005. 37: p. 2478-2503.

96. Cunningham, C.H., et al., *Positive contrast magnetic resonance imaging of cells labeled with magnetic nanoparticles.* Magnetic Resonance in Medicine, 2005. 53(5): p. 999-1005.

97. Polyak, B. and G. Friedman, *Magnetic targeting for site-specific drug delivery: applications and clinical potential.* Expert Opin. Drug Delivery, 2009. 6(1): p. 53-70.

98. Johannsen, M., et al., *Magnetic fluid hyperthermia (MFH)reduces prostate cancer growth in the orthotopic Dunning R3327 rat model.* Prostate, 2005. 64(3): p. 283-92.

99. Hafeli, U.O., et al., *Effective targeting of magnetic radioactive 90Y-microspheres to tumor cells by an externally applied magnetic field. Preliminary in vitro and in vivo results.* Nucl Med Biol, 1995. 22(2): p. 147-55.

100. Hafeli, U.O., et al., *Magnetically directed poly(lactic acid) 90Y-microspheres: novel agents for targeted intracavitary radiotherapy.* J Biomed Mater Res, 1994. 28(8): p. 901-8.

101. Jurgons, R., et al., *Drug loaded magnetic nanoparticles for cancer therapy.* Journal of Physics: Condensed Matter, 2006. 18(38): p. S2893-S2902.

102. Lubbe, A.S., C. Alexiou, and C. Bergemann, *Clinical applications of magnetic drug targeting.* J Surg Res, 2001. 95(2): p. 200-6.

103. Lubbe, A.S., C. Bergemann, and C. Alexiou, *Targeting tumors with magnetic drugs.* Tumor Targeting in Cancer Therapy, 2002: p. 379-388.

104. Lubbe, A.S., et al., *Preclinical experiences with magnetic drug targeting: tolerance and efficacy.* Cancer Res, 1996. 56(20): p. 4694-701.

105. Mosbach, K. and U. Schroder, *Preparation and application of magnetic polymers for targeting of drugs.* FEBS Lett, 1979. 102(1): p. 112-6.

106. Senyei, A., K. Widder, and G. Czerlinski, *Magnetic guidance of drug-carrying microspheres.* Journal of Applied Physics, 1978. 49(6): p. 3578-83.

107. Widder, K.J., A.E. Senyel, and G.D. Scarpelli, *Magnetic microspheres: a model system of site specific drug delivery in vivo.* Proc Soc Exp Biol Med, 1978. 158(2): p. 141-6.

108. Chorny, M., et al., *Magnetically driven plasmid DNA delivery with biodegradable polymeric nanoparticles.* Faseb J (in press), 2007.

109. Mah, C., et al., *Improved method of recombinant AAV2 delivery for systemic targeted gene therapy.* Mol Ther, 2002. 6(1): p. 106-12.

110. Mah, C., et al., *Microsphere-Mediated Delivery of Recombinant AAV Vectors In Vitro And In Vivo.* Mol Ther, 2000. 1: p. S239-242.

111. Plank, C., et al., *Magnetofection: enhancement and localization of gene delivery with magnetic particles under the influence of a magnetic field.* J Gene Med, 2000. 2(24).

112. Muthana, M., et al., *A novel magnetic approach to enhance the efficacy of cell-based gene therapies.* Gene Ther, 2008. 15(12): p. 902-10.

113. Pislaru, S.V., et al., *Magnetically targeted endothelial cell localization in stented vessels.* J Am Coll Cardiol, 2006. 48(9): p. 1839-45.

114. Polyak, B., et al., *High field gradient targeting of magnetic nanoparticle-loaded endothelial cells to the surfaces of steel stents.* Proceedings of the National Academy of Sciences of the United States of America, 2008. 105(2): p. 698-703.

115. Ritter, J.A., et al., *Application of high gradient magnetic separation principles to magnetic drug targeting.* Journal of Magnetism and Magnetic Materials, 2004. 280(2-3): p. 184-201.

116. Pislaru, S.V., et al., *Magnetic forces enable rapid endothelialization of synthetic vascular grafts.* Circulation, 2006. 114(1 Suppl): p. I314-8.

117. Kamau, S.W., et al., *Enhancement of the efficiency of non-viral gene delivery by application of pulsed magnetic field.* Nucleic Acids Res., 2006. 34(5): p. e40/1-e40/8.

118. Kuhn, S.J., et al., *Proteolytic Surface Functionalization Enhances in Vitro Magnetic Nanoparticle Mobility through Extracellular Matrix.* Nano Letters, 2006. 6(2): p. 306-312.

119. Kuhn, S.J., D.E. Hallahan, and T.D. Giorgio, *Characterization of superparamagnetic nanoparticle interactions with extracellular matrix in an in vitro system.* Ann Biomed Eng, 2006. 34(1): p. 51-8.

120. Mondalek, F.G., et al., *The permeability of SPION over an artificial three-layer membrane is enhanced by external magnetic field.* Journal of Nanobiotechnology, 2006. 4(4).

121. Rotariu, O., et al., *The guidance of magnetic colloids in simulated tissues for targeted drug delivery.* Journal of Optoelectronics and Advanced Materials, 2007. 9(4): p. 942-945.

122. Crick, F.H.C. and A.F.W. Hughes, *The physical properties of cytoplasm: a study by means of the magnetic particle method.* . Exp. Cell Res., 1950. 1: p. 37–80.

123. Dobson, J., *Remote control of cellular behaviour with magnetic nanoparticles.* Nature Nanotechnology, 2008. 3(3): p. 139-143.

124. Hamoudeh, M., et al., *Elaboration of PLLA-based superparamagnetic nanoparticles: Characterization, magnetic behaviour study and in vitro relaxivity evaluation.* International Journal of Pharmaceutics, 2007. 338(1-2): p. 248-257.

125. Massart, R., *Preparation of aqueous magnetic liquids in alkaline and acidic media.* IEEE Trans. Magn., 1981. MAG-17(2): p. 1247-8.

126. Ali, S.A., P.J. Doherty, and D.F. Williams, *Mechanisms of polymer degradation in implantable devices. 2. Poly(DL-lactic acid).* J Biomed Mater Res, 1993. 27(11): p. 1409-18.

127. Anderson, J.M. and M.S. Shive, *Biodegradation and biocompatibility of PLA and PLGA microspheres.* Advanced Drug Delivery Reviews, 1997. 28(1): p. 5-24.

128. Chu, C.C., *The degradation and biocompatibility of suture materials.* Critical Reviews in Biocompatibility, 1985. 1(3): p. 261-322.

129. Williams, D.F., *Review. Biodegradation of surgical polymers.* Journal of Materials Science, 1982. 17(5): p. 1233-46.

130. Liu, X., et al., *Synthesis and characterization of highly-magnetic biodegradable poly(d,l-lactide-co-glycolide) nanospheres.* J Control Release, 2007. 119(1): p. 52-8.

131. Gref, R., G. Miralles, and E. Dellacherie, *Polyoxyethylene-coated nanospheres: effect of coating on zeta potential and phagocytosis.* Polymer International, 1999. 48(4): p. 251-256.

132. Sahoo, S.K., et al., *Residual polyvinyl alcohol associated with poly (D,L-lactide-co-glycolide) nanoparticles affects their physical properties and cellular uptake.* Journal of Controlled Release, 2002. 82(1): p. 105-114.

133. Goya, G.F., V. Grazu, and M.R. Ibarra, *Magnetic nanoparticles for cancer therapy.* Current Nanoscience, 2008. 4(1): p. 1-16.

134. Ivkov, R., et al., *Application of High Amplitute Alternating Magnetic Fields for Heat Induction of Nanoparticles Localized in Cancer.* Clinical Cancer Research, 2005. 11(19): p. 7093-7193.

135. Johannsen, M., et al., *Clinical hyperthermia of prostate cancer using magnetic nanoparticles: presentation of a new interstitial technique.* International Journal of Hyperthermia, 2005. 21(7): p. 637-47.

136. Moroz, P., S.K. Jones, and B.N. Gray, *Magnetically mediated hyperthermia: current status and future directions.* Int J Hyperthermia, 2002. 18(4): p. 267-84.

137. MacDonald, C., et al., *Time-varied magnetic field enhances transport of magnetic nanoparticles in viscous gel.* Nanomedicine, 2010. 5(1): p. 65-76.

138. Johnson, B., et al., *Magnetically responsive, pclitazel-loaded biodegradable nanoparticles for treatment of vascular disease: preparation, characterizaton and in vitro evaluation of anti-proliferative potential.* Current Drug Delivery, 2010. 7(4): p. 263-273.

139. Wang, G.N. and X.G. Su, *The synthesis and bio-applications of magnetic and fluorescent bifunctional composite nanoparticles.* Analyst, 2011. 136(9): p. 1783-1798.

140. LaConte, L., N. Nitin, and G. Bao, *Magnetic nanoparticle probes.* Materials today, 2005. 8(5): p. 32-38.

141. Mornet, S., et al., *Magnetic nanoparticle design for medical diagnosis and therapy.* Journal of Materials Chemistry, 2004. 14(14): p. 2161-2175.

142. Smith, C.A.M., et al., *The effect of static magnetic fields and tat peptides on cellular and nuclear uptake of magnetic nanoparticles.* Biomaterials, 2010. 31(15): p. 4392-4400.

143. Tresilwised, N., et al., *Boosting Oncolytic Adenovirus Potency with Magnetic Nanoparticles and Magnetic Force.* Molecular Pharmaceutics, 2010. 7(4): p. 1069-1089.

144. Okada, H. and H. Toguchi, *BIODEGRADABLE MICROSPHERES IN DRUG-DELIVERY.* Critical Reviews in Therapeutic Drug Carrier Systems, 1995. 12(1): p. 1-99.

145. Kim, D., et al., *Biofunctionalized magnetic-vortex microdiscs for targeted cancer-cell destruction.* Nature Materials, 2010. 9: p. 165-171.

146. Ale-Agha, N., C. Albrecht, and L. Klotz, *Loss of gap junctional intercellular communication in rat lung epithelial cells exposed to carbon or silica-based nanoparticles.* Biol Chem, 2010.

147. Patel, S., et al., *Human corneal endothelial cell transplantation in a human ex vivo model.* Investigative Ophthalmology and Visual Science, 2009. 50(5): p. 2123-2131.

148. Mitragotri, S., *Transdermal drug delivery using low-frequency sonophoresis.* BioMEMS Biomed. Nanotechnol., 2006. 3: p. 223-236.

149. Mitragotri, S., D. Blankschtein, and R. Langer, *Ultrasound-mediated transdermal protein delivery.* Science, 1995. 269(5225): p. 850-3.